

NEW INSIGHTS ON POREWATER GEOCHEMISTRY
IN ORGANIC-RICH COASTAL SEDIMENTS

by

ALEXANDER F. LAMORE

NATASHA DIMOVA, COMMITTEE CHAIR

YUEHAN LU

GEOFF TICK

JULIA A. CHERRY

A THESIS

Submitted in partial fulfillment of the requirements
for the degree of Master of Science
in the Department of Geological Sciences
in the Graduate School of
The University of Alabama

TUSCALOOSA, ALABAMA

2020

Copyright Alexander F. Lamore 2020
ALL RIGHTS RESERVED

ABSTRACT

Previous studies of groundwater nutrient dynamics in coastal Baldwin County, AL indicate that groundwater is contaminated with NO_3^- . However, recently, nutrient fluxes' mass-balance indicates positive fluxes of reduced nitrogen species, NH_4^+ and dissolved organic nitrogen (DON), while NO_3^- fluxes were negative. Further, it was suggested that geochemical transformations within an organic-rich layer comprising the subterranean estuary (STE) in Mobile Bay could be responsible for the observed changes in the groundwater-derived nitrogen fluxes. This study aims to examine the nitrogen geochemical transformations occurring in organic-rich shallow coastal sediments and to identify the quantity and quality of carbon exported by groundwater. In a laboratory-based study, sediment cores with identified organic-rich layers collected from a hypoxia-impacted shoreline of Mobile Bay were incubated with $400\mu\text{M}$ and $800\mu\text{M}$ NO_3^- solutions, natural groundwater (GW), and ultra-pure carbon-free water (UPCFW) to evaluate how the sediment reacts to different NO_3^- loading. Findings from the incubation studies show that the organic-rich sediments are indeed responsible for the NO_3^- loss in groundwater as all treatments with NO_3^- amendments experienced NO_3^- removal. Also, that the organic-rich sediments are a source of reduced N, in the form of DON and NH_4^+ , evidenced by net-N production observed in three of four treatments and the N produced correlates with DON, and that higher NO_3^- loading promotes increased DON production. Additionally, both DNRA and denitrification occurred, but the dominant pathway of NO_3^- removal was denitrification. Average NO_3^- removal rates increased with increases in NO_3^- loading, but complete NO_3^- removal was not observed. The STE sediment has the potential to denitrify

significant amounts of anthropogenic NO_3^- , however, in the process producing NH_4^+ , DON, DOC, and DIC.

DEDICATION

This thesis is dedicated to my family, my colleagues and friends at The University of Alabama, and my partner for their never-ending support and encouragement throughout this educational journey.

LIST OF ABBREVIATIONS AND SYMBOLS

| | |
|-------------------|--|
| cm | centimeter(s) |
| d | day(s) |
| DNRA | dissimilatory nitrate reduction to ammonium |
| DO | dissolved oxygen |
| DIC | dissolved inorganic carbon |
| DIC _{OM} | dissolved inorganic carbon from the remineralization of organic matter |
| DIN | dissolved inorganic nitrogen |
| DISL | Dauphin Island Sea Lab |
| DOC | dissolved organic carbon |
| DOM | dissolved organic matter |
| DON | dissolved organic nitrogen |
| GW | groundwater |
| m | meter(s) |
| N _{ex} | nitrogen excess |
| ODC | oxygen deplete chamber |
| OM | organic matter |
| POM | particulate organic matter |
| SGD | submarine groundwater discharge |
| SRB | sulfate reducing bacteria |
| STE | subterranean estuary |

| | |
|-------|------------------------------|
| T | time |
| TA | total alkalinity |
| TDN | total dissolved nitrogen |
| TN | total nitrogen |
| UPCFW | ultra-pure carbon-free water |
| VPDB | Vienna Peedee belemnite |
| XRD | x-ray diffraction |
| Y | year(s) |
| % | percentage |
| ‰ | per mil |

ACKNOWLEDGMENTS

I would like to express my sincerest appreciation for my advisor and mentor, Dr. Natasha Dimova. Dr. Dimova has guided me throughout my secondary education journey since the junior year of my undergraduate studies. Without her support and guidance, I would not be in the position I am today. I would also like to thank Dr. Yuehan Lu for all the wisdom and guidance she has shared with me throughout this process. Dr. Lu has consistently allowed my access to her labs and equipment and has treated me like one of her own students; for that, I am incredibly grateful. Additionally, I am very appreciative of the advice and support given by my committee members, Dr. Geoff Tick, and Dr. Julia Cherry. I cannot express enough thanks for the help from my fellow graduate student colleagues, especially Shuo Chen. Shuo was always willing to help me with any questions I had. From simple answers to complex issues, Shuo always was happy to help. The person perhaps the most deserving of an acknowledgment is Dr. Daniel Montiel. Daniel introduced me to the fascinating research being done in Dr. Dimova's lab and took me under his wing when I was only a sophomore. Every step of the way, Daniel has been there for me as both a friend and a mentor, and I don't think I could ever fully express my gratitude. Finally, I must thank Laura Linn at Dauphin Island Sea Lab for conducting the nutrient analysis. Without her excellent communication and patience, this thesis research wouldn't have been possible.

CONTENTS

| | |
|--|-----|
| ABSTRACT | ii |
| DEDICATION | iv |
| LIST OF ABBREVIATIONS AND SYMBOLS | v |
| ACKNOWLEDGMENTS | vii |
| LIST OF TABLES | xi |
| LIST OF FIGURES | xii |
| INTRODUCTION | 1 |
| MATERIALS AND METHODS..... | 5 |
| Site Description..... | 5 |
| Sediment Core Material Collection and Characterization | 5 |
| X-Ray diffraction (XRD)..... | 6 |
| Heavy metal composition | 7 |
| $\delta^{15}\text{N}$ - $\delta^{13}\text{C}$ assessments in sediments | 7 |
| Radiocarbon (^{14}C , $t_{1/2}=5,730$ yrs) dating | 8 |
| Incubation Experiments Setup and Porewater Analyses | 9 |
| Total alkalinity (TA) and auxiliary parameters | 11 |
| Nitrogen speciation | 11 |
| Nitrate removal | 12 |
| Dissolved organic carbon (DOC)..... | 12 |
| Dissolved inorganic carbon (DIC)..... | 12 |

| | |
|---|----|
| Dissolved organic matter (DOM) | 13 |
| RESULTS | 15 |
| Sediment Core Stratigraphy and Physical/Chemical Properties | 15 |
| Mineral composition | 17 |
| Heavy metal concentrations in sediment | 17 |
| Sediment $\delta^{13}\text{C}$ and $\delta^{15}\text{N}$ compositions | 18 |
| Radiocarbon (^{14}C , $t_{1/2}=5,730$ yrs) dating | 18 |
| Porewater Composition After Incubations..... | 19 |
| Dissolved organic nitrogen (DON)..... | 19 |
| Ammonium (NH_4^+)..... | 20 |
| Nitrate (NO_3^-)..... | 20 |
| Nitrite (NO_2^-) | 21 |
| Dissolved organic carbon (DOC)..... | 22 |
| Dissolved inorganic carbon (DIC)..... | 23 |
| Dissolved organic matter (DOM) quality | 24 |
| N- And C-Balances in Porewater..... | 26 |
| Nitrogen excess (N_{ex})..... | 26 |
| Nitrate removal rates..... | 27 |
| DIC from the mineralization of organic matter (DIC_{OM}) | 28 |
| Calculated DOC and DIC theoretical fluxes entrained by SGD..... | 29 |
| DISCUSSION..... | 31 |
| Age of The Organic-Rich Sediment Layer | 31 |
| Theoretical Basis Of N-Biogeochemical Transformations in Organic-Rich Marine Sediments | 31 |

| | |
|--|----|
| N Budget Assessments..... | 34 |
| N production | 34 |
| Nitrate removal pathways and rates | 38 |
| DOM Compositional Changes and Mineralization Of OM..... | 40 |
| DOM compositional changes..... | 41 |
| Mineralization of OM | 42 |
| Hypothetical Effectiveness of Anthropogenic Nitrogen Loading Removal | 48 |
| CONCLUSION..... | 51 |
| REFERENCES | 52 |
| APPENDIX I | 60 |

LIST OF TABLES

Table 1: Results from incubations60

Table 2: Sediment physical, chemical, and hydraulic properties.....66

LIST OF FIGURES

| | |
|---|----|
| <p>Figure 1: Left: Image of sediment core PH10 with tape measure for reference. Right: Diagram representing stratigraphy and grain size classification of sediment cores used for this study.....</p> | 15 |
| <p>Figure 2: Grain size distribution (in mm) of sediment from core PH10 collected from The STE. Each line represents the grain size distribution for a 5cm section of core.....</p> | 16 |
| <p>Figure 3: Depth profile (in cm) of (A) DON, (B) NH₄, (C) NO₃⁻, and (D) NO₂⁻ from the UPCFW, GW, 400μM and 800μM treatments. Measured in μM. Shaded areas indicate the organic-rich sediment layers.....</p> | 22 |
| <p>Figure 4: Depth profile (in cm) of DOC from the UPCFW, GW, 400μM, and 800μM treatments, measured in μM. Shaded areas indicate the organic-rich sediment layers</p> | 23 |
| <p>Figure 5: Depth profiles (in cm) of DIC (in μM) from the (A) UPCFW, (B) GW, (C) 400μM, and (D) 800μM treatments. Shaded areas indicate the organic-rich sediment layers.....</p> | 24 |
| <p>Figure 6: Average nitrate removal rates (μM/hr) from the 800μM, 400μM, and GW treatments. Dark bars represent averages from the organic-rich layer while light bars represent averages from the lower-organic layers. Error bars represent standard deviation within each treatment.</p> | 27 |
| <p>Figure 7: Average percentage DIC from the remineralization of organic matter from the UPCFW, GW, 400μM, and 800μM treatments. Dark bars represent the organic rich sediment layers while the light bars represent the lower-organic layers. Error bars represent standard deviation within each treatment.</p> | 28 |
| <p>Figure 8: (A) theoretical DOC fluxes entrained by SGD from the UPCFW, GW, 400μM, and 800μM treatments measured in mmol/day. (B) theoretical DOC fluxes entrained by SGD from the UPCFW, GW, 400μM, and 800μM treatments measured in mmol/day. Error bars represent standard deviation within each treatment.....</p> | 30 |

Figure 9: Left diagram depicts the sequence of early diagenetic reactions occurring in Surficial sediments (the figure is a compilation of different sources, mostly from Gaillard JF 1999, and Floelich et al., 1979). Fluxes of POM and DOM and anthropogenic nitrate entering the system are indicated on top. The figure on the right shows the N-cycle from Madigan et al. (2017)32

Figure 10: Depth profile (in cm) of dissolved TN from UPCFW treatment (A), GW treatment (B), 400µM treatment (C), and 400µM treatment (D) measured in µM. Dashed lines represent TN of the system at the beginning of each treatment. Shaded areas indicate the organic-rich sediment layers.....34

Figure 11: Cross plot N_{ex} (in µM) vs. the amount of NO_3^- added to the incubations (in µM) demonstrating a linear relationship with an $R^2 = 0.96$35

Figure 12: N_{ex} vs. DON in UPCFW treatment (A), N_{ex} vs. DON in GW treatment (B), N_{ex} vs. DON in 800µM treatment (C), and N_{ex} vs. DON in 400µM treatment (D). All data is in µM.36

Figure 13: Cross plot N_{ex} (in µM) vs. DOC (in µM) from the UPCFW treatment demonstrating a linear relationship with an $R^2 = 0.61$ 37

Figure 14: Depth profile (in cm) of the mineral goethite XRD peak intensity in percentage (upper x axis) and Fe concentration in mg/kg of sediment (lower x axis) from ICP-OES metal cations analysis. (B) Depth profile of Fe (lower x axis) and Mn (upper x axis) in in mg/kg of sediment from ICP-OES metal cations analysis. Shaded areas indicate the organic-rich sediment layers.....38

Figure 15: Visual representation of the excitation and emission of (left to right) component 1, component 2, and component 3 from DOM analysis.....41

Figure 16: DOM component intensity in porewater after treatment and from pre-treatment sediment (PTS) shaker experiments reported in %43

Figure 17: Average % DIC from the remineralization of organic matter from the UPCFW, GW, 400µM and 800µM treatments46

Figure 18: Cross plots of DON vs DOC in porewater from the organic-rich sediment for the (A) UPCFW, (B) GW, (C) 400µM, and (D) 800µM treatments48

INTRODUCTION

Coastal hypoxia has been observed globally and has detrimental effects on ecosystems, causing harm to coastal marine life, including large scale fish kill events (Loesch, 1960; Montiel, 2018; Peterson et al., 2016). It is widely accepted that enhanced nutrient input is the main driving factor of coastal hypoxia. Many studies point to riverine input as the primary source of nutrients that ultimately creates hypoxic events, such as the Gulf of Mexico dead zone (Dybas, 2005; Fennel & Testa, 2019; Osterman, Poore, Swarzenski, Senn, & Dimarco, 2009; Rabalais & Turner, 2001). However, recently it has been suggested that in some cases, nutrient input via submarine groundwater discharge (SGD) can play a more critical role (Knee & Jordan, 2013; Mccoy & Corbett, 2009; Montiel et al., 2019; Null et al., 2012; Slomp & Cappellen, 2004). Before entering coastal waters, SGD percolates through the shallow coastal aquifer, known as the *subterranean estuary* (STE). The STE is an ideal environment where steep chemical gradients, created by mixing reduced and oxidized pore fluids, drive concurrently critical biogeochemical reactions (Moore, 1999). Recent studies have found that groundwater flowing through the STE can carry anoxic water high in nutrients into coastal waters through SGD (Couturier, Tommi-morin, Sirois, Rao, & Nozais, 2017; Erler et al., 2014; Montiel et al., 2019; Peterson et al., 2016; Slomp & Cappellen, 2004).

Due to the concurrent impacts of terrestrial and marine forcing, STEs are non-steady-state systems, where chemical equilibrium and the typical sequence of redox reactions are often disturbed (Santos, Eyre, & Huettel, 2012; Sundby, 2006). For example, oscillating oxic and anoxic conditions due to seasonal groundwater flow variations and tidal pumping in coastal

sediments allow for coupled nitrification-denitrification to co-occur (Aller, 1994). On the other hand, alternative nitrate reduction pathways such as dissimilatory nitrate reduction to ammonium (DNRA) and anaerobic ammonium oxidation (anammox) have also been observed (Kroeger & Charette, 2008; Montiel et al., 2019; Rocha, Ibanhez, & Leote, 2009; Sáenz et al., 2012). In hydrogeology, net nutrient exports through SGD are typically calculated by assessing nutrient concentrations in inland groundwater and applying local groundwater flow rates to calculate net fluxes, assuming conservative chemical transport (Kroeger and Charette, 2008). However, chemical transport in the STE is rarely conservative, suggesting the STE can act either as a sink of nutrients from fresh groundwater, or a source of nutrients through biogeochemical processes (Beck et al., 2007; Charette & Sholkovitz, 2002; Charette, Sholkovitz, & Hansel, 2005; Hays & Ullman, 2007; Windom, Moore, Niencheski, & Jahnke, 2006).

Anthropogenic nutrient loading in the STE has been an area of concern due to the recent and vast development of coastal regions (Null et al., 2012). High levels of total dissolved nitrogen (TDN) and dissolved organic nitrogen (DON) in groundwater have been linked to the magnitude of anthropogenic nitrogen (N) inputs. Nevertheless, although the presence of certain speciations of N in the STE is still poorly understood, it has been strongly suggested to be related to the complexity of the N transformations during transport (Kroeger, Cole, & Valiela, 2006). The presence of organic matter (OM) is essential to facilitating N transformations, specifically N mineralization of organic matter (Couturier et al., 2017; Kroeger & Charette, 2008; Montiel et al., 2019; Santoro, 2010; Santos et al., 2008). Many studies on dissolved inorganic nitrogen (DIN) in the STE have been conducted (Boehm, Paytan, Shellenbarger, & Davis, 2006; Kroeger & Charette, 2008; Rocha et al., 2009), but DON and geochemical reactions occurring within the STE overall still remains poorly understood.

The three key elements linked to the development of hypoxia in coastal waters are (1) increased nutrient loading, (2) fast production of particulate and dissolved organic matter (POM and DOM), and (3) oxygen consumption from the degradation of OM (Gray et al., 2002). In addition to anthropogenic activities, high nutrient loading can be generated in SGD through the mineralization of OM in anoxic and OM-rich coastal sediments (Montiel et al., 2019; Slomp & Cappellen, 2004; Song, Luo, Zhao, & Christie, 2003). Based on that, the STE provides ideal conditions to meet the elements linked to hypoxia by Gray et al. (2002). For example, Ho et al. (2019) reported findings of bottom water hypoxia during the summer in areas experiencing high SGD contribution in the northern Gulf of Mexico, Mississippi Bight (Mississippi, USA). Further, Kroeger, Cole, and Valiela (2006) found that NH_4^+ and DON were the primary N species delivered by SGD to Tampa Bay (Florida, USA). Also, in Martinique Beach on the Magdalen Islands (Quebec, Canada) SGD rich in NH_4^+ and DON was reported to discharge from the STE into the coastal waters (Couturier et al., 2017). Lastly, in Turkey Point (Florida, USA) in the north-eastern Gulf of Mexico, Santos et al. (2008) also reported fluxes of primarily DON and NH_4^+ from SGD. The common denominator in all these cases is the presence of OM, which was found to be critical in producing reduced N fluxes (i.e. NH_4^+ and DON). Such severe reduced conditions create a high demand for oxygen in further oxidation and microorganism respiration processes (Burford & Bremner, 1975). Indeed, in Hampyeong Bay (South Korea) SGD derived DOM was identified as an essential source for both DOC and DON to the coastal waters (Kim, Waska, Kwon, Suryaputra, & Kim, 2012). In the northern Gulf of Mexico, a recent study by Montiel et al. (2019) in Mobile Bay (Alabama, USA) further linked the large DON and NH_4^+ fluxes from SGD in hypoxia-impacted coastal water to the presence of an organic-rich sediment layer in the shallow coastal aquifer.

To better understand N dynamics in shallow coastal aquifers and the fundamental role of organic carbon in areas impacted by SGD-influenced hypoxia, I studied pore water biogeochemistry in sediment cores collected from the STE in the northern Gulf of Mexico. Such a laboratory-based approach eliminates some of the uncertainty inherent to field-based studies and provides better insights into the biogeochemistry that occurs in the porous sediment found within the STE. This work focuses on investigating several critical factors and questions including: (1) what net biogeochemical transformations do nutrients (NO_3^- , NO_2^- , NH_4^+ , DON, DIC, and DOC) undergo as pore water with controlled composition incubates in the STE organic-rich coastal sediment; (2) whether or not organic-rich sediment acts as a source or sink for nutrients, as well as how different loadings of NO_3^- affects biogeochemical reactions; (3) what the fundamental role of carbon is, including carbon production/consumption in addition to the quality of organic matter that regulates the bioavailability of carbon; and (4) what is the age of the organic-rich sediment layer?

I hypothesize that in response to NO_3^- loading the organic-rich sediment would be a source of carbon and reduced nitrogen species and must play a critical role in producing the biogeochemical transformations of nitrogen and OM observed. I suspect that increased NO_3^- loading will produce increased carbon and reduced nitrogen production. Additionally, I hypothesized that the organic-rich sediment layer was buried during the last sea level transgression. Further I suggest that the biogeochemical transformations occurring within the organic-rich sediment layer have an impact at the regional level.

MATERIALS AND METHODS

Site Description

The sediment cores that will be used for this laboratory study were collected at a site located on the eastern shore of Mobile Bay south of Fairhope in Baldwin County in southwestern Alabama, USA. The shallow lithology of the study area consists of a Miocene to Holocene sequence of sand strata interbedded by clay layers (Gillett, Raymond, Moore, & Tew, 2000). Groundwater percolates from inland Baldwin county towards the bay where it ultimately discharges due to the positive regional groundwater gradient (Tew et al., 2018). The organic-rich layer is buried roughly 0.5-2m below the surface throughout the study area within the surficial aquifer unit (Montiel et al. 2018).

Sediment Core Material Collection And Characterization

To examine the biogeochemical transformations occurring in organic-rich sediments, I collected 11 sediment cores (PH-1 through PH11), each ~2m in length, from within the STE from different depths of a coastal site on the southeast shore of Mobile Bay, AL that has been impacted by SGD influenced hypoxia (Montiel, 2018). All cores were recovered from within a 2m² plot of the shoreline using a GeoProbe model 5410 direct push technology (DPT). The sediment cores with the most successful collection, i.e. with visually undisturbed sediment layers and length minimum 150 cm were PH-7 (l=185cm), PH-10 (l=190cm), and PH-11 (l=175cm). Sediment cores PH-7 and PH-11 captured the STE as described in Montiel et al. (2019) and

therefore were selected to be used in laboratory incubations experiments examining the geochemical transformations. Sediment core PH-10 was used for identifying the in-situ sediment conditions, i.e. mineralogical composition, metals composition, hydraulic conductivity, bulk density, porosity, grains size, water content, and sediment $\delta^{15}\text{N}$ - $\delta^{13}\text{C}$. These three cores also had visually well-reproducible stratigraphy and, according to descriptions by Montiel et al. (2019), capture the STE in this coastal site. All three sediment cores were divided into 5-cm sections for further physical and chemical analyses.

Sediment core PH-10 was divided into 38 sections and analyzed for density, porosity, and grain size following methods detailed by Lambe (1951)). Grain size distribution was determined using eight decreasing screen size (2.36-0.053mm) stacked sieves (Fisher Scientific USA standard), and sediment was classified using the Wentworth scale (Wentworth, 1922). Hydraulic conductivities were determined following the Hazen method using the 10th percentile finer grain size in millimeters (Hazen, 1893). Water content was determined following ASTM method D2216-10. Organic matter content was determined following ASTM method 2974-87 via mass differential after combustion in a furnace at 550°C for four hours.

X-ray diffraction (XRD)

To determine the mineralogical composition of the recovered sediment core (PH-10), I examined the sediment fraction of them using the XRD method. The XRD analyses were conducted following a modified method from Cook et al. (1975). Due to the sediment being majority quartz sand, XRD clay slides were created in leu of bulk XRD analysis. Following a method modified from Foos and Quick (1988), sediment was pulverized using an agate mortar and pestle, then suspended in ultra-pure-carbon free water (UPCFW) and allowed to settle

slightly so the heavy materials (i.e. quartz) fell out of suspension according to Stoke's law. The upper layer of the sediment slurry was decanted into a vacuum filter apparatus where it was filtered through 0.45 μ m membranes. The resultant clay film was rolled off the filter membrane and onto a glass slide for XRD analysis via Bruker D8 X-ray diffractometer.

Heavy metal composition

Heavy metal concentrations (reported as mg/kg dry sediment) of PH-10 were assessed using partial (99%) acid digestion of 1g sediment following EPA method 3051A and then analyzed for metal cations using a Perkin-Elmer ICP-OES with a precision of $\pm 4\%$. Sediment samples were weighed, acidified with 10mL concentrated ARISTAR PLUS trace metal grade nitric acid (c.HNO₃), and placed into a microwave digestion unit. After cooling to room temperature, the nitric acid sediment leachate was filtered through 0.45 μ m syringe filters and placed into pre-cleaned centrifuge tubes for instrument analysis.

$\delta^{15}\text{N}$ - $\delta^{13}\text{C}$ assessments in sediments

Sediment samples ranging from 30mg (high organic content) to 300mg (low organic content) from PH-10 were acidified to remove the effect of carbonate (Arens, Jahren, & Kendrick, 2014) and bulk $\delta^{15}\text{N}$ - $\delta^{13}\text{C}$ were measured using a EACF-IRMS system with an Elemental Combustion System (ECS 4010) coupled to a Gas Source-IRMS operating in a continuous flow mode, interfaced with a Finnigan MAT Conflo III at the Alabama Stable Isotope Laboratory (ASIL). The $\delta^{13}\text{C}$ values were calculated relative to Vienna Peedee belemnite (VPDB) with an accuracy of 0.2‰, and the $\delta^{15}\text{N}$ values were calculated relative to the

atmospheric nitrogen (AIR) standard with an accuracy of 0.3%. Carbon and nitrogen weight percent and the C/N ratio were measured using an ECS 4010 thermal conductivity detector.

Radiocarbon analysis

To determine the age of sediment depositions of the shallow layers of the STE, material collected from the sediment within the two cores designated for incubation experiments (i.e. PH-7 and PH-11) was used for radiocarbon analysis. Both cores were examined carefully for carbon-containing pieces such as plant/wood fragments and shells. A total of 13 samples, six from PH-7 and seven from PH-11 were collected (Piotrowska, Blaauw, Mauquoy, & Chambers, 2011). These samples were chosen based on the position within the core and the quantity and quality of the material. All collected samples were within either the upper or lower organic-rich layer. Two bivalve shell fragments were identified in core PH-11, but due to the lack of the entire shell and uncertainty about the species of the shells, those samples were eliminated. The remaining samples contained three wood fragments and six plant fragments collected from cores PH-11 and PH-7. All three wood fragments were well preserved, two were from the upper organic-rich layer, and one was from the lower organic-rich layer. In addition to the wood fragments, the best-preserved plant fragment from the lower organic-rich layer was selected. Samples chosen for radiocarbon analysis that were well preserved and contained abundant carbon consisted of two from the upper organic-rich layer (samples PH7-11 and PH11-11) and two samples from the lower organic-rich layer (samples PH7-22 and PH11-24) (Piotrowska et al., 2011). All samples were inspected under a microscope at 45x magnification and any debris/sediment grains were removed. The samples were then placed into an ultrasonic bath containing ultra-pure carbon-free water for 30 minutes to remove any debris and then put into an oven at 50°C for 48 hours to dry.

Dried and cleaned samples were sent to the National Ocean Sciences Accelerator Mass Spectrometry (NOSA-MS) facility at Woods Hole Oceanographic Institute (WHOI) for radiocarbon analyses.

Incubation Experiments Setup and Porewater Analyses

The overarching goal of this work is to examine the geochemical transformations in pore water of saturated natural sediments from hypoxia-impacted areas under different levels of NO_3^- loadings mimicking different regimes of anthropogenic agricultural impacts. Thus, sediments from cores PH-7 and PH-11 were subsequently incubated with: (1) ultra-pure carbon-free water (UPCFW), (2) groundwater collected from the aquifer near the study site (GW), (3) a-400 μM and (4) a-800 μM NO_3^- amended solution. The UPCFW used for incubations and to make the nitrate solutions was UV treated, 18.2ohm resistance. The GW solution used contained NO_3^- (252 μM), DON (156 μM), and negligible amounts of NH_4^+ and NO_2^- (< 1 μM). The NO_3^- solutions were prepared with >99% ACS grade sodium nitrate (NaNO_3) supplied by Alfa Aesar. After cutting each core in 5-cm sections, there were 35 total samples from PH-11 and 37 from PH-7. These individual sections were placed into pre-baked (organic carbon-free) glass jars labeled by depth. Incubation solutions were brought to anoxic conditions ($\text{DO} < 0.2 \text{ mg/L}$) by bubbling UPC grade argon (or He) through the solutions while within an O_2 -deplete chamber (ODC) that was also previously deoxygenated before inserting the solutions. Before every incubation the jars with sediment in them were allowed to equilibrate with the O_2 -depleted atmosphere within the ODC and then incubated with 120mL of prepared solutions to best represent in-situ conditions (Engström, Dalsgaard, Hulth, & Aller, 2005; Hansen, Thamdrup, & Jorgensen, 2000; Hulth, Aller, & Gilbert, 1999; Martens & Berner, 1974). After the jars

equilibrated and had anoxic solutions added, they were capped and incubated for five days within the ODC. I chose this time of incubation because it is the best representation of groundwater residence time within the STE of the study site (Montiel et al., 2018). The concentration of O₂ within the ODC was monitored continuously using an atmospheric oxygen sensor (Vernier, Accuracy ± 1%) to maintain low oxygen levels (below 2%). After the five-day incubation, while still inside the ODC, 75mL porewater aliquots were withdrawn from each jar using syringes, filtered through 0.45µm syringe filters, and placed into pre-cleaned air-tight 55mL centrifuge tubes. I used this specific amount to satisfy detection limits for the following analyses: 30mL for nutrient analysis (NO₃⁻ + NO₂⁻, NO₂⁻, NH₄⁺, and TN), 10 mL for NO₃⁻ stable isotope analysis (¹⁸O and ¹⁵N), and 35mL for DOC, DOM and total alkalinity (TA) analysis. Aliquots earmarked for TA, DOC and DOM were analyzed as soon as possible after collection, while the rest of the aliquots were frozen for later analysis. Between each treatment, the sediment jars were drained of excess solution, and stored refrigerated (below 4°C) until the next treatment. In total, seven incubations were performed: one GW treatment, duplicate UPCFW treatments, duplicate 400µM NO₃⁻ treatments, and duplicate 800µM NO₃⁻ treatments. All incubations were conducted in the order of lowest to highest NO₃⁻ concentrations (i.e. UPCFW first, followed by GW, then 400µM NO₃⁻ and lastly 800µM NO₃⁻). The same core was used for all treatments discussed in the results and discussion below as of the duplicate analyses, treatments using core PH-7 yielded lowest and better controlled oxygen level throughout the incubation period. Using the same core will allow the data to be more comparable and ensuring that the treatments with the best-controlled oxygen deplete conditions will be most representative of in-situ conditions.

Total alkalinity (TA) and auxiliary parameters

An aliquot from each pore water incubation was collected and analyzed immediately for total alkalinity (TA) as CaCO_3 following Hach method 10239 using a Hach DR1900 spectrophotometer with a precision of $\pm 1.4\text{ppm}$. Sample temperature ($\pm 0.3^\circ\text{C}$), dissolved oxygen (DO) ($\pm 0.2\text{ mg L}^{-1}$), conductivity ($\pm 1\ \mu\text{S cm}^{-1}$), and pH were measured in-situ before collection using a YSI Pro 2030 handheld instrument. Before each use, the instrument was calibrated for DO and pH accuracy following the calibration procedure manual provided by YSI.

Nitrogen speciation

Total Nitrogen (TN), nitrite (NO_2^-), nitrate (as $((\text{NO}_2^- + \text{NO}_3^-) - \text{NO}_2^-)$), and ammonium (NH_4^+) analyses in pore water before and after incubations were conducted by Dauphin Island Sea Lab (DISL) using a Skalar San++ segmented flow autoanalyzer with automatic in-line sample digestion. The analytical error of the instrument was $\pm 5\%$ for all analyses. For this study, I define total dissolved nitrogen (TN) as $\text{DIN} + \text{DON}$, where DIN is measured as $(\text{NO}_3^- + \text{NO}_2^-) + \text{NH}_4^+$ and quantify and qualify DON. Excess nitrogen (N_{ex}) was calculated by subtracting the amount of nitrogen added to the system for each incubation from the total nitrogen measured after incubation completion (Eq. 1). I also accounted for the carried amount NO_3^- from a previous incubation. DON was calculated from the difference of TN and the sum of dissolved inorganic nitrogen species (equation 2).

$$N_{\text{ex}} = TN_{\text{after}} - (N_{\text{added}} + N_{\text{before}}) \quad \text{Eq. (1)}$$

$$DON = TN - \sum \text{DIN} \quad \text{Eq. (2)}$$

Where TN_{before} represents the NO_3^- in porewater carried over from the previous incubation (in μM). This term was calculated by using porosity and bulk density of the sediment to calculate

the volume of water trapped in the pore space between incubations. The porewater volume was multiplied by the TN concentrations measured in μM from the previous incubation to account for TN carried over in the pore spaces to the next incubation. TN_{added} (in μM) represents nitrogen added to the system as NaNO_3 and TN_{after} (in μM) represents the TN measured post five-day treatment.

Nitrate removal

The rate of NO_3^- removal for this study was calculated as the change of NO_3^- in two consecutive sediment sections:

$$R = \frac{AC - (MC - \text{NO}_3^-_{\text{UPCFW}})}{T} \quad \text{Eq. (6)}$$

Where: R= rate of nitrate removal in $\mu\text{M}/\text{hr}$, AC = amendment NO_3^- concentration for each incubation in μM (GW= $252\mu\text{M NO}_3^-$, $400\mu\text{M} = 400\mu\text{M NO}_3^-$, and $800\mu\text{M} = 800\mu\text{M NO}_3^-$), MC = measured NO_3^- concentration for section of core in each incubation in μM , $\text{NO}_3^-_{\text{UPCFW}}$ is the measured NO_3^- concentration in μM for each sample from the UPCFW treatment, and T time (hours).

Dissolved organic carbon (DOC)

DOC in pore water after incubation was measured in the Organic Geochemistry Laboratory at The University of Alabama (UA) following a method described in Lu et al. (2015) using a Shimadzu TOC-V total organic carbon analyzer with an accuracy of $\pm 2\%$.

Dissolved inorganic carbon (DIC)

DIC in pore water after incubation was calculated from TA, salinity, temperature, and pH using R (version 3.6.1) package AquaENV as described by Hofmann et al. (2010). The

AquaENV software was designed for low-salinity (S as low as 0) estuarine applications. Total DIC was calculated as $\sum \text{CO}_2$, and DIC sourced from the remineralization of organic matter was determined following equation 3 (Rao, Malkin, Hidalgo-martinez, & Meysman, 2016; Rao, Malkin, & Meysman, 2014). Percentage DIC from the remineralization of organic matter (% DIC_{OM}) was calculated by subtracting DIC from remineralization of organic matter, from total DIC, then dividing by total DIC and multiplying by 100.

$$\text{DIC}_{\text{OM}} = \text{TotDIC} - \text{TA}(\text{r}_{\text{Ca:TA}}) \quad \text{Eq. (3)}$$

Where DIC_{OM} represents DIC from the remineralization of organic matter in (μM), TotDIC represents total DIC in porewater (μM), and $\text{TA}(\text{r}_{\text{Ca:TA}})$ represents TA corrected for CaCO_3 dissolution in (μM).

$$(\% \text{ DIC}_{\text{OM}}) = \frac{\text{TotDIC} - \text{DIC}_{\text{OM}}}{\text{TotDIC}} * 100 \quad \text{Eq. (4)}$$

Where DIC_{OM} and TotDIC are calculated in μM

Dissolved organic matter (DOM)

DOM absorbance was measured using a UV-1800 Shimadzu spectrophotometer at the Molecular Eco-Geochemistry laboratory at The University of Alabama. To determine DOM quality pre-incubation, sediment from core PH10 was mixed with UPCFW at a ratio of 1:20 by mass. The mixtures were agitated continuously for 42 hours on an orbital shaker at 300 rpm, followed by centrifugation at 4,000 rpm for 20 minutes. The upper liquid layer was carefully transferred to a new vial using a pipette and the leachable DOM in these samples was further analyzed for absorbance and fluorescence properties (i.e., Excitation-Emission Matrix coupled with Parallel Factor Analysis), following the analytical methods described in detail in Lu et al. (2014) and Lu et al. (2015). Porewater samples from the incubation treatments required no pre-

treatment and were analyzed as soon as possible after collection. Briefly, samples were allowed to come to room temperature and were placed in a 1cm pathlength quartz cuvette. Samples high in DOC were diluted using fresh UPCFW so that the optical properties could be accurately recorded. 190 to 670nm wavelengths were scanned at a 1nm interval. Three-dimensional fluorescence excitation-emission matrices (EEMs) were measured using a Horiba Jobin-Yvon FLuoromax-3 spectrofluorometer. Wavelengths 250-520nm were measured at 3nm intervals. The data was then normalized relative to the area under the water Raman peak at excitation wavelength 350nm (Cory & Mcknight, 2005). Parallel factor analysis (PARAFAC) was completed in MATLAB using the DrEEM toolbox to convert the fluorescence spectra into the main identifiable components based on the location of emission and excitation peaks (Stedmon & Bro, 2008). The final models were validated using the split-half analysis (Murphy, Stedmon, Graeber, & Bro, 2013). The relative abundance of each component was determined using equation 5.

$$\%F_{Ci} = F_{Ci} / TF \times 100 = F_{Ci} / (\sum_{i=1}^3 F_{Ci}) \times 100 \quad \text{Eq. (5)}$$

Where F_{Ci} represents the fluorescence intensity and TF represents the total fluorescence intensity.

RESULTS

Sediment Core Stratigraphy and Physical/Chemical Properties

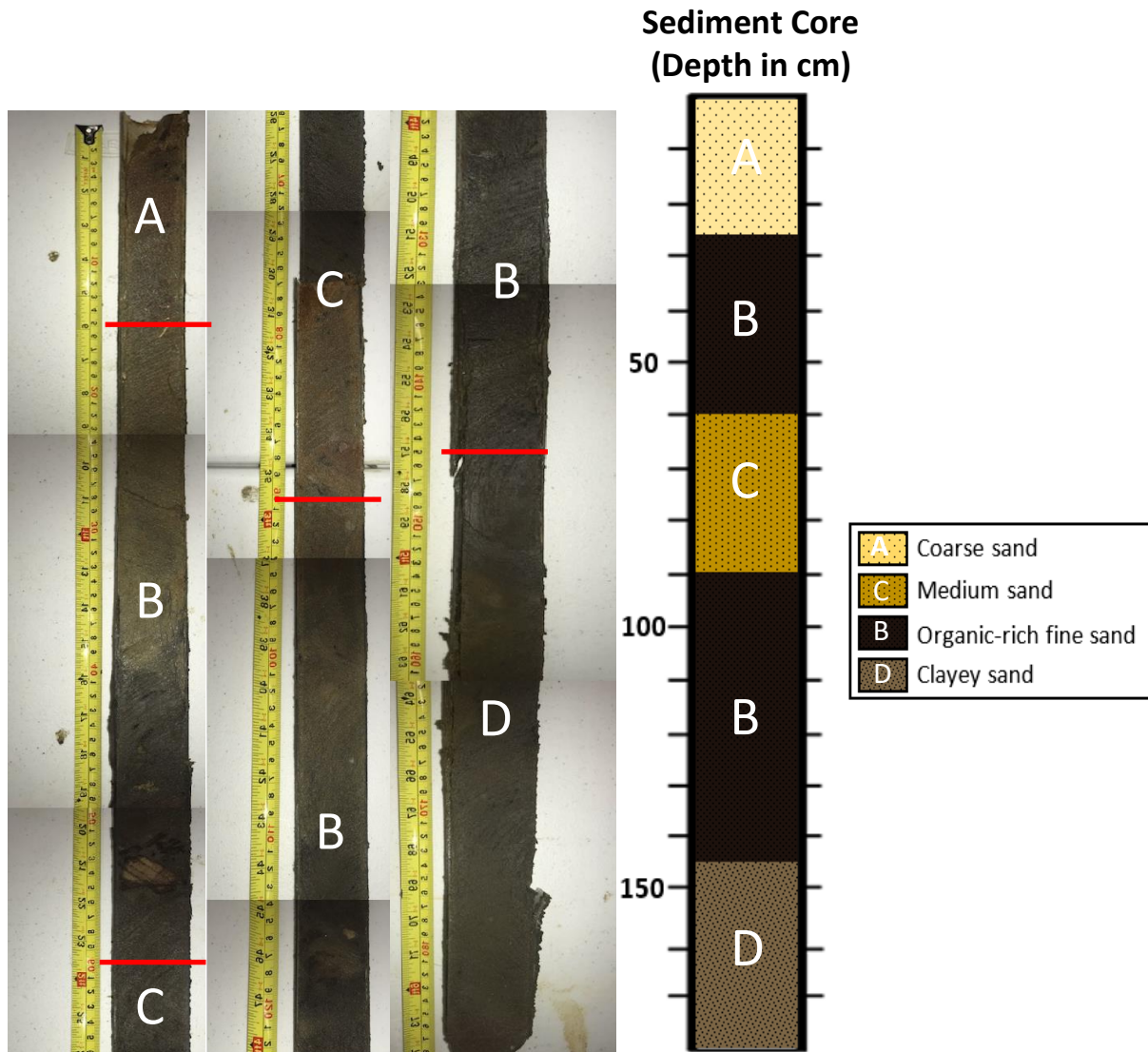


Figure 1: Left: Image of sediment core PH10 with tape measure for reference. Right: Diagram representing stratigraphy and grain size classification of sediment cores used for this study.

The collected cores demonstrate systematic stratigraphy with an uppermost coarse sand layer up to 25cm depth with $2 \pm 1\%$ average organic content followed by the organic-rich layer

discontinuously as a 35cm upper (25-60cm depth) and 55cm lower (90-145cm depth) organic-rich fine sand with a maximum average $22 \pm 3.2\%$ organics content. Between the two sections of high organic content there is a 30cm medium sand layer (60-90cm depth) with $2 \pm 1\%$ average organic content. Beneath the lower organic-rich fine sand section through the remainder of the core is low-organic clayey-sand, with $3 \pm 2\%$ average organic content (Figure 1). Going forward, sediment layers B are what I will refer to as the “organic-rich sediment layer” while sediment layers A, C, and D I collectively refer to as the “lower-organic sediment layer”. Sediment grain size analysis was conducted to determine the D10 grain size for Hazen hydraulic conductivity calculations (Figure 2). Average D10, or the grain size where 10% of sediment grains are smaller, varied by layer with the top coarse sand layer (A) having an average D10 of 0.16mm, and average D10 of 0.13mm within the organic-rich sediment (B), and average D10s of 0.15 and 0.16 in the medium sand layer (C), and clayey-sand layers (D) respectively. The sediment throughout has moderate permeability, with an average hydraulic conductivity $K=1.3 \pm 0.6$ mday^{-1} ($n=20$) in the organic-rich sediment layers, and $K=1.7 \pm 0.6$ mday^{-1} ($n=18$) in the lower-organic layers.

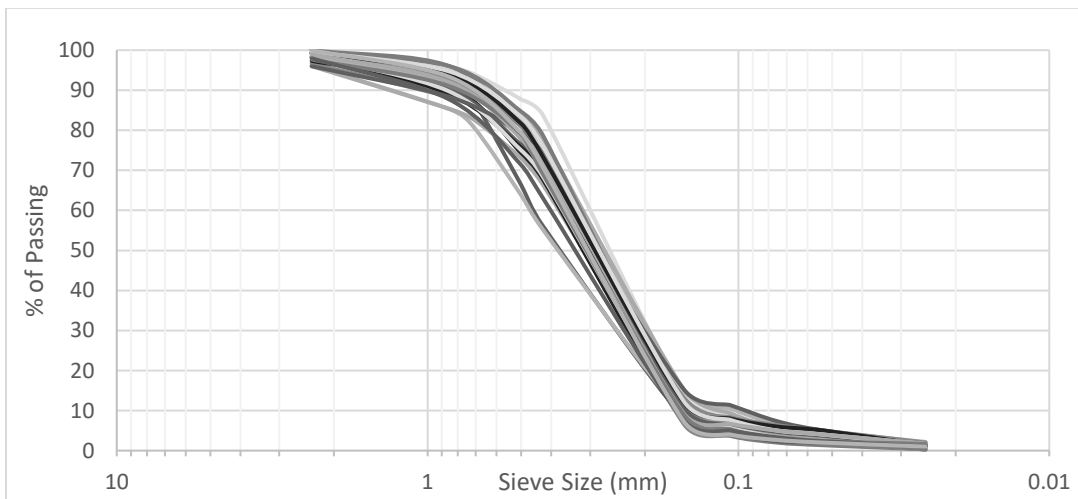


Figure 2: Grain size distribution (in mm) of sediment from core PH10 collected from the STE. Each line represents the grain size distribution for a 5cm section of core.

Mineral composition

Based on the XRD analyses I found that quartz was the mineral that had the highest percentage intensity throughout all samples. Montmorillonite ((Na,Ca)_{0,3}(Al,Mg)₂Si₄O₁₀(OH)₂•n(H₂O)), microcline (KAlSi₃O₈), albite (NaAlSi₃O₈), kaolinite (Al₂Si₂O₅(OH)₄), goethite (Fe³⁺O(OH)), nordstrandite Al(OH)₃, nontronite (Na_{0.3}Fe₂((Si,Al)₄O₁₀)(OH)₂•nH₂O), and glauconite ((K,Na)(Fe³⁺,Al,Mg)₂(Si,Al)₄O₁₀(OH)₂) minerals were all present at up to 20% intensity readings throughout. All of the minerals peaked in intensity between 20 and 40cm depth where OM content was highest, especially kaolinite, nordstrandite, and nontronite which peaked at 51, 74.2, and 16.7%, respectively. Goethite had consistently highest percent intensity, followed by kaolinite and nordstrandite, which had very similar results. See full mineralogical results in Table 2 in Appendix I

Heavy metal concentrations in sediment

The results from ICP-OES analysis of trace and major metals Zn, As, Cd, Cu, Ni, Pb, Sr, V, Cr, Ti, Mn, B, Ca, Al, Fe, Mg, K, and Na did not indicate instances of metals at higher than EPA maximum levels (U.S. EPA, 1993). Of all metals, the ones with the most potential biological impact, Fe and Mn, were present in sediment with average concentrations of 10,979 ± 7256 mg/kg (n=38) and 35 ± 29 mg/kg (n=38), respectively. Fe was the metal measured in the highest concentration throughout sediment core PH10. All metals analyzed had higher average concentrations within the organic-rich sediment sections, with the exceptions of As, B, Cd, Fe, and Ti, where average concentrations were higher in the lower-organic sediment sections. See Table 2 in Appendix I for full metals results.

Sediment $\delta^{13}\text{C}$ and $\delta^{15}\text{N}$ compositions

The C-content in the non-organic-rich sediment averaged $2,900 \pm 1,859$ mgC/kg (n=18) of sediment and over four times higher (avg. $12,656 \pm 15,124$ mg/kg, n=20) within the upper and lower organic-rich layers. The total amount of N in the sediment followed a similar trend as the C where the higher average value, 722 ± 903 mg/kg (n=20), was found within the organic-rich layer. In contrast, average N was lower (202 ± 219 mg/kg (n=18)) in the non-organic-rich layers. The average C/N ratio for the organic layers was 17 ± 3.3 (n=20). The average C/N ratio for the low-organic sediment was 22 ± 5.0 (n=18). Average $\delta^{13}\text{C}$ within the organic-rich layer was $-25.8 \pm 3.3\text{‰}$ and average $\delta^{15}\text{N}$ was $2.16 \pm 1.1\text{‰}$ (n=20). Average $\delta^{13}\text{C}$ within the low-organic sediment was $-24.9 \pm 1.8\text{‰}$ (n=18) and average $\delta^{15}\text{N}$ was $2.6\text{‰} \pm 0.95\text{‰}$ (n=18). See Table 2 in Appendix I for full $\delta^{13}\text{C}$ and $\delta^{15}\text{N}$ results.

Radiocarbon (^{14}C , $t_{1/2}=5,730$ yrs) dating

All but sample PH7-11 from both cores (PH-7 and PH-11) resulted in modern radiocarbon ages, which means they were buried post-1950 (Olsson 1970). ^{14}C ages were calculated following equations 6-8 as described by WHOI NOSAMS. Sample PH7-11 collected from core PH-7 from 55cm depth had a $\Delta^{14}\text{C} = -19.5\text{‰}$ and $\delta^{13}\text{C} = -24.24\text{‰}$ with fraction modern = 0.99 for a radiocarbon age of 90 ± 15 years pre-1950 (buried around 1860). The other sample from core PH-7, sample PH7-22, retrieved from 110cm depth had a $\Delta^{14}\text{C} = 218.65\text{‰}$ and $\delta^{13}\text{C} = -24.44\text{‰}$ with fraction modern = 1.2, meaning deposition was post-1950. Sample PH11-11 retrieved from core PH-11 from 55cm depth had a $\Delta^{14}\text{C} = 59.58\text{‰}$ and $\delta^{13}\text{C} = -26.84\text{‰}$ with fraction modern = 1.1, meaning deposition was post-1950. The other sample from core PH-11,

PH11-24 retrieved from 125cm depth had a $\Delta^{14}\text{C} = 104.1\text{‰}$ and $\delta^{13}\text{C} = -28.08\text{‰}$ with fraction modern = 1.1 meaning deposition occurred post 1950. See Table 2 in Appendix I for full results.

$$Fm_c = Fm - Fm_b \frac{Fm_s - Fm}{Fm_s} \quad \text{Eq. (6)}$$

Fm_c represents the blank corrected fraction modern, Fm_b represents the $^{14}\text{C}/^{12}\text{C}$ ratio of the blank, Fm represents the sample fraction modern, and Fm_s represents the modern reference.

$$Fm_{\delta^{13}\text{C}} = Fm_c * \left(\frac{(1 - \frac{25}{1000})}{(1 + \delta^{13}\text{C}/1000)} \right)^2 \quad \text{Eq. (7)}$$

$Fm_{\delta^{13}\text{C}}$ represents the fraction modern corrected for $\delta^{13}\text{C}$ and Fm_c represents blank corrected fraction modern

$$Age = -8033 \ln (Fm_{\delta^{13}\text{C}}) \quad \text{Eq. (8)}$$

Porewater Composition After Incubations

Dissolved organic nitrogen (DON)

DON was highest in porewater from the 800 μM incubation, followed by 400 μM , GW, and UPCFW incubations (Figure 3 A). In the 800 μM treatment, average DON in porewater retrieved from sediments of the organic-rich layers was 19% lower ($479 \pm 102\mu\text{M}$ (n=20)) than average DON in the lower-organic layers ($570 \pm 73\mu\text{M}$ (n=17)). In the 400 μM incubation, average DON in the organic-rich layers was 7% higher ($200 \pm 56\mu\text{M}$ (n=20)) than average DON in the lower-organic layers ($186 \pm 80\mu\text{M}$ (n=12)). In the GW treatment, average DON in the organic-rich layers was 34% higher ($156 \pm 28\mu\text{M}$ (n=20)) than average DON in porewater retrieved from sediments of the lower-organic layers ($103 \pm 39\mu\text{M}$ (n=17)). In the UPCFW incubation, average DON in the organic-rich layers was 22% higher ($55 \pm 49\mu\text{M}$ (n=20)) than

average DON in the lower-organic layers ($43 \pm 17\mu\text{M}$ ($n=17$)). See Table 1 in Appendix I for full results

Ammonium (NH_4^+)

Ammonium was highest in porewater from UPCFW incubation, followed by $400\mu\text{M}$ treatment, while $800\mu\text{M}$ treatment and GW incubation had similar ammonium results (Figure 3 B). In the $800\mu\text{M}$ incubation, average ammonium in porewater retrieved from sediments of the organic-rich layers was 21% higher ($28 \pm 16\mu\text{M}$ ($n=20$)) than average ammonium in the lower-organic layers ($22 \pm 8\mu\text{M}$ ($n=17$)). In the $400\mu\text{M}$ treatment, average ammonium in the organic-rich layers was 39% higher ($62 \pm 51\mu\text{M}$ ($n=20$)) than average ammonium in porewater retrieved from sediments of the lower-organic layers was ($38 \pm 34\mu\text{M}$ ($n=12$)). In the GW incubation, average ammonium in the organic-rich layers was 23% higher ($31 \pm 9\mu\text{M}$ ($n=20$)) than average ammonium in the lower-organic layers ($24 \pm 15\mu\text{M}$ ($n=17$)). In the UPCFW treatment, average ammonium in porewater retrieved from sediments of the organic-rich layers was 15% higher ($92 \pm 16\mu\text{M}$ ($n=20$)) than average ammonium in the lower-organic layers ($78 \pm 20\mu\text{M}$ ($n=17$)). See Table 1 in Appendix I for full results.

Nitrate (NO_3^-)

Overall, NO_3^- was highest in the incubations with the highest added NO_3^- amendment of $800\mu\text{M}$, followed by the $400\mu\text{M}$, then GW, and UPCFW treatments (Figure 3 C). In the $800\mu\text{M}$ incubation, the average NO_3^- in porewater retrieved from the sediments of the organic-rich layers was 21% lower ($619 \pm 136\mu\text{M}$ ($n=20$)) than the average NO_3^- in the lower-organic layers ($750 \pm 90\mu\text{M}$ ($n=17$)). In the $400\mu\text{M}$ treatment, average NO_3^- in the organic-rich layers was 1% higher

($235 \pm 77\mu\text{M}$ (n=20)) than average NO_3^- in porewater retrieved from sediments of the lower-organic layers ($232 \pm 94\mu\text{M}$ (n=12)). In the GW incubation, the average NO_3^- in the organic-rich layers was 6% lower ($93 \pm 27\mu\text{M}$ (n=20)) than average NO_3^- in the lower-organic layers ($99 \pm 35\mu\text{M}$ (n=17)). In the UPCFW treatment, average NO_3^- in the organic-rich layers was 6% higher ($1.7 \pm 0.7\mu\text{M}$ (n=20)) than average NO_3^- in the lower-organic layers ($1.6 \pm 1\mu\text{M}$ (n=170)). See Table 1 in Appendix I for full results.

Nitrite (NO_2^-)

Nitrite was highest in porewater from the $800\mu\text{M}$ incubation, followed by GW, then $400\mu\text{M}$ and UPCFW incubations (Figure 3 D). In the $800\mu\text{M}$ treatment, average nitrite in porewater retrieved from sediments of the organic-rich layers was 21% higher ($34 \pm 19\mu\text{M}$ (n=20)) than average nitrite in the lower-organic layers ($27 \pm 12\mu\text{M}$ (n=17)). In the $400\mu\text{M}$ incubation, average nitrite in the organic-rich layers was 25% higher ($12 \pm 12\mu\text{M}$ (n=20)) than average nitrite in the lower-organic layers ($9 \pm 10\mu\text{M}$ (n=12)). In the GW treatment, average nitrite in the organic-rich layers was 8% lower ($13 \pm 5\mu\text{M}$ (n=20)) than average nitrite in porewater retrieved from sediments of the lower-organic layers ($14 \pm 6\mu\text{M}$ (n=17)). In the UPCFW incubation, nitrite measured was below $1.7\mu\text{M}$. See Table 1 in Appendix I for full results.

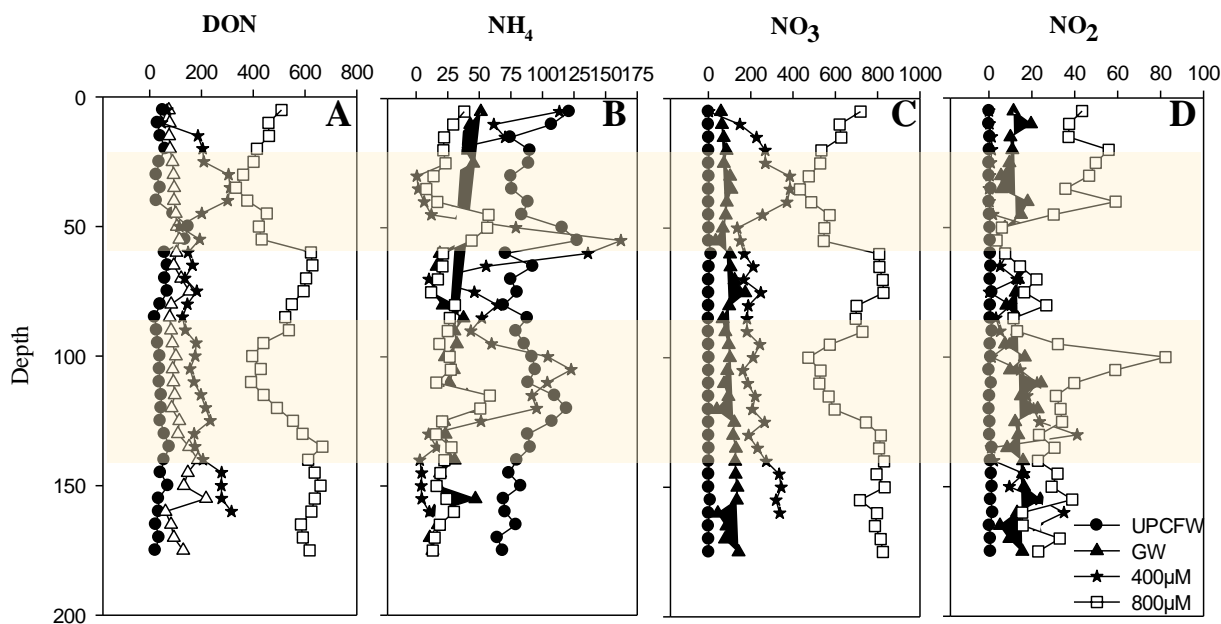


Figure 3: Depth profile (in cm) of (A) DON, (B) NH_4 , (C) NO_3^- , and (D) NO_2^- from the UPCFW, GW, $400\mu\text{M}$ and $800\mu\text{M}$ treatments. Measured in μM . Shaded areas indicate the organic-rich sediment layers

Dissolved organic carbon (DOC)

DOC was highest in porewater from the UPCFW incubation, followed by GW, $800\mu\text{M}$ and $400\mu\text{M}$ incubation (Figure 4). In the $800\mu\text{M}$ treatment, average DOC in the organic-rich layers was 35% higher ($630 \pm 596\mu\text{M}$ ($n=20$)) than average DOC in porewater retrieved from the lower-organic layers ($408 \pm 482\mu\text{M}$ ($n=17$)). In the $400\mu\text{M}$ incubation, average DOC in the organic-rich layers was 37% higher ($187 \pm 199\mu\text{M}$ ($n=20$)) than average DOC in porewater retrieved from sediments in the lower-organic layers ($117 \pm 133\mu\text{M}$ ($n=12$)). In the GW treatment, average DOC in porewater retrieved from sediments in the organic-rich layers was 20% higher ($675 \pm 604\mu\text{M}$ ($n=20$)) than average DOC in the lower-organic layers ($537 \pm 819\mu\text{M}$ ($n=17$)). In the UPCFW incubation, average DOC in the organic-rich layers was 32% higher

($1,102 \pm 801\mu\text{M}$ ($n=20$)) than average DOC in porewater retrieved from sediments in the lower-organic layers ($754 \pm 447\mu\text{M}$ ($n=17$)). See Table 1 in Appendix I for full results.

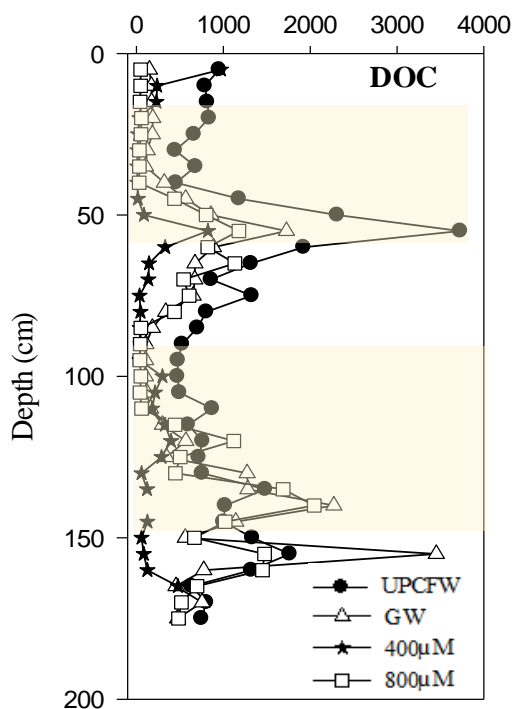


Figure 4: Depth profile (in cm) of DOC from the UPCFW, GW, 400µM, and 800µM treatments, measured in µM. Shaded areas indicate the organic-rich sediment layers

Dissolved inorganic carbon (DIC)

DIC was highest in porewater from the 400µM incubation, followed by UPCFW incubation, while the 800µM and GW incubations had similar results (Figure 5). In the 800µM treatment, average DIC in the organic-rich layers was 20% higher ($649 \pm 347\mu\text{M}$) than average DIC in the lower-organic layers ($518 \pm 297\mu\text{M}$). In the 400µM incubation, average DIC in the organic-rich layers was 38% lower ($2,775 \pm 4,603\mu\text{M}$) than average DIC in porewater retrieved from sediments of the lower-organic layers ($3,809 \pm 3,825\mu\text{M}$). In the GW treatment, average DIC in the organic-rich layers was 17% lower ($606 \pm 256\mu\text{M}$) than average DIC in the lower-organic layers ($712 \pm 458\mu\text{M}$). In the UPCFW incubation, average DIC in porewater retrieved

from sediments of the organic-rich layers was 6% higher ($998 \pm 289\mu\text{M}$) than average DIC in the lower-organic layers ($941 \pm 486\mu\text{M}$). See Table 1 in Appendix I for full results.

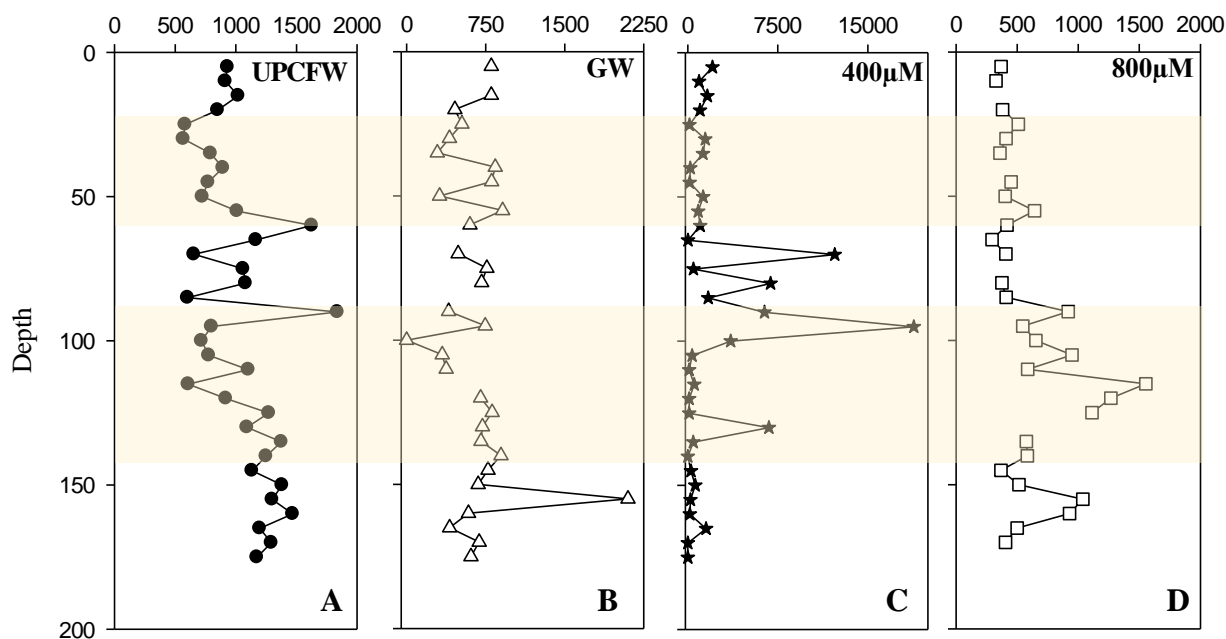


Figure 5: Depth profiles (in cm) of DIC (in μM) from the (A) UPCFW, (B) GW, (C) 400 μM , and (D) 800 μM treatments. Shaded areas indicate the organic-rich sediment layers.

Dissolved organic matter (DOM) quality

Three dominant molecular components of DOM (C1-C3) were found through DOM analysis of porewater at excitation-emission maximum ranges of 285-320nm (C1), <250-421nm (C2), and 270-304nm (C3) (Figure 15). Component 1 corresponds to humic-like terrestrial degradation product organic matter and has been described as complex degradation products from biological activity (D'Andrilli et al. 2019). Component 2 is tannin/phenylalanine protein-like organic compounds, it has been reported as prevalent at low DOC:DON ratios, and has been linked to amino acids produced by phytoplankton, cyanobacteria, bacteria, and algae in stress

conditions that mineralize the original DOM into nutrients (Brogi, Jung, Ha, & Hur, 2019).

Component 3 corresponds to tryptophan/tyrosine protein-like organic compounds and has been described as highly bioavailable, associated with microbial activity, linked to DON. Further, this component was said to occur due to the free release of amino acids that occurs during the breakdown of organic matter (Cawley, 2012; Dalmagro et al., 2019). This component is also found to be enriched in groundwater (Hu et al., 2016).

I found that in the porewater after the incubation with UPCFW, component 2 (i.e. tannin/phenylalanine protein-like DOM) was the primary component with an average intensity of $47 \pm 14\%$ (n=9), component 3 (i.e. tryptophan/tyrosine protein-like DOM) average intensity was $28 \pm 8\%$ (n=9), while component 2 (i.e. humic-like terrestrial DOM) was the least prevalent at an average intensity of $27 \pm 12\%$ (n=9). From the GW incubation, component 2 was the primary component at $40 \pm 8\%$, while component 3 was the second-highest component at $36 \pm 3\%$ (n=11), and lastly, component 1 was least prevalent at $24 \pm 9\%$ (n=11). From the $400\mu\text{M}$ incubation, component 2 was the primary component at $46 \pm 16\%$ (n=10), next component 3 was the second most prevalent component at $35 \pm 10\%$ (n=10), least prevalent was component 1 at $20 \pm 11\%$ (n=10). From $800\mu\text{M}$ incubation, component 3 was the primary component at $40 \pm 4\%$ (n=11), then Component 2 was the second most prevalent component at $37 \pm 4\%$ (n=11), and Component 3 was least prevalent at $22 \pm 6\%$ (n=11). DOM from core PH-10 representing pre-treatment sediment DOM conditions reported highest average intensity from component 2 at $52 \pm 12\%$ (n=38), while component 3 had the second highest average intensity at $32 \pm 9\%$ (n=38), and the average intensity for component 1 was $15 \pm 8\%$ (n=38).

N- And C-Balances In Porewater

Nitrogen excess (N_{ex})

Based on the TN results in porewater prior and after incubations (Eq. 1), I found that N_{ex} was highest in porewater from the 800 μ M incubation, followed by 400 μ M incubation, GW incubation, and UPCFW incubation (Table 1 in Appendix I). In the 800 μ M treatment, the average N_{ex} in the organic-rich layers was 21% lower ($478 \pm 104\mu$ M (n=20)), accounting for an average of 73 ± 5 % of the total nitrogen measured per sample, than average N_{ex} in porewater retrieved from sediments of the low-organic layers was $577 \pm 74\mu$ M (n=17)), accounting for an average of 75 ± 3 % of the total nitrogen measured per sample. The average N_{ex} in the organic-rich layers in the 400 μ M incubation average was 11% higher ($293 \pm 57\mu$ M (n=20)), accounting for an average of 96 ± 0.78 % of the total nitrogen measured per sample, than the average N_{ex} in the low-organic layers ($262 \pm 83\mu$ M (n=12)), accounting for an average of 96 ± 1.5 % of the total nitrogen measured per sample. In the GW treatment, the average N_{ex} in porewater retrieved from sediments of the organic-rich layers was 3% lower ($116 \pm 28\mu$ M (n=20)), accounting for an average of 74 ± 9 % of the total nitrogen measured per sample, than average N_{ex} in the low-organic layers ($119 \pm 47\mu$ M (n=17)), accounting for an average of 79 ± 7 % of the total nitrogen measured per sample. In the UPCFW treatment, average N_{ex} in the organic-rich layers was 28% higher ($61 \pm 43\mu$ M (n=20)), accounting for an average of 45 ± 14 % of the total nitrogen measured per sample, than average N_{ex} in porewater retrieved from sediments of the low-organic layers ($44 \pm 27\mu$ M (n=17)), accounting for an average of 39 ± 18 % of the total nitrogen measured per sample. See Table 1 in Appendix I for full results.

Nitrate removal rates

Nitrate removal (calculated in $\mu\text{M hr}^{-1}$) was highest in porewater from the 800 μM incubation, followed by 400 μM incubation, and then GW incubation (Figure 6). In the 800 μM treatment, average nitrate removal in the organic-rich layers was 13% higher ($1.7 \pm 1.1 \mu\text{M hr}^{-1}$ (n=20)) than average nitrate removal in porewater from sediment in the lower-organic layers ($0.5 \pm 0.7 \mu\text{M hr}^{-1}$ (n=17)). In the 400 μM incubation, average nitrate removal in the organic-rich layers was 60% higher ($1.4 \pm 0.6 \mu\text{M hr}^{-1}$ (n=20)) than average nitrate removal in the lower-organic layers ($1.5 \pm 0.8 \mu\text{M hr}^{-1}$ (n=12)). In the GW treatment, average nitrate removal in the organic-rich layers was 13% higher ($1.4 \pm 0.22 \mu\text{M hr}^{-1}$ (n=20)) than average nitrate removal in porewater from sediment in the lower-organic layers ($1.3 \pm 0.3 \mu\text{M hr}^{-1}$ (n=17)). See Table 1 in Appendix I for full results.

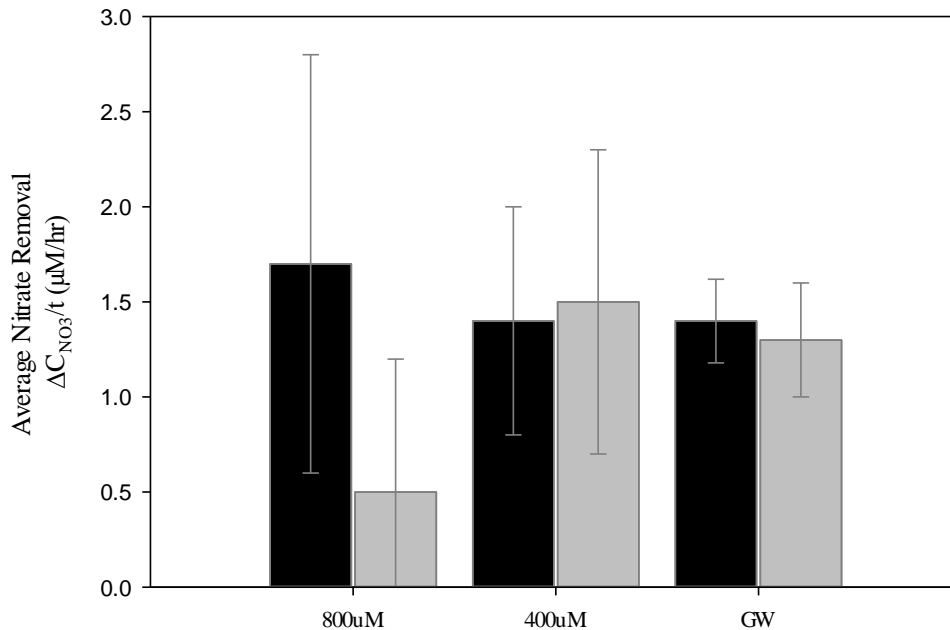


Figure 6: Average nitrate removal rates ($\mu\text{M/hr}$) from the 800 μM , 400 μM , and GW treatments. Dark bars represent averages from the organic-rich layer while light bars represent averages from the lower-organic layers. Error bars represent standard deviation within each treatment.

DIC from remineralization of organic matter (DIC_{OM})

Using equation 3, I calculated the percentage DIC from the mineralization of OM. DIC_{OM} was highest in 400 μ M incubation, followed by 800 μ M incubation, then GW incubation, and lastly by UPCFW incubation (Figure 7). In the 800 μ M incubation, average DIC_{OM} in the organic-rich layers was $90 \pm 1\%$ (n=20) and average DIC_{OM} in the low-organic layers was $90 \pm 1\%$ (n=17). In the 400 μ M incubation, average DIC_{OM} in the organic-rich layers was $94 \pm 0.4\%$ (n=20) and average DIC_{OM} in the low-organic layers was $94 \pm 3\%$ (n=12). In the GW incubation, average DIC_{OM} in the organic-rich layers was $89 \pm 0.5\%$ (n=20) and average DIC_{OM} in the low-organic layers was $89 \pm 1\%$ (n=17). In the UPCFW incubation, average DIC_{OM} in the organic-rich layers was $88 \pm 0.4\%$ (n=20) and average DIC_{OM} in the low-organic layers was $88 \pm 0.39\%$ (n=17). See Table 1 in Appendix I for full results.

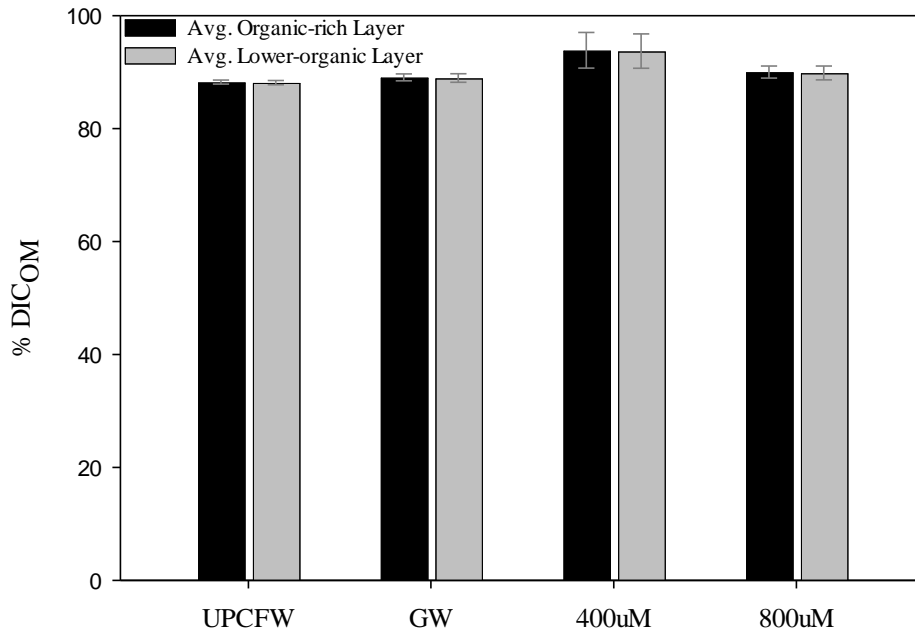


Figure 7: Average percentage DIC from the remineralization of organic matter from the UPCFW, GW, 400 μ M, and 800 μ M treatments. Dark bars represent the organic-rich sediment layers while the light bars represent the lower-organic layers. Error bars represent standard deviation within each treatment.

Calculated DOC and DIC theoretical fluxes entrained by SGD

Using average seasonal groundwater fluxes to Mobile Bay from the southeastern shore during the wet season ($3.8 \pm 1.3 \times 10^5 \text{ m}^3 \text{ day}^{-1}$) and during the dry season ($2.3 \pm 1 \times 10^5 \text{ m}^3 \text{ day}^{-1}$) calculated by Montiel et al. (2018), and the overall average DOC values from these incubation studies (Table 1, Appendix I), I was able to determine the theoretical DOC fluxes to this coastal site that experiences hypoxia. Average DOC fluxes from porewater in sediment in the 800 μM incubation were $127 \pm 128 \text{ mmol day}^{-1}$ during the dry season and $209 \pm 125 \text{ mmol day}^{-1}$ during the wet season (Figure 8 A). Average DOC fluxes from the 400 μM treatment were $42 \pm 51 \text{ mmol day}^{-1}$ during the dry season and $69 \pm 84 \text{ mmol day}^{-1}$ during the wet season. Average DOC fluxes from porewater in sediment in the GW incubation were $146 \pm 159 \text{ mmol day}^{-1}$ during the dry season and $242 \pm 269 \text{ mmol day}^{-1}$ during the wet season. The average DOC fluxes from the UPCFW treatment were $237 \pm 145 \text{ mmol day}^{-1}$ during the dry season and $392 \pm 246 \text{ mmol day}^{-1}$ during the wet season.

Applying the same groundwater fluxes to average DIC measured, I was able to calculate theoretical DIC fluxes (Figure 8 B). Average DIC fluxes from porewater in sediment in the 800 μM treatment was $142 \pm 127 \text{ mmol day}^{-1}$ during the dry season and $234 \pm 125 \text{ mmol day}^{-1}$ during the wet season. The average DIC fluxes from the 400 μM incubation were $740 \pm 955 \text{ mmol day}^{-1}$ during the dry season and $1,223 \pm 1,578 \text{ mmol day}^{-1}$ during the wet season. Average DIC fluxes from porewater in sediment in the GW treatment was $154 \pm 77 \text{ mmol day}^{-1}$ during the dry season and $257 \pm 121 \text{ mmol day}^{-1}$ during the wet season. Average DIC fluxes from the UPCFW incubation was $232 \pm 71 \text{ mmol day}^{-1}$ during the dry season and $385 \pm 115 \text{ mmol day}^{-1}$ during the wet season.

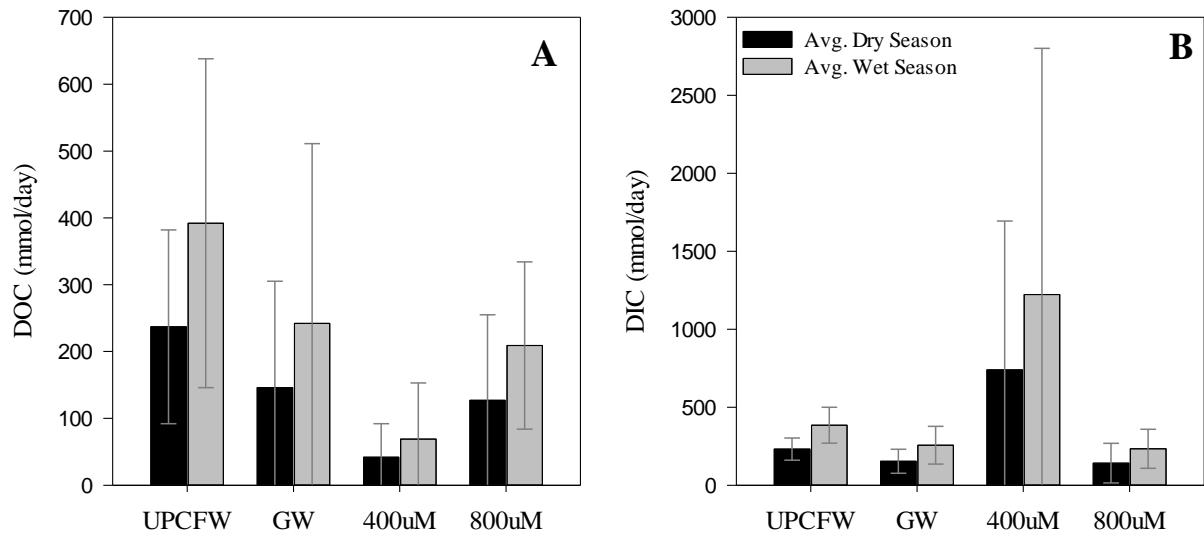


Figure 8: (A) theoretical DOC fluxes entrained by SGD from the UPCFW, GW, 400µM, and 800µM treatments measured in mmol/day. (B) theoretical DIC fluxes entrained by SGD from the UPCFW, GW, 400µM, and 800µM treatments measured in mmol/day. Error bars represent standard deviation within each treatment.

DISCUSSION

Age of Organic-Rich Sediment Layer

I found that the organic-rich layer was buried within the last 160 years. Initially, I hypothesized that the organic-rich sediment layer observed 25-50cm below the surface along the eastern shore of Mobile Bay had been buried during the last sea level transgression about 6000 years ago. However, radiocarbon dating performed on samples from the organic-rich sediment revealed ages as early as modern (buried post 1950), and as old as 90 ± 15 years (buried around 1860) (Table 2, Appendix I).

Theoretical Basis Of N-Biogeochemical Transformations in Organic-Rich Sediments

In an anoxic reducing environment with a high content of OM, which is typical for wetlands and estuaries, N undergoes complex biogeochemical transformations. Each pathway of these transformations can be influenced by a wide variety of environmental factors, including temperature, salinity, dissolved oxygen (DO), substrate availability of nitrate + nitrite ($\text{NO}_3^- + \text{NO}_2^-$), ammonium (NH_4^+), dissolved organic carbon (DOC), and hydrogen sulfide (H_2S) (Cornwell et al., 1999; Dalsgaard et al., 2005; Seitzinger et al., 2006). In an ideal system, there is an order in which electron acceptors are available for organisms to respire OM within the sediment column (Figure 9).

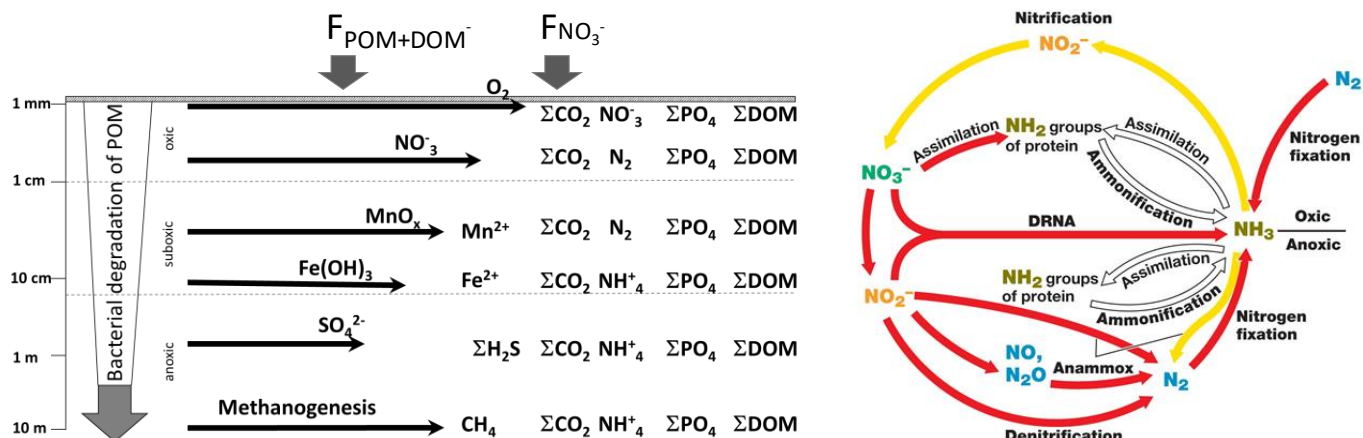


Figure 9: Left diagram depicts the sequence of early diagenetic reactions occurring in surficial sediments (the figure is a compilation of different sources, mostly from Gaillard JF 1999, and Floelich et al., 1979). Fluxes of POM and DOM and anthropogenic nitrate entering the system are indicated on top. The figure on the right shows the N-cycle from Madigan et al. (2017)

In the sequences of diagenetic reactions where NO_3^- is used as the electron acceptor, different bacteria reduce NO_3^- either partially to NO_2^- , or to gaseous N species (NO , N_2O), or completely to N_2 via denitrification. In the process, dissolved organic nitrogen (DON) and carbon (DOC) are released to the environment as a byproduct as well (Sipler & Bronk, 2015). Through their life cycle, microbes utilize C and N in a specific C/N ratio resulting in increased microbial biomass.

If the POM sediment C/N ratio is higher than 30 (i.e. significantly more C than N), then microorganisms prefer nitrogen in the form of NO_3^- (or NH_4^+) from the environment to support their metabolic needs in a process called *assimilatory nitrate reduction* or *immobilization* (Brewer & Brown, 2012; Reuter, Gensel, Elvert, & Zak, 2020). When sediment C/N ratios are below 20 (i.e. C is more limiting or there is an abundance of N), microbial communities degrade OM more completely and release NH_4^+ to the environment through *mineralization of OM* (also called *ammonification*). Therefore, the availability of C and N in the environment dictates microbial activity and, ultimately, the N-pathway transformations as well.

Research conducted near a coastal site impacted by hypoxia in the northern Gulf of Mexico has shown high NO_3^- concentrations in groundwater; however, a more recent study indicated that SGD to Mobile Bay through the STE, has very low NO_3^- fluxes but extremely high NH_4^+ and DON fluxes (Montiel, Lamore, Stewart, & Dimova, 2018; Murgulet & Tick, 2009). Using evidence from sediment core stratigraphic composition and shallow geophysical exploration, it was demonstrated that SGD percolates through organic-rich sediment deposits at these sites. The organic-rich layer previously has been reported as having a maximum organic content of up to 36% and was also identified in the northwest portion of Mobile Bay was also identified (Montiel et al., 2018). However, based on my observations, the shallow organic-rich layer is discontinuous, existing as upper and lower organic-rich layers with maximum organic content of up to 26%. Because shorelines are high energy environments, it is possible that the upper and lower organic-rich layers observed might have been one continuous layer that was potentially disturbed at some point in the past. Similar sediment organic-rich layers (i.e. peat layers) are not uncommon in estuarine systems on the continental shelves worldwide. For example, they have been described in Cape Lookout Bight (North Carolina, USA) by Klump and Martens (2019); in the Pearl River Delta (Guangdong, China) by Jiao et al., (2010); in the Neuse River Estuary (North Carolina, USA) by Null et al., (2011); and on Raratonga Island (Cook Islands) by Erler et al. (2014). It is possible that many estuaries coastlines across the world could have a similar organic-rich layer as well, being that the effects of the last sea level transgression were far reaching.

N Budget Assessments

N production:

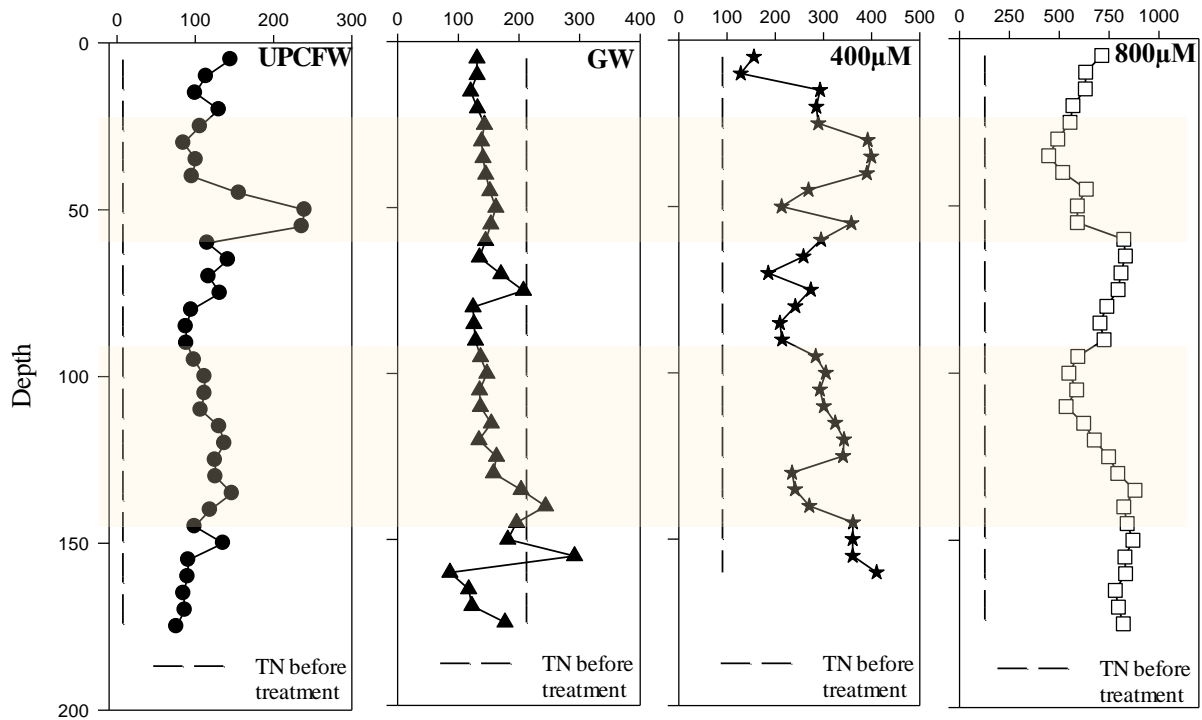


Figure 10: Depth profile (in cm) of dissolved TN from UPCFW treatment (A), GW treatment (B), 400 μM treatment (C), and 400 μM treatment (D) measured in μM . Dashed lines represent TN of the system at the beginning of each treatment. Shaded areas indicate the organic-rich sediment layers.

During this laboratory incubation study, I found that the TN after each incubation was consistently above the level of nitrogen added to the system for all treatments but the GW treatment (Figure 10), suggesting an overall net gain of nitrogen in the dissolved phase. I found that the highest increase was the result of the incubation with UPCFW (>100x), whereas the TN in the incubation with GW was generally lower than the baseline. The GW solution used

contained DON and NO_3^- , making baseline TN higher than the lab prepared solutions with solely NO_3^- -N.

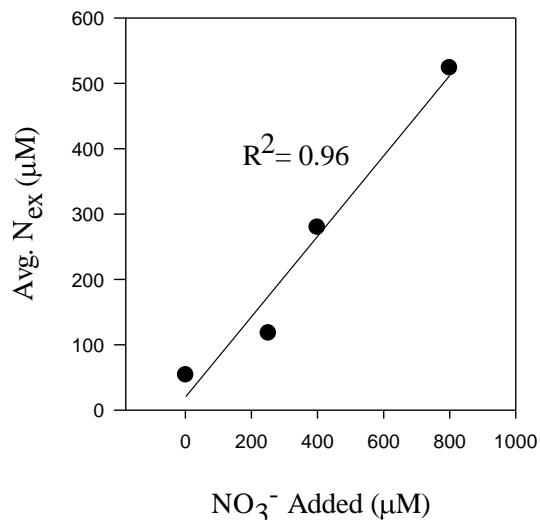


Figure 11: Cross plot N_{ex} (in μM) vs. the amount of NO_3^- added to the incubations (in μM) demonstrating a linear relationship with an $R^2 = 0.96$

Based on these results and using equation 7, I was able to calculate N_{ex} and I found a linear correlation ($R^2=0.96$) between the amount of the added NO_3^- and the average N_{ex} calculated at the end of the incubations (Figure 11). I observed that both N_{ex} and DON follow very similar trends for all experiments during these incubations. When plotted DON versus N_{ex} , I found robust correlations ($R^2=0.83 - 0.91$) from all treatments (Figure 12). These results strongly suggest that the observed N_{ex} in the system is due to extra DON most likely produced from the bacterial transformation and mobilization of sediment organic matter (Blackburn et al. 1996; Burdige and Zheng 1998; Eyre and Ferguson 2002; Cook et al. 2004).

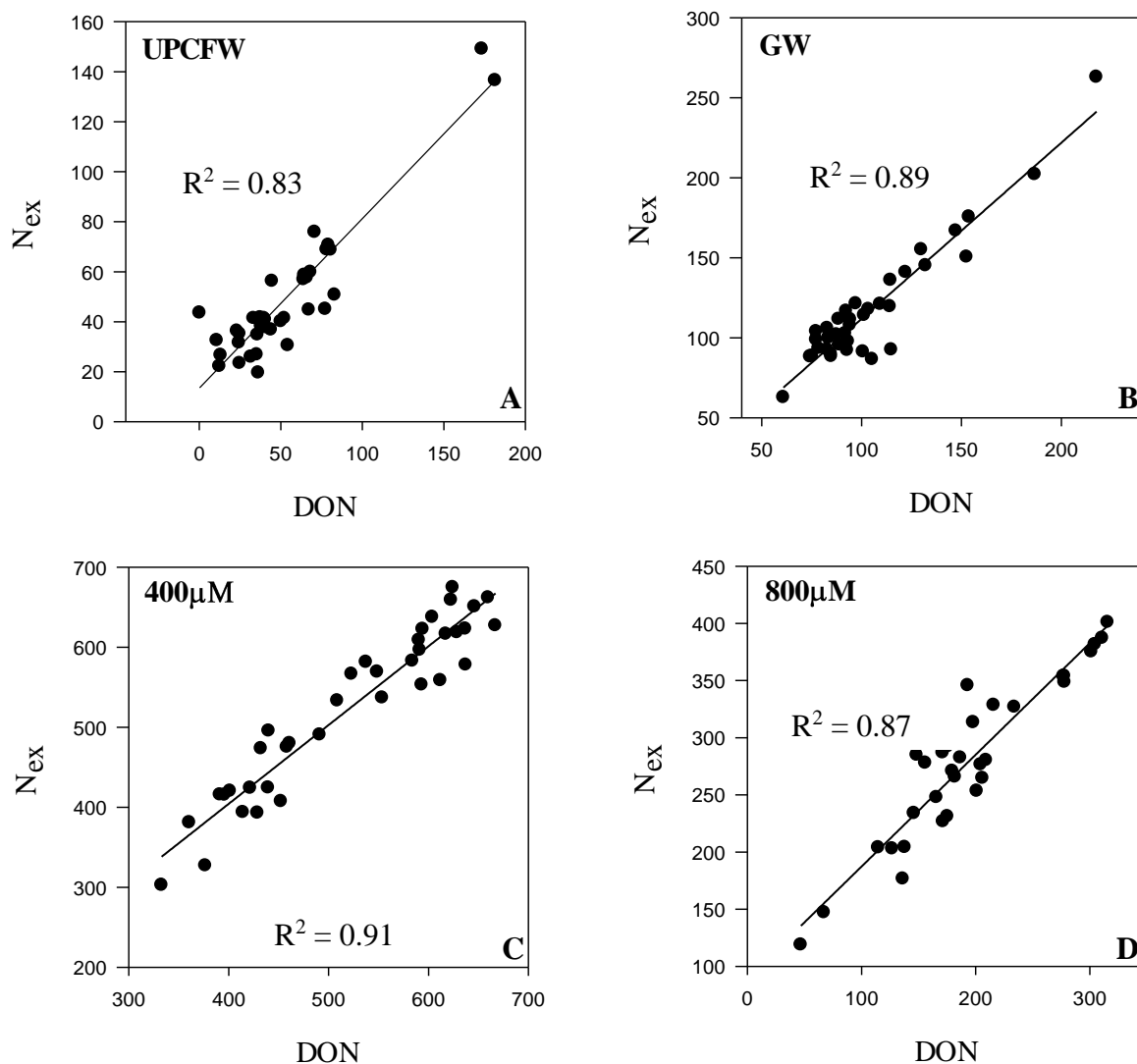


Figure 12: N_{ex} vs. DON in UPCFW treatment (A), N_{ex} vs. DON in GW treatment (B), N_{ex} vs. DON in 800 μM treatment (C), and N_{ex} vs. DON in 400 μM treatment (D). All data is in μM .

There is also a strong correlation between N_{ex} and DOC ($R^2 = 0.61$) during the UPCFW treatment (Figure 13). This could be due to dissolution of DOC and DON during the UPCFW treatment, as it was the first treatment conducted, or potentially that in the absence of NO_3^- the transformation of organic matter/ammonification case is facilitated by different, potentially more easily accessible electron donors (e.g. Fe^{3+} , SO_4^{2-}) as evidenced by the high DIC and %DIC_{OM} from the UPCFW treatment (Figure 9).

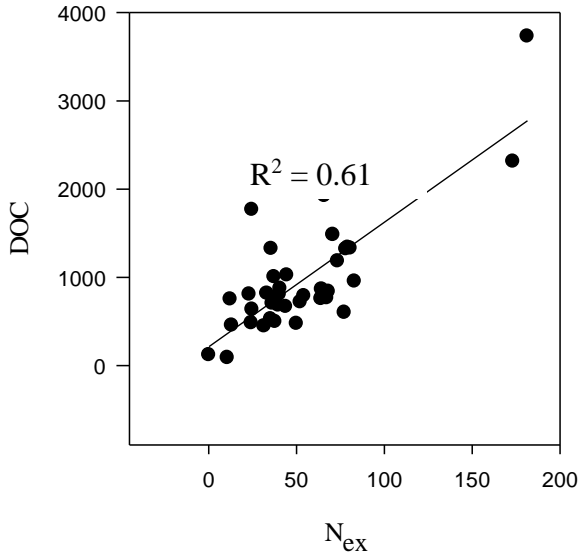


Figure 13: Cross plot N_{ex} (in μM) vs. DOC (in μM) from the UPCFW treatment demonstrating a linear relationship with an $R^2 = 0.61$

Analysis of metals concentrations in the sediment material confirms the presence of Fe in high concentrations (avg. $10,979 \pm 7,255$ mg/kg) and Mn in low concentrations (avg. 35 ± 29 mg/kg) within the sediment leachate. However, these metals are most likely bound to a mineral within its structure. For example, the Fe bearing mineral goethite ($\text{Fe}^{3+}\text{O}(\text{OH})$) was one of the most prevalent minerals aside from quartz identified in the sediment, and it is not uncommon in nature for goethite to accommodate Mn within its structure in place of Fe (Liu et al., 2018). I did not identify any Mn bearing minerals in the sediment and Mn concentrations in sediment leachate were orders of magnitude lower than Fe concentrations. Nevertheless, Fe, Mn, and goethite followed a very similar trend suggesting goethite as the source of Mn and Fe observed, making them biologically unavailable (Figure 14).

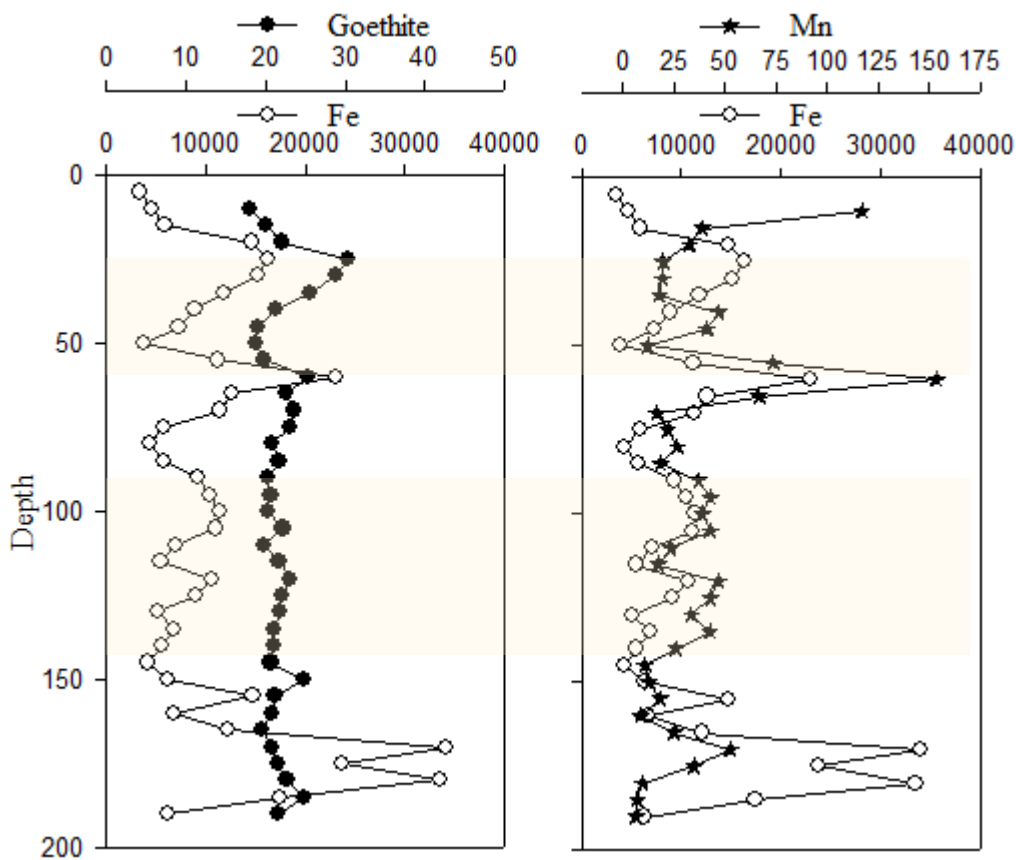


Figure 14: (A) Depth profile (in cm) of the mineral goethite XRD peak intensity in percentage (upper x axis) and Fe concentration in mg/kg of sediment (lower x axis) from ICP-OES metal cations analysis. (B) Depth profile of Fe (lower x axis) and Mn (upper x axis) in in mg/kg of sediment from ICP-OES metal cations analysis. Shaded areas indicate the organic-rich sediment layers.

Nitrate removal pathways and rates

During all incubations, I found a significant decrease (between 15 and 62%) of the total NO_3^- added to the sediment systems. The results from the $800\mu\text{M}$ treatment clearly indicate that the sediment layers with higher organic content remove more NO_3^- compared to the lower-organic matter sections (Figure 3 C). Although a significant decrease of NO_3^- in the pore water after incubations was observed during the treatments, I also found that the added NO_3^- to the system was not removed completely (Figure 3 C). Furthermore, I found that the average total amount of NO_3^- removed from each incubation was very similar. For example, during the GW treatment it

is $156 \pm 15 \mu\text{M}$ ($62 \pm 12\%$), from the $400\mu\text{M}$ treatment, it was $156 \pm 84 \mu\text{M}$ ($39 \pm 20\%$), and during the $800\mu\text{M}$ treatment is $121 \pm 128\mu\text{M}$ ($15 \pm 16\%$). The similar average total amount of NO_3^- removed combined with the incomplete NO_3^- removal (between 15 and 62%) can potentially be the result of short incubation times or NO_3^- saturation. NO_3^- saturation was observed in marsh sediments at concentrations between 70 and $150\mu\text{M}$ NO_3^- (Koop-jakobsen & Giblin, 2010), so NO_3^- saturation during the high NO_3^- treatments is possible. With the current results, I cannot confirm or reject the hypothesis of too short incubation time because I maintained the same incubation times for all treatments.

Using the results from the NO_3^- and the coupled behavior with other measured parameters (e.g. NH_4^+ , NO_2^-), I suggest that the two most likely processes of removal of NO_3^- from the system are primarily denitrification and secondarily DNRA (Figure 9). This hypothesis is supported by the fact that NO_2^- concentrations increased with increasing NO_3^- (Figure 3 D). NO_2^- was measured in all incubations with added NO_3^- , but not in the UPCFW treatment where the measure NO_2^- concentrations were very low (avg. $0.69 \pm 0.49\mu\text{M}$) indicating low rates (or absence) of denitrification. I attributed the NH_4^+ detected in all treatments as a result of the concurrent occurrence of DNRA, which contributes to an additional removal of NO_3^- . However, I suggest that the abundant NH_4^+ detected in this system can also be explained by the process of ammonification. This suggestion is strongly supported by the large excess of NH_4^+ measured from the UPCFW treatment which was carried in the absence of NO_3^- loading, and thus suggests the only source of NH_4^+ is the POM.

To quantify the removal of NO_3^- and be able to compare the efficiency of removal between treatments, I calculated the parameter “nitrate removal rate, R” using equation 6. I found that the NO_3^- removal rates from the $400\mu\text{M}$ and GW incubations on average were similar, yet they did

not differ significantly between the organic-rich (1.4 ± 0.6 and $1.4 \pm 0.22 \mu\text{M hr}^{-1}$, respectively) and lower-organic layers (1.5 ± 0.8 and $1.3 \pm 0.3 \mu\text{M hr}^{-1}$ respectively) (Figure 6). Conversely, I found that the NO_3^- removal rates during the $800\mu\text{M}$ treatment were more than three times higher within the organic-rich layers ($1.7 \pm 1.1\mu\text{M hr}^{-1}$) than within the low-organic sediment ($0.5 \pm 0.7 \mu\text{M hr}^{-1}$) (Figure 6). One potential explanation for the difference between the $800\mu\text{M}$ and the $400\mu\text{M}/\text{GW}$ incubations is the order in which the incubations were conducted. It is possible that readily bioavailable OM in the low-organic layers, where C/N ratios were low even pre-incubation treatments, were consumed before the $800\mu\text{M}$ incubation occurred, thus limiting NO_3^- removal in these sections. I found that higher OM content promotes higher removal rates. In sediment with organic content greater than 5%, the average NO_3^- removal rates were 7% higher in the GW treatment, 16% higher in the $400 \mu\text{M}$ treatment, and 60% higher in the $800\mu\text{M}$ treatment compared to sediment with organic content less than 5%. Increased denitrification in sediments with increasing organic carbon content has also been noted by others (Caffrey, Sloth, Kaspar, & Blackburn, 1993; Pfenning & McMahon, 1996; Saunders & Kalff, 2001).

DOM Compositional Changes and Mineralization Of OM

I identified three unique molecular components of DOM representative of DOM compositional shifts caused by environmental degradation induced by anthropogenic NO_3^- loading. For simplicity, I refer to these components as, Component 1, Component 2 and Component 3 (Figure 15).

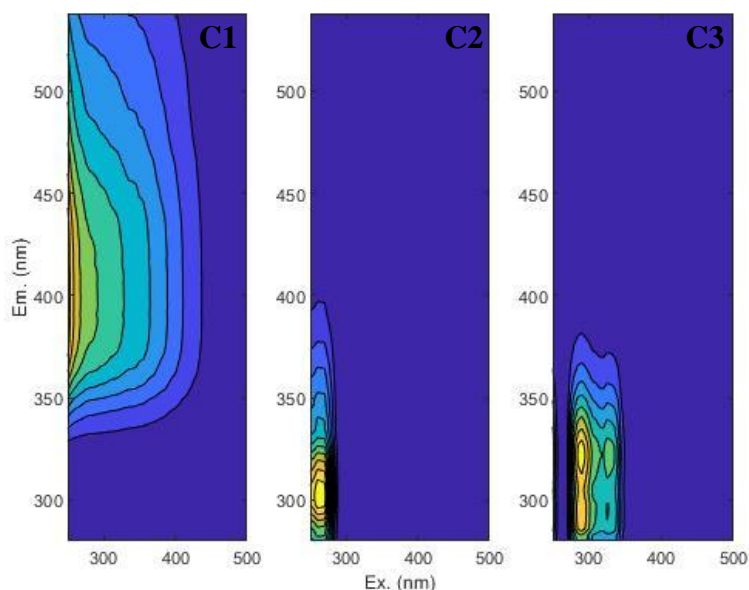


Figure 15: Visual representation of the excitation and emission of (left to right) component 1, component 2, and component 3 from DOM analysis

DOM compositional changes

Based on the trends in component 3 intensity, I suggest that component 3 is most representative of DOM compositional changes caused by anthropogenic NO_3^- loading (Figure 16). It has been linked to DON produced by the degradation of OM by microbial communities that have been observed in areas impacted by anthropogenic NO_3^- loading (Cawley, 2012; Dalmagro et al., 2019). Supporting this hypothesis is the observation that component 3 is most prevalent ($40 \pm 4\%$) from the highest NO_3^- treatment ($800\mu\text{M}$). Also, component 3 intensity is high in pre-treatment sediment (PTS) ($32 \pm 9\%$), indicating that this component is prevalent in the STE sediment right after collection as well. Furthermore, the anthropogenic NO_3^- free UPCFW treatment had the lowest component 3 intensity ($28 \pm 8\%$), which was likely in part residual from the sediment as evidenced by the high PTS component 3 intensity. The natural GW solution used for the incubation, collected from near the study site, also had DON in solution, unlike any other treatment. While I did not analyze the DOM of the GW solution, I suspect the large component 3 percentage intensity from the GW treatment ($36 \pm 3\%$) was due to the DON in the GW solution added to the DON produced during incubation. These findings support that

component 3 is the component most representative of DOM compositional changes caused by anthropogenic NO_3^- loading because it has high intensities in PTS and the treatment most representative of natural conditions (GW), as well as being high (between 35 and 40%) in the high NO_3^- treatments (400 μM and 800 μM).

Mineralization of OM

Based on this study, I strongly suggest that consistent mineralization of OM occurred in all incubations and the degree to which it occurs depended on the amount NO_3^- added to the different treatments. Direct evidence of this was found in the compositional changes of the products of OM. I found that the presence of Component 1 which represents humic-like degradation products or terrestrial OM and its intensity was lowest in PSDOM (15%), while the other treatments reported similar component 1 intensities (between 20 and 25%) (Figure 16). Additional evidence is that I found that the amount of these degradation products of terrestrial organic matter increases with increased OM decomposition. Furthermore, component 1 has also been described as being positively correlated with DON and DOC (Painter et al., 2018), both of which are also products of the transformation and mobilization of sediment OM. As component 1 is produced during times of highest organic matter decomposition, the similar overall presence of this component across all incubations is indicative that generally, organic matter was not a limiting factor in the incubations (D'Andrilli et al., 2019).

The high concentrations of DOC from UPCFW and GW treatments, coupled with the also relatively high NH_4^+ concentrations (Figure 3 B, Figure 4) suggest that the sediment organic matter is indeed the source of NH_4^+ through ammonification in the treatments with the absence of or low NO_3^- conditions. Component 1 which is positively correlated with DOC matched the

DOC trend for all treatments, strongly supporting the terrestrial organic matter degradation by biological activity seen in all incubations (D'Andrilli et al., 2019; Painter et al., 2018).

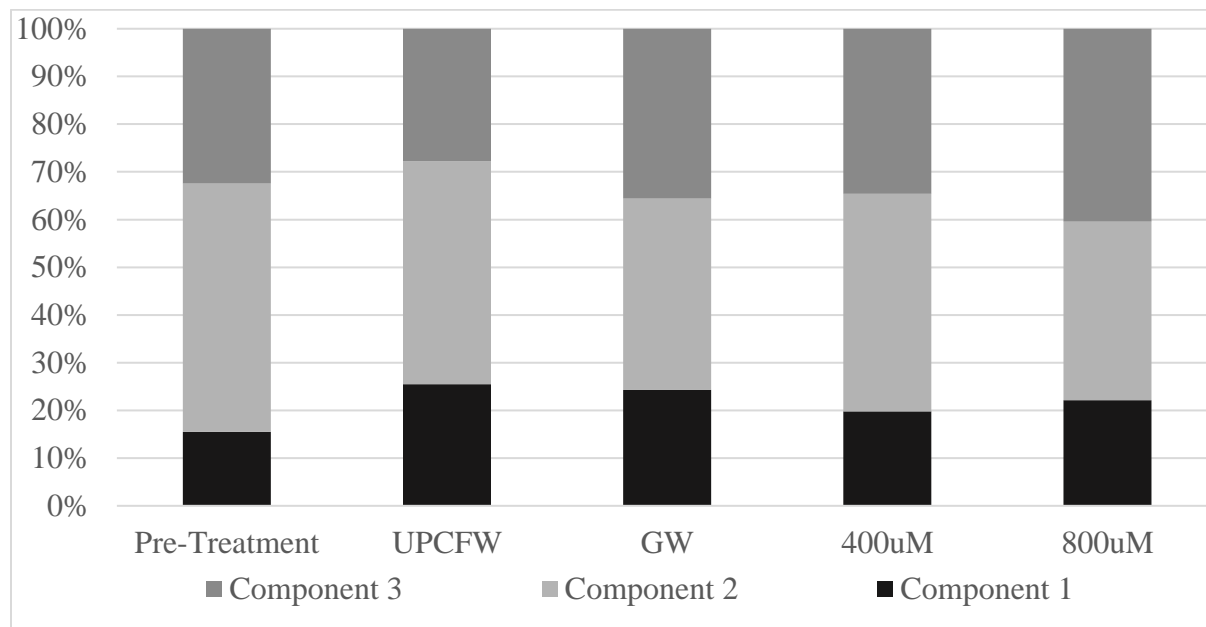


Figure 16: DOM component intensity in porewater after treatment and from pre-treatment sediment (PTS) shaker experiments reported in %.

I found that trends in component 2 intensity further support consistent mineralization of OM and that increasing NO_3^- concentrations created a less stressful environment for the microbial community (Figure 16). Component 2 intensity was highest in PTS and the UPCFW treatment and as NO_3^- concentrations increased, component 2 intensity decreased, suggesting that the microbial community was under less stress because component 2 is protein-like DOM linked to OM produced in-situ by microorganisms under stress conditions that have been linked to high DON concentrations (Brogi et al., 2019; D'Andrilli, Foreman, Sigl, Priscu, & Mcconnell, 2017). Furthermore, component 2 was generally the most prevalent component of all treatments,

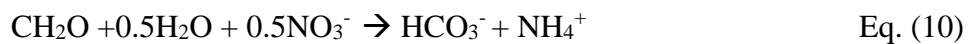
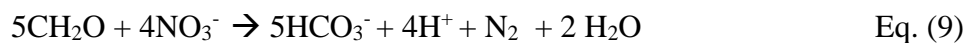
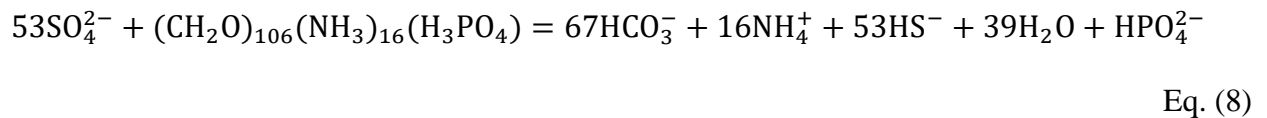
therefore, its large presence reinforces the evidence of consistent mineralization of OM demonstrated by the trends in component 1 intensity.

As additional evidence for the mineralization of OM, I also found significant dissolved carbon (both DIC and DOC) from all treatments; where the incubations with the lowest NO_3^- treatments had the highest DOC (Figure 4). DOC was highest from UPCFW incubation ($990 \pm 619\mu\text{M}$) and was significantly higher than the other treatments suggesting increased mineralization of organic matter. High intensity of DOM component 2 from the UPCFW treatment, representing DOM produced under stress conditions, supports increased DOC production through enhanced OM degradation in the absence of added NO_3^- .

I suggest that some DOC produced during organic matter degradation is also consumed during the incubation period, which could be why DOC was observed as lowest from the $400\mu\text{M}$ and $800\mu\text{M}$ treatments as microbial activity would be highest. This hypothesis is supported by the trends of component 3 intensity, which is produced and consumed in-situ by microorganisms. Since component 3 intensity is generally higher from treatments with higher NO_3^- , this suggests that more DOC produced during degradation of OM could also be consumed (Dalmagro et al., 2019).

I found that DIC decreased with increasing NO_3^- conditions, except for the $400\mu\text{M}$ incubation, and that most of the DIC measured in all incubations (between 88 and 94%) is the result of the remineralization of OM (Figure 17). DIC can be produced as a result of the oxidation of organic matter through several microbially mediated processes, including SO_4^{2-} reduction (Eq. 8), denitrification (Eq. 9) and DNRA (Eq. 10). I found compelling evidence that suggests co-occurrence of SO_4^{2-} reduction during the first three treatments. DIC is unusually high from the $400\mu\text{M}$ incubation, and $94 \pm 2\%$ of the DIC in this incubation is result of the

mineralization of OM. Through the process of POM respiration using SO_4^{2-} as an electron donor, DIC and NH_4^+ are produced (Mucci et al., 2000) (Figure redox sequence). NO_3^- reducing bacteria (NRB) are able to degrade a wider range of OM types including larger polymers, while SRB prefer smaller, less complex organic molecules (Nedwell, 1984). OM that is released by the NO_3^- reduction process may be suitable for SRB and can potentially allow for increased SO_4^{2-} reduction (Laverman, Pallud, Abell, & Cappellen, 2012). Therefore, I believe a significant amount of the high DIC and NH_4^+ in the 400 μM incubation is due to the co-occurrence of SO_4^{2-} reduction (Eq. 8) (Figure 3 B, Figure 5 C) as supported by the large presence of SO_4^{2-} reducing bacteria (SRB) naturally within the STE sediment (Adyasari, Hassenruck, Montiel, & Dimova, 2020). I suggest that SO_4^{2-} reduction increased as NO_3^- concentration increased through the first three treatments, producing the DIC trends seen. SO_4^{2-} reduction was likely highest during the 400 μM treatment due to the high NO_3^- (compared to GW and UPCFW) promoting increased nitrate reduction and OM production, leading to the depletion of SO_4^{2-} in the sediment. DIC was lowest from the 800 μM treatment, likely because SO_4^{2-} was depleted during the 400 μM treatment, eliminating a source of DIC. While SO_4^{2-} was not measured in this study, during the analyses of the porewater samples from these incubations, there was analytical interference in some samples with the suspected cause being SO_4^{2-} presence (DISL Lab pers. comm.), specifically from the first three incubations (UPCFW, GW, and 400 μM).



The results from the 400 μ M treatment showed that the percent of DIC_{OM} generally increases with increasing NO₃⁻ loading (Figure 17). The anomalously high DIC_{OM} in 400 μ M incubation thus could be explained with the co-occurrence of SO₄²⁻ and NO₃⁻ reduction.

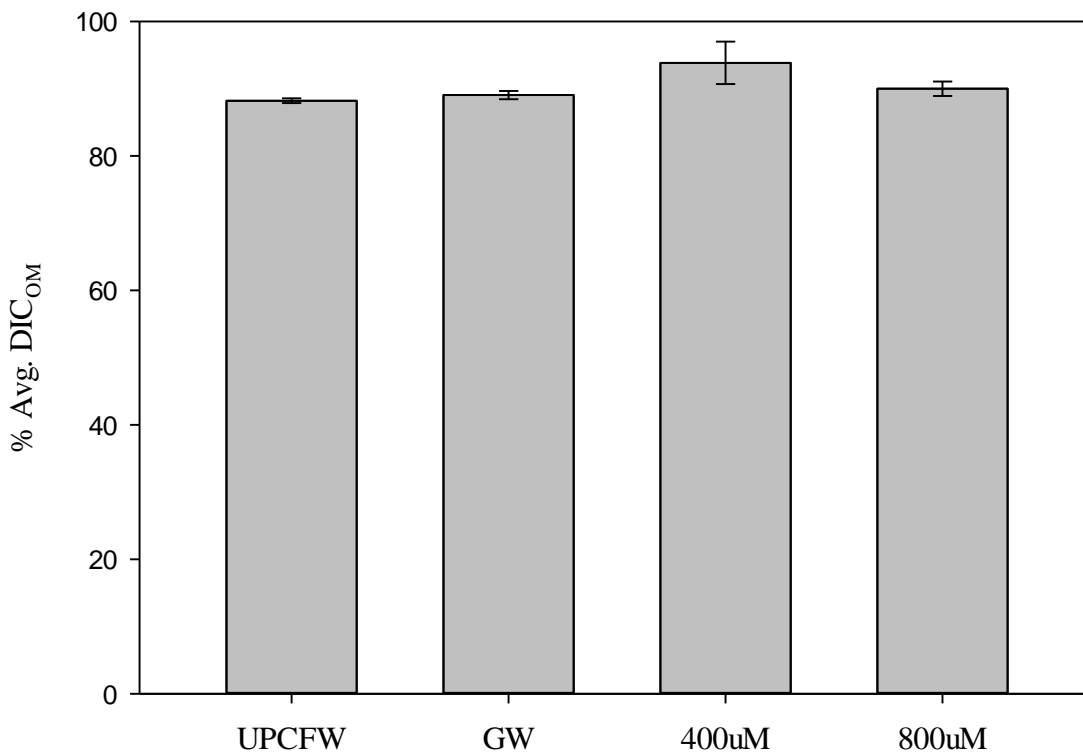


Figure 17: Average % DIC from the remineralization of organic matter from the UPCFW, GW, 400 μ M and 800 μ M treatments

I found high correlation between DON and DOC in porewater from the organic-rich sediment in all treatments but the 400 μ M (UPCFW $R^2 = 0.77$, GW $R^2 = 0.59$, 400 μ M $R^2 = 0.05$ and 800 μ M $R^2 = 0.48$), suggesting that the same processes produce both DON and DOC (Figure 18). DON is a byproduct of the degradation of OM and up to 41% of dissolved inorganic nitrogen uptake is later re-released as DON, according to a study of estuarine phytoplankton

(Bronk, Gilbert, & Ward, 1994). I have already established that N_{ex} (which represents N that's source is not accounted for) is correlated with DON, so the correlations between DON and DOC coupled with the correlations between DON and N_{ex} strongly supports the degradation of soil OM during microbial processes.

However, I did not find a correlation between DON and DOC for the 400 μ M incubation, and the 400 μ M incubation also had the lowest DOC of all the incubations. I suspect the lack of correlation is primarily due to the co-occurrence of SO_4^{2-} reduction during this incubation, which would have increased DOC consumption and produced more DIC as evidenced, explaining the results observed (Laverman et al., 2012).

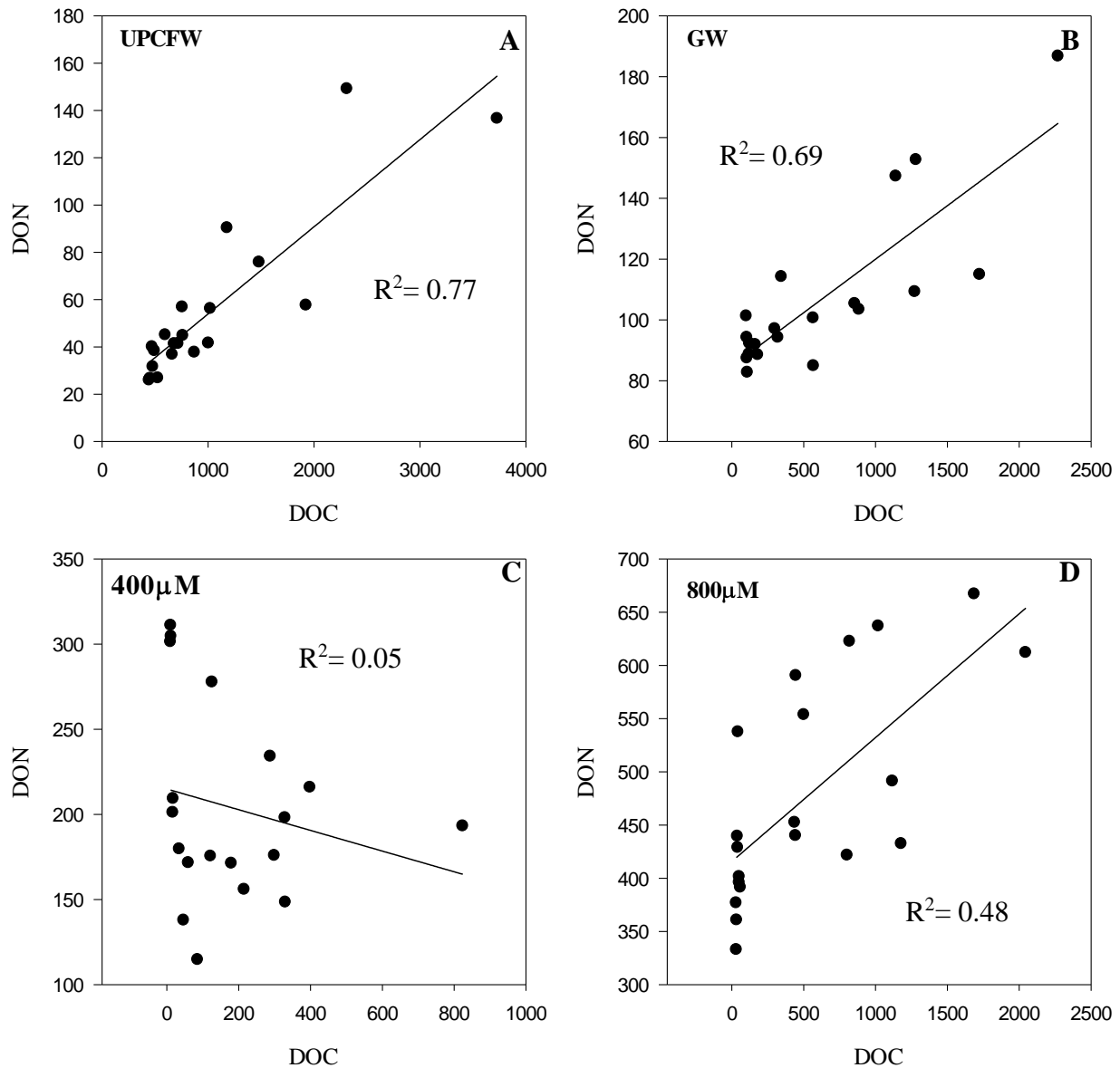


Figure 18: Cross plots of DON vs DOC in porewater from the organic-rich sediment for the (A) UPCFW, (B) GW, (C) 400µM, and (D) 800µM treatments

Hypothetical Effectiveness of Anthropogenic Nitrogen Loading Removal

Using the findings of this study and available nitrogen fertilizer usage data from 2007 for cotton crops in Alabama, I calculated anthropogenic nitrogen removal's theoretical limits by denitrification in organic-rich coastal sediment. Cotton is the second most grown crop in

Alabama and the fifth most grown crop in the county surrounding the study site with 40.7km² of cropland as of 2012 (USDA 2012) and receives an average of 0.15kgN/km² (USDA 2019) of nitrogen fertilizer, so this analysis can help give an understanding of the environments natural ability to attenuate anthropogenic nitrogen loading. Several assumptions were made to complete these calculations: (1) all nitrogen applied to cotton crops was applied as NO₃⁻, (2) all nitrogen that was not consumed by crops was transported away via groundwater, (3) organic matter content is homogeneously distributed across the entire eastern shore, (4) all nitrogen in groundwater in Baldwin County ultimately percolated through the coastal sediment on the eastern shore, (5) NO₃⁻ removal does not occur before reaching the STE.

Globally, only 42-47% of nitrogen added to agricultural lands is utilized by crops and removed as crop products (Zhang, 2017), leaving 53-58% of the nitrogen to be lost to the environment. Denitrification is a crucial process to help mitigate the effects of anthropogenic NO₃⁻ loading. The general chemical reaction is shown in equation 5 (Eljamal, Jinno, & Hosokawa, 2006). Applying a total groundwater seepage area of 3.8x10⁶m² (Montiel et al., 2018) for the eastern shore of Mobile Bay, and average organic matter content within the organic-rich sediment layer, I determined that there is 7.41kg/m² of OM present across the seepage area of the eastern shore. Applying the reaction stoichiometry from equation 5, I was able to determine that 0.6 kg of OM (as CH₂O) per kg of NO₃⁻ is required for denitrification. Theoretically, to denitrify the total amount of NO₃⁻ applied to cotton that is lost to the environment, only 1.94% of the total organic matter across the eastern shore would be consumed. While data was not available for nitrogen fertilizer usage on other crops near the study site, it is safe to assume that there is sufficient OM present to denitrify excess anthropogenic nitrogen sourced from other agriculture as only 1.94% is required for cotton, the fifth most grown crop in Baldwin County. Even

factoring in the generality of these calculations and the assumptions made, it is safe to say that currently, the organic matter present within the STE is capable of mitigating anthropogenic NO_3^- loading, provided enough residence time within the organic-rich sediment in the STE.

CONCLUSION

I found that the organic-rich sediment layer is indeed a source of reduced N, in the form of DON and NH_4^+ , and that higher NO_3^- loading promotes increased DON production, supporting my initial hypothesis. Many biogeochemical transformations occurred including NO_3^- removal, which was observed in all treatments with added NO_3^- and the highest NO_3^- removal rates were observed within the organic rich sediment during the treatment with the highest NO_3^- loading (800 μM treatment), while the lowest NO_3^- removal rates were observed in the lower-organic sediment during the same treatment. All treatments, except the GW treatment, experienced net N production in the form of DON that is produced as a direct result of the mineralization of sediment OM during microbial NO_3^- reduction, DNRA, and likely SO_4^{2-} reduction. I found that both DNRA and denitrification likely occurred, but the dominant pathway of NO_3^- removal was denitrification and average NO_3^- removal rates increased with increased NO_3^- loading. I found that DOC and DIC are both released during mineralization of OM, demonstrating that the biogeochemical transformations occurring in the STE sediment are a source of carbon. Contrary to my hypothesis, the organic-rich sediment layer was not buried during the last sea level transgression, but rather was likely buried within the last century. Applying my findings to the regional scale, I determined that the organic-rich sediment layer along the eastern shore of Mobile Bay has the potential to denitrify significant amounts of anthropogenic NO_3^- , however in the process producing large amounts of NH_4^+ , DON, DOC, and DIC.

REFERENCES

- Adyasari, D., Hassenruck, C., Montiel, D., & Dimova, N. (2020). Microbial community composition across a coastal hydrological system affected by submarine groundwater discharge (SGD). *PLoS ONE*, 1–26. <https://doi.org/10.1371/journal.pone.0235235>
- Aller, R. C. (1994). Bioturbation and remineralization of sedimentary organic matter: effects of redox oscillation. *Chemical Geology*, 114(3–4), 331–345.
- Arens, N. C., Jahren, A. H., & Kendrick, D. C. (2014). Carbon isotope stratigraphy and correlation of plant megafossil localities in the Hell Creek Formation of eastern Montana, USA. *The Geological Society of America*, 503(05), 149–171. [https://doi.org/10.1130/2014.2503\(05\)](https://doi.org/10.1130/2014.2503(05)).
- Beck, A. J., Tsukamoto, Y., Tovar-sanchez, A., Huerta-diaz, M., Bokuniewicz, H. J., & San, S. A. (2007). Importance of geochemical transformations in determining submarine groundwater discharge-derived trace metal and nutrient fluxes. *Applied Geochemistry*, 22, 477–490. <https://doi.org/10.1016/j.apgeochem.2006.10.005>
- Blackburn, T. H., Hall, P. O. J., Hulth, S., & Landen, A. (1996). Organic-N loss by efflux and burial associated with a low efflux of inorganic N and with nitrate assimilation in Arctic sediments (Svalbard, Norway). *Marine Ecology Progress Series*, 141, 283–293.
- Boehm, A. B., Paytan, A., Shellenbarger, G. G., & Davis, K. A. (2006). Composition and flux of groundwater from a California beach aquifer: Implications for nutrient supply to the surf zone. *Continental Shelf Research*, 26, 269–282. <https://doi.org/10.1016/j.csr.2005.11.008>
- Brewer, C. E., & Brown, R. C. (2012). 5.18 Biochar. In *Comprehensive Renewable Energy* (pp. 357–384). Elsevier.
- Brogi, S. R., Jung, J. Y., Ha, S.-Y., & Hur, J. (2019). Seasonal differences in dissolved organic matter properties and sources in an Arctic fjord: Implications for future conditions. *Science of the Total Environment*, 694, 133740. <https://doi.org/10.1016/j.scitotenv.2019.133740>
- Bronk, D. A., Gilbert, P. M., & Ward, B. B. (1994). Nitrogen Uptake, Dissolved Organic Nitrogen Release, and New Production. *Science*, 265(5180), 1843–1846.
- Burdige, D. J., & Zheng, S. (1998). The biogeochemical cycling of dissolved organic nitrogen in estuarine sediments. *Limnology and Oceanography*, 43, 1796–1813.

- Burford, J. R., & Bremner, J. M. (1975). RELATIONSHIPS BETWEEN THE DENITRIFICATION CAPACITIES OF SOILS AND TOTAL , WATER-SOLUBLE AND READILY DECOMPOSABLE SOIL ORGANIC MATTER. *Soil Biology Biochemistry*, 7, 389–394.
- Caffrey, J. M., Sloth, N. P., Kaspar, H. F., & Blackburn, T. H. (1993). Effect of organic loading on nitrification and denitrification in a marine sediment microcosm. *FEMS Microbiology Ecology*, 12, 159–167.
- Cawley, K. M. (2012). Characterising the sources and fate of dissolved organic matter in Shark Bay , Australia : a preliminary study using optical properties and stable carbon isotopes. *Marine and Freshwater Research*, 63, 1098–1107.
- Charette, M. A., & Sholkovitz, E. R. (2002). Oxidative precipitation of groundwater-derived ferrous iron in the subterranean estuary of a coastal bay. *Geophysical Research Letters*, 29(10), 1–4.
- Charette, M. A., Sholkovitz, E. R., & Hansel, C. M. (2005). Trace element cycling in a subterranean estuary: Part 1. Geochemistry of the permeable sediments. *Geochimica et Cosmochimica Acta*, 69(8), 2095–2109.
- Cook, H. E., Johnson, P. D., Matti, J. C., & Zemmels, I. (1975). *METHODS OF SAMPLE PREPARATION AND X-RAY DIFFRACTION DATA ANALYSIS, X-RAY MINERALOGY LABORATORY, DEEP SEA DRILLING PROJECT, UNIVERSITY OF CALIFORNIA, RIVERSIDE*.
- Cook, P. L. M., Eyre, B. D., Leeming, R., & Butler, E. C. V. (2004). Benthic Fluxes of nitrogen in the tidal reaches of a turbid, high-nitrate sub-tropical river. *Estuarine Coastal and Shelf Science*, 59, 675–685.
- Cory, R. M., & Mcknight, D. M. (2005). Fluorescence Spectroscopy Reveals Ubiquitous Presence of Oxidized and Reduced Quinones in Dissolved Organic Matter. *Environmental Science and Technology*, 39(21), 8142–8149. <https://doi.org/10.1021/es0506962>
- Couturier, M., Tommi-morin, G., Sirois, M., Rao, A., & Nozais, C. (2017). Nitrogen transformations along a shallow subterranean estuary. *Biogeosciences*, 14, 3321–3336.
- D’Andrilli, J., Foreman, C. M., Sigl, M., Priscu, J. C., & Mcconnell, J. R. (2017). A 21 000-year record of fluorescent organic matter markers in the WAIS Divide ice core. *Climate of the Past*, 13, 533–544. <https://doi.org/10.5194/cp-13-533-2017>
- D’Andrilli, J., Junker, J. R., Foreman, C. M., Smith, H. J., & Scholl, E. A. (2019). DOM composition alters ecosystem function during microbial processing of isolated sources. *Biogeochemistry*, 142(2), 281–298. <https://doi.org/10.1007/s10533-018-00534-5>

- Dalmagro, H. J., Lathuilli, M. J., Sallo, F. S., Guerreiro, M. F., Jr, O. B. P., Arruda, P. H. Z. De, ... Johnson, M. S. (2019). Streams with Riparian Forest Buffers versus Impoundments Differ in Discharge and DOM Characteristics for Pasture Catchments in Southern Amazonia. *Water*, *11*(390), 1–20. <https://doi.org/10.3390/w11020390>
- Dybas, C. L. (2005). Dead Zones Spreading in World Oceans. *BioScience*, *55*(7), 552–557.
- Eljamal, O., Jinno, K., & Hosokawa, T. (2006). Denitrification of Secondary Wastewater Using Sawdust. *Memoirs of the Facults of Engineering, Kyushu University*, *66*(2), 115–128.
- Engström, P. I. A., Dalsgaard, T., Hulth, S. H., & Aller, R. C. (2005). Anaerobic ammonium oxidation by nitrite (anammox): Implications for N₂ production in. *Geochemica et Cosmochemica Acta*, *69*(8), 2057–2065. <https://doi.org/10.1016/j.gca.2004.09.032>
- Erler, D. V, Santos, I. R., Zhang, Y., Tait, D. R., Befus, K. M., Hidden, A., ... Eyre, B. D. (2014). Nitrogen transformations within a tropical subterranean estuary. *Marine Chemistry*, *164*, 38–47. <https://doi.org/10.1016/j.marchem.2014.05.008>
- Eyre, B. D., & Ferguson, A. J. P. (2002). Comparison of carbon production and decomposition , benthic nutrient fluxes and denitrification in seagrass , phytoplankton , benthic microalgae- and macroalgae- dominated warm-temperate Australian lagoons. *Marine Ecology Progress*, *229*, 43–59.
- Fennel, K., & Testa, J. M. (2019). Biogeochemical Controls on Coastal Hypoxia. *Annual Review of Marine Science*, *11*, 105–129.
- Foos, A. M., & Quick, T. J. (1988). Preparation of oriented clay mounts with uniform thickness for XRD analysis. *Geoscience World*, 759–760.
- Gillett, B., Raymond, D. E., Moore, J. D., & Tew, B. H. (2000). *HYDROGEOLOGY AND VULNERABILITY TO CONTAMINATION OF MAJOR AQUIFERS IN ALABAMA : AREA 13*. Tuscaloosa, AL.
- Gray, J. S., Wu, R. S. S., & Ying, Y. O. (2002). Effects of hypoxia and organic enrichment on the coastal marine environment. *Marine Ecology Progress Series*, *238*, 249–279. <https://doi.org/10.3354/meps238249>
- Hansen, J. W., Thamdrup, B., & Jorgensen, B. (2000). Anoxic incubation of sediment in gas-tight plastic bags: a method for biogeochemical process studies. *Marine Ecology*, *208*, 273–282.
- Hays, R. L., & Ullman, W. J. (2007). Dissolved Nutrient Fluxes through a Sandy Estuarine Beachface (Cape Henlopen , Delaware , U . S . A .): Contributions from Fresh Groundwater Discharge , Seawater Recycling , and Diagenesis. *Estuaries and Coasts*, *30*(4), 710–724.

- Ho, P., Joon, M., Howden, S. D., & Shiller, A. M. (2019). Temporal and spatial distributions of nutrients and trace elements (Ba , Cs , Cr , Fe , Mn , Mo , U , V and Re) in Mississippi coastal waters : In fl uence of hypoxia , submarine groundwater discharge , and episodic events. *Continental Shelf Research*, 175(December 2018), 53–69. <https://doi.org/10.1016/j.csr.2019.01.013>
- Hofmann, A. F., Soetaert, K., Middelburg, J. J., & Meysman, F. J. R. (2010). AquaEnv : An Aqua tic Acid – Base Modelling Env ironment in R. *Aquatic Geochemistry*, 16, 507–546. <https://doi.org/10.1007/s10498-009-9084-1>
- Hu, Y., Lu, Y., Edmonds, J. W., Liu, C., Wang, S., Das, O., ... Zheng, C. (2016). Hydrological and land use control of watershed exports of dissolved organic matter in a large arid river basin in northwestern China. *Journal of Geophysical Research: Biogeosciences*, 466–478. <https://doi.org/10.1002/2015JG003082>.Received
- Hulth, S., Aller, Ro. C., & Gilbert, F. (1999). Coupled anoxic nitrification / manganese reduction in marine sediments. *Geochemica et Cosmochemica Acta*, 63(1), 49–66.
- Ingrid U. Olsson. (1970). The use of Oxalic acid as a Standard. In *Radiocarbon Variations and Absolute Chronology: Proceedings of the 12th Nobel Symposium* (p. 17). New York: John Wiley & Sons.
- Jiao, J. J., Wang, Y., Cherry, J. A., Wang, X., & Wen, D. (2010). Abnormally High Ammonium of Natural Origin in a Coastal Aquifer-Aquitard System in the Pearl River Delta , China. *Environmental Science and Technology*, 44(19), 7470–7475.
- Kim, T.-H., Waska, H., Kwon, E., Suryaputra, I. G. N., & Kim, G. (2012). Production, degradation, and flux of dissolved organic matter in the subterranean estuary of a large tidal flat. *Marine Chemistry*, 142–144, 1–10.
- Klump, J. V., & Martens, C. S. (2019). Biogeochemical cycling in an organic rich coastal marine basin — II . Nutrient sediment-water exchange processes Biogeochemical cycling in an organic rich coastal marine basin-II . Nutrient sediment-water exchange processes. *Geochemica et Cosmochemica Acta*, 45(June), 101–121. [https://doi.org/10.1016/0016-7037\(81\)90267-2](https://doi.org/10.1016/0016-7037(81)90267-2)
- Knee, K. L., & Jordan, T. E. (2013). Spatial Distribution of Dissolved Radon in the Choptank River and Its Tributaries : Implications for Groundwater Discharge and Nitrate Inputs. *Estuaries and Coasts*, 36, 1237–1252. <https://doi.org/10.1007/s12237-013-9619-y>
- Koop-jakobsen, K., & Giblin, A. E. (2010). The effect of increased nitrate loading on nitrate reduction via denitrification and DNRA in salt marsh sediments. *Limnology and Oceanography*, 55(2), 789–802.
- Kroeger, K. D., & Charette, M. A. (2008). Nitrogen biogeochemistry of submarine groundwater discharge. *Limnology and Oceanography*, 53(3), 1025–1039.

- Kroeger, K. D., Cole, M. L., & Valiela, I. (2006). Groundwater-transported dissolved organic nitrogen exports from coastal watersheds. *Limnology and Oceanography*, 51(5), 2248–2261.
- Lambe, T. W. (1951). *Soil Testing for Engineers*. (T. W. Lambe & R. V. Whitman, Eds.). New York: John Wiley & Sons.
- Laverman, A. M., Pallud, C., Abell, J., & Cappellen, P. Van. (2012). Comparative survey of potential nitrate and sulfate reduction rates in aquatic sediments. *Geochemica et Cosmochemica Acta*, 77, 474–488. <https://doi.org/10.1016/j.gca.2011.10.033>
- Liu, H., Lu, X., Li, M., Zhang, L., Pan, C., Zhang, R., & Li, J. (2018). Structural Incorporation of Manganese into Goethite and Its Enhancement of Pb (II) Adsorption. *Environmental Science and Technology*, 52, 4719–4727. <https://doi.org/10.1021/acs.est.7b05612>
- Loesch, H. (1960). Sporadic Mass Shoreward Migrations of Demersal Fish and Crustaceans in Mobile Bay , Alabama. *Ecology*, 41(2), 292–298.
- Lu, Y., Edmonds, J. W., Yamashita, Y., Zhou, B., Jaegge, A., & Baxley, M. (2015). Spatial variation in the origin and reactivity of dissolved organic matter in Oregon-Washington coastal waters. *Ocean Dynamics*, 65, 17–32. <https://doi.org/10.1007/s10236-014-0793-7>
- Madigan, M. T., Martinko, J. M., Bender, K. S., Buckey, D. H., & Stahl, D. A. (2017). Redox cycle for nitrogen. In *Brock Biology of Microorganisms* (14th ed., p. 661). Pearson.
- Martens, C. S., & Berner, R. A. (1974). Methane Production in the Interstitial Waters of Sulfate-Depleted Marine Sediments Author (s): Christopher S . Martens and Robert A . Berner Published by : American Association for the Advancement of Science Stable URL : <https://www.jstor.org/stable/173>. *Science*, 185(4157), 1167–1169.
- Mccooy, C. A., & Corbett, D. R. (2009). Review of submarine groundwater discharge (SGD) in coastal zones of the Southeast and Gulf Coast regions of the United States with management implications. *Journal of Environmental Management*, 90(1), 644–651. <https://doi.org/10.1016/j.jenvman.2008.03.002>
- Montiel, D. (2018). *Comparing the Magnitude and Mechanisms of Submarine Groundwater Discharge (SGE) and Associated Fluxes in Estuaries and Coastal Karst Systems: The Examples of Mobile Bay (USA) and Maro-Cerro Gordo (Spain)*. The University of Alabama.
- Montiel, D., Lamore, A., Stewart, J., & Dimova, N. (2018). Is Submarine Groundwater Discharge (SGD) Important for the Historical Fish Kills and Harmful Algal Bloom Events of Mobile Bay ? *Estuaries and Coasts*, 1–24.
- Montiel, D., Lamore, A., Stewart, J., Lambert, J., Honeck, J., Lu, Y., ... Dimova, N. (2019). Natural groundwater nutrient fluxes exceed anthropogenic inputs in an ecologically impacted estuary. Lessons learned from Mobile Bay, Alabama. *Biogeochemistry*, 145, 1–33. <https://doi.org/https://doi.org/10.1007/s10533-019-00587-0>

- Moore, W. S. (1999). The subterranean estuary : a reaction zone of ground water and sea water. *Marine Chemistry*, 65, 111–125.
- Mucci, A., Sundby, B., Gehlen, M., Arakaki, T., Zhong, S., & Silverberg, N. (2000). The fate of carbon in continental shelf sediments of eastern Canada : a case study. *Deep-Sea Research II*, 47, 733–760.
- Murgulet, D., & Tick, G. R. (2009). Assessing the extent and sources of nitrate contamination in the aquifer system of southern Baldwin County, Alabama. *Environmental Geology*, 58(5), 1051–1065. <https://doi.org/10.1007/s00254-008-1585-5>
- Murphy, K. R., Stedmon, C. A., Graeber, D., & Bro, R. (2013). Fluorescence spectroscopy and multi-way techniques. PARAFAC. *Analytical Methods*, 5(23). <https://doi.org/10.1039/c3ay41160e>
- Nedwell, D. B. (1984). The Input and Mineralization of Organic Carbon in Anaerobic Aquatic Sediments. *Advances in Microbial Ecology*, 7, 93–131.
- Null, K. A., Corbett, D. R., Demaster, D. J., Burkholder, J. M., Thomas, C. J., & Reed, R. E. (2011). Estuarine , Coastal and Shelf Science Porewater advection of ammonium into the Neuse River Estuary, North Carolina, USA. *Estuarine, Coastal and Shelf Science*, 95(2–3), 314–325. <https://doi.org/10.1016/j.ecss.2011.09.016>
- Null, K. A., Dimova, N. T., Knee, K. L., Esser, B. K., Swarzenski, P. W., Singleton, M. J., ... Paytan, A. (2012). Submarine Groundwater Discharge-Derived Nutrient Loads to San Francisco Bay : Implications to Future Ecosystem Changes. *Estuaries and Coasts*, 35, 1299–1315. <https://doi.org/10.1007/s12237-012-9526-7>
- Osterman, L. E., Poore, R. Z., Swarzenski, P. W., Senn, D. B., & Dimarco, S. F. (2009). The 20th-century development and expansion of Louisiana shelf hypoxia , Gulf of Mexico. *Geo-Marine Letters*, 29, 405–414. <https://doi.org/10.1007/s00367-009-0158-2>
- Painter, S. C., Lapworth, D. J., Woodward, E. M. S., Kroeger, S., Evans, C. D., Mayor, D. J., & Sanders, R. J. (2018). Science of the Total Environment Terrestrial dissolved organic matter distribution in the North Sea. *Science of the Total Environment*, 630, 630–647. <https://doi.org/10.1016/j.scitotenv.2018.02.237>
- Peterson, R. N., Moore, W. S., Chappel, S. L., Viso, R. F., Libes, S. M., & Peterson, L. E. (2016). A new perspective on coastal hypoxia : The role of saline groundwater. *Marine Chemistry*, 179, 1–11. <https://doi.org/10.1016/j.marchem.2015.12.005>
- Pfenning, K. S., & McMahon, P. B. (1996). Effect of nitrate, organic carbon, and temperature on potential denitrification rates in nitrate-rich riverbed sediments. *Journal of Hydrology*, 187, 283–295.
- Piotrowska, N., Blaauw, M., Mauquoy, D., & Chambers, F. M. (2011). Constructing deposition chronologies for peat deposits using radiocarbon dating. *Mires and Peat*, 7(10), 1–14.

- Rabalais, N. N., & Turner, R. E. (2001). *Gulf of Mexico Hypoxia*. Washington, DC: American Geophysical Union.
- Rao, A. M. F., Malkin, S. Y., Hidalgo-martinez, S., & Meysman, F. J. R. (2016). ScienceDirect The impact of electrogenic sulfide oxidation on elemental cycling and solute fluxes in coastal sediment. *Geochemica et Cosmochemica Acta*, *172*, 265–286. <https://doi.org/10.1016/j.gca.2015.09.014>
- Rao, A. M. F., Malkin, S. Y., & Meysman, F. J. R. (2014). Estuarine , Coastal and Shelf Science Alkalinity production in intertidal sands intensi fi ed by lugworm bioirrigation. *Estuarine, Coastal and Shelf Science*, *148*, 36–47. <https://doi.org/10.1016/j.ecss.2014.06.006>
- Reuter, H., Gensel, J., Elvert, M., & Zak, D. (2020). Evidence for preferential protein depolymerization in wetland soils in response to external nitrogen availability provided by a novel FTIR routine. *Biogeosciences*, *17*, 499–514.
- Rocha, C., Ibanhez, J., & Leote, C. (2009). Benthic nitrate biogeochemistry affected by tidal modulation of Submarine Groundwater Discharge (SGD) through a sandy beach face , Ria Formosa , Southwestern Iberia. *Marine Chemistry*, *115*(1–2), 43–58. <https://doi.org/10.1016/j.marchem.2009.06.003>
- Sáenz, J. P., Hopmans, E. C., Rogers, D., Henderson, P. B., Charette, M. A., Schouten, S., ... Eglinton, T. I. (2012). Distribution of anaerobic ammonia-oxidizing bacteria in a subterranean estuary. *Marine Chemistry*, *136–137*, 7–13. <https://doi.org/10.1016/j.marchem.2012.04.004>
- Santoro, A. E. (2010). Microbial nitrogen cycling at the saltwater – freshwater interface. *Hydrogeology Journal*, *18*, 187–202. <https://doi.org/10.1007/s10040-009-0526-z>
- Santos, I. R., Burnett, W. C., Chanton, J., Mwashote, B., Suryaputra, I. G. N. A., & Dittmar, T. (2008). Nutrient biogeochemistry in a Gulf of Mexico subterranean estuary and groundwater- derived fluxes to the coastal ocean. *Limnology and Oceanography*, *53*(2), 705–718.
- Santos, I. R., Eyre, B. D., & Huettel, M. (2012). The driving forces of porewater and groundwater fl ow in permeable coastal sediments : A review. *Estuarine, Coastal and Shelf Science*, *98*. <https://doi.org/10.1016/j.ecss.2011.10.024>
- Saunders, D. ., & Kalff, J. (2001). Denitrification rates in the sediments of Lake Memphremagog, Canada–USA. *Water Research*, *35*(8), 1897–1904.
- Sipler, R. E., & Bronk, B. A. (2015). Dynamics of dissolved organic nitrogen, in: Biogeochemistry of marine dissolved organic matter. In *Biogeochemistry of Marine Dissolved Organic Matter (Second Edition)* (pp. 127–232). Academic Press.
- Slomp, C. P., & Cappellen, P. Van. (2004). Nutrient inputs to the coastal ocean through submarine groundwater discharge: controls and potential impact. *Journal of Hydrology*, *295*(1–4), 64–86.

- Song, J., Luo, Y. M., Zhao, Q. G., & Christie, P. (2003). Novel use of soil moisture samplers for studies on anaerobic ammonium fluxes across lake sediment – water interfaces. *Chemosphere*, *50*, 711–715.
- Stedmon, C. A., & Bro, R. (2008). Characterizing dissolved organic matter fluorescence with parallel factor analysis : a tutorial. *Limnology and OCEANOGRAPHY: METHODS*, *6*, 572–579.
- Sundby, B. (2006). Transient state diagenesis in continental margin muds. *Marine Chemistry*, *102*(1–2), 2–12. <https://doi.org/10.1016/j.marchem.2005.09.016>
- Tew, B. H., Cook, M. R., O’Neil, P. E., Durrough-Pritchard, J., Ponta, G. M., Hinson, A. S., & Reynolds, A. L. (2018). *ASSESSMENT OF GROUNDWATER RESOURCES IN ALABAMA 2010-2016*. Tuscaloosa, AL.
- Windom, H. L., Moore, W. S., Niencheski, L. F. H., & Jahnke, R. A. (2006). Submarine groundwater discharge : A large , previously unrecognized source of dissolved iron to the South Atlantic Ocean, *102*, 252–266. <https://doi.org/10.1016/j.marchem.2006.06.016>
- Zhang, X. (2017). A plan for efficient use of nitrogen fertilizers. *Nature*, *543*, 322–323.

APPENDIX I

Table 1: Results from incubations

| Treatment | Sample ID | Depth | NO ₂ ⁻ | NH ₄ ⁺ | NO ₃ ⁻ | DON | N _{ex} | NO ₃ ⁻ removal | DOC | TA | DIC | DIC _{OM} | C1 | C2 | C3 |
|-----------|-----------|-------|------------------------------|------------------------------|------------------------------|-------|-----------------|--------------------------------------|--------|--------|--------|-------------------|------|------|------|
| | | | μM | | | | | μM/hr | μM | | | % | | | |
| UPCFW | PH7-1 | 5 | 0.2 | 121.3 | 0.6 | 50.7 | 422.6 | | 951.7 | 851.3 | 931.2 | 89.0 | | | |
| | PH7-2 | 10 | 0.0 | 107.3 | 0.4 | 30.5 | 254.2 | | 787.1 | 880.2 | 913.2 | 88.4 | | | |
| | PH7-3 | 15 | 0.5 | 74.7 | 2.3 | 41.3 | 344.4 | | 814.8 | 975.2 | 1019.8 | 88.5 | | | |
| | PH7-4 | 20 | 0.3 | 90.1 | 1.7 | 59.8 | 498.4 | | 836.7 | 804.3 | 851.0 | 88.7 | | | |
| | PH7-5 | 25 | 0.0 | 89.0 | 1.2 | 36.8 | 306.9 | | 663.8 | 555.5 | 580.8 | 88.5 | | | |
| | PH7-6 | 30 | 0.1 | 75.1 | 2.9 | 25.9 | 216.2 | | 444.8 | 532.5 | 566.1 | 88.7 | | | |
| | PH7-7 | 35 | 1.0 | 75.8 | 1.1 | 41.3 | 344.3 | | 680.1 | 738.4 | 790.4 | 88.8 | | | |
| | PH7-8 | 40 | 0.1 | 88.6 | 1.2 | 26.7 | 222.2 | | 454.3 | 906.2 | 894.5 | 87.8 | 18.5 | 47.7 | 33.8 |
| | PH7-9 | 45 | 0.3 | 83.7 | 2.0 | 90.4 | 753.0 | | 1180.8 | 724.4 | 770.0 | 88.7 | | | |
| | PH7-10 | 50 | 0.6 | 115.8 | 2.9 | 149.1 | 1242.6 | | 2310.8 | 719.4 | 722.8 | 88.1 | | | |
| | PH7-11 | 55 | 0.6 | 127.7 | 2.0 | 136.5 | 1137.6 | | 3728.3 | 980.1 | 1009.7 | 88.4 | 39.9 | 29.9 | 30.2 |
| | PH7-12 | 60 | 0.7 | 70.8 | 12.8 | 57.6 | 480.2 | | 1924.2 | 1623.6 | 1625.7 | 88.0 | | | |
| | PH7-13 | 65 | 0.9 | 92.4 | 3.4 | 68.9 | 574.1 | | 1318.3 | 1180.0 | 1165.7 | 87.9 | | | |
| | PH7-14 | 70 | 0.6 | 75.0 | 0.9 | 58.6 | 488.4 | | 860.0 | 661.4 | 654.9 | 87.9 | | | |
| | PH7-15 | 75 | 1.4 | 80.0 | 1.5 | 68.7 | 572.3 | | 1327.5 | 1062.1 | 1060.1 | 88.0 | 17.9 | 51.4 | 30.7 |
| | PH7-16 | 80 | 0.7 | 69.1 | 1.2 | 40.8 | 340.4 | | 804.8 | 1083.1 | 1080.0 | 88.0 | | | |

| | | | | | | | | | | | | | |
|--------|-----|-----|-------|-----|------|-------|--------|--------|--------|------|------|------|------|
| PH7-17 | 85 | 0.6 | 88.0 | 0.4 | 19.6 | 163.2 | 701.8 | 603.5 | 600.9 | 87.9 | | | |
| PH7-18 | 90 | 1.6 | 79.0 | 0.6 | 26.9 | 223.9 | 526.2 | 1817.4 | 1836.6 | 88.1 | 17.1 | 73.8 | 9.1 |
| PH7-19 | 95 | 0.6 | 85.6 | 1.4 | 31.6 | 263.4 | 478.8 | 787.3 | 798.5 | 88.2 | | | |
| PH7-20 | 100 | 0.9 | 91.7 | 2.6 | 40.0 | 333.6 | 472.9 | 725.4 | 717.1 | 87.9 | | | |
| PH7-21 | 105 | 0.1 | 94.4 | 1.8 | 38.4 | 319.9 | 494.6 | 709.4 | 776.1 | 89.0 | 14.6 | 65.5 | 19.8 |
| PH7-22 | 110 | 1.2 | 88.6 | 1.0 | 37.7 | 314.5 | 871.7 | 1038.1 | 1102.0 | 88.7 | | | |
| PH7-23 | 115 | 0.4 | 109.6 | 1.3 | 45.1 | 375.5 | 596.7 | 587.5 | 606.9 | 88.4 | | | |
| PH7-24 | 120 | 0.2 | 119.1 | 0.8 | 44.8 | 373.1 | 762.5 | 879.2 | 917.8 | 88.5 | 21.8 | 45.7 | 32.5 |
| PH7-25 | 125 | 0.5 | 107.5 | 1.4 | 41.4 | 344.6 | 717.3 | 1255.9 | 1271.4 | 88.1 | | | |
| PH7-26 | 130 | 0.4 | 88.4 | 1.8 | 56.8 | 473.7 | 756.2 | 1071.1 | 1091.6 | 88.2 | | | |
| PH7-27 | 135 | 1.4 | 90.4 | 2.6 | 75.8 | 631.9 | 1481.7 | 1378.8 | 1376.1 | 88.0 | 30.2 | 36.6 | 33.2 |
| PH7-28 | 140 | 0.7 | 79.8 | 2.3 | 56.2 | 468.2 | 1021.7 | 1238.9 | 1250.3 | 88.1 | | | |
| PH7-29 | 145 | 1.1 | 73.5 | 1.2 | 41.6 | 346.9 | 1003.3 | 1140.0 | 1133.1 | 87.9 | 32.3 | 35.2 | 32.6 |
| PH7-30 | 150 | 1.5 | 82.9 | 1.4 | 70.6 | 588.7 | 1335.8 | 1421.8 | 1380.7 | 87.6 | | | |
| PH7-31 | 155 | 0.8 | 69.2 | 9.8 | 35.1 | 292.8 | 1765.0 | 1320.9 | 1300.2 | 87.8 | | | |
| PH7-32 | 160 | 1.8 | 70.5 | 1.0 | 34.7 | 289.2 | 1323.3 | 1464.7 | 1468.7 | 88.0 | | | |
| PH7-33 | 165 | 0.2 | 79.1 | 0.9 | 23.3 | 194.5 | 633.9 | 1194.0 | 1196.5 | 88.0 | 37.1 | 35.2 | 27.7 |
| PH7-34 | 170 | 0.7 | 64.3 | 1.4 | 36.3 | 302.7 | 804.8 | 1282.9 | 1293.5 | 88.1 | | | |
| PH7-35 | 175 | 0.8 | 68.5 | 2.1 | 22.1 | 184.3 | 749.2 | 1112.0 | 1174.2 | 88.6 | | | |
| PH7-36 | 180 | 1.8 | 59.8 | 3.2 | 32.5 | 271.0 | 804.8 | 1413.8 | 1398.5 | 87.9 | | | |
| PH7-37 | 185 | 0.3 | 32.5 | 3.3 | 43.5 | 362.7 | 749.2 | 1336.8 | 1328.5 | 87.9 | | | |

GW

| Sample ID | Depth | NO ₂ ⁻ | NH ₄ ⁺ | NO ₃ ⁻ | DON | N _{ex} | NO ₃ ⁻ removal | DOC | TA | DIC | DIC _{OM} | C1 | C2 | C3 |
|-----------|-------|------------------------------|------------------------------|------------------------------|------|-----------------|--------------------------------------|-------|-------|-------|-------------------|------|------|------|
| | | μM | | | | | μM/hr | μM | | | % | | | |
| PH7-1B | 5 | 11.4 | 51.2 | 58.7 | 74.2 | 88.3 | 1.6 | 149.5 | 708.4 | 803.2 | 89.4 | | | |
| PH7-2B | 10 | 19.6 | 42.8 | 63.7 | 77.3 | 98.8 | 1.6 | 173.5 | | | | 23.6 | 42.1 | 34.2 |
| PH7-3B | 15 | 10.0 | 32.8 | 72.5 | 75.2 | 88.6 | 1.5 | 175.4 | 727.4 | 803.5 | 89.1 | | | |

| | | | | | | | | | | | | | | |
|---------|-----|------|------|-------|-------|-------|-----|--------|--------|--------|------|------|------|------|
| PH7-4B | 20 | 10.9 | 39.1 | 85.7 | 78.4 | 93.4 | 1.4 | 188.3 | 420.6 | 458.3 | 89.0 | | | |
| PH7-5B | 25 | 9.5 | 45.1 | 73.1 | 88.5 | 111.6 | 1.5 | 182.2 | 440.6 | 524.8 | 89.9 | | | |
| PH7-6B | 30 | 5.6 | 26.9 | 102.9 | 92.3 | 116.7 | 1.3 | 123.6 | 399.7 | 406.4 | 88.2 | 20.7 | 41.4 | 37.9 |
| PH7-7B | 35 | 5.9 | 25.8 | 108.2 | 94.3 | 111.5 | 1.2 | 105.2 | 279.8 | 291.4 | 88.5 | | | |
| PH7-8B | 40 | 18.0 | 33.4 | 86.9 | 94.2 | 107.8 | 1.4 | 321.1 | 781.3 | 841.1 | 88.9 | 11.5 | 49.4 | 39.2 |
| PH7-9B | 45 | 15.0 | 36.2 | 81.9 | 100.6 | 91.2 | 1.4 | 566.8 | 680.4 | 806.8 | 89.9 | | | |
| PH7-10B | 50 | 7.5 | 50.1 | 67.8 | 105.3 | 86.6 | 1.6 | 856.7 | 269.8 | 313.7 | 89.7 | | | |
| PH7-11B | 55 | 4.1 | 38.4 | 33.9 | 114.9 | 92.6 | 1.8 | 1725.8 | 839.3 | 911.3 | 88.9 | 43.5 | 25.9 | 30.6 |
| PH7-12B | 60 | 12.9 | 18.7 | 102.2 | 103.4 | 117.9 | 1.4 | 885.8 | 540.5 | 601.8 | 89.2 | | | |
| PH7-13B | 65 | 18.3 | 16.4 | 104.5 | 92.8 | 92.1 | 1.3 | 673.1 | | | | | | |
| PH7-14B | 70 | 13.5 | 20.8 | 123.7 | 122.0 | 141.0 | 1.1 | 670.8 | 431.6 | 489.2 | 89.4 | | | |
| PH7-15B | 75 | 12.5 | 13.2 | 173.9 | 153.8 | 175.6 | 0.7 | 652.5 | 683.4 | 761.9 | 89.2 | 18.1 | 47.9 | 34.0 |
| PH7-16B | 80 | 8.1 | 21.1 | 98.2 | 83.3 | 99.8 | 1.3 | 336.1 | 671.4 | 711.9 | 88.7 | | | |
| PH7-17B | 85 | 13.3 | 37.5 | 67.2 | 77.3 | 104.0 | 1.6 | 182.8 | | | | | | |
| PH7-18B | 90 | 13.2 | 30.3 | 80.0 | 82.8 | 105.9 | 1.5 | 109.2 | 367.7 | 399.2 | 88.9 | 41.3 | 23.6 | 35.2 |
| PH7-19 | 95 | 7.5 | 32.3 | 96.1 | 87.4 | 101.9 | 1.3 | 106.2 | 639.4 | 745.3 | 89.7 | | | |
| PH7-20B | 100 | 16.8 | 22.9 | 101.3 | 101.3 | 114.2 | 1.3 | 102.2 | | | | | | |
| PH7-21B | 105 | 9.8 | 29.8 | 89.0 | 88.8 | 95.7 | 1.4 | 120.9 | 299.7 | 338.0 | 89.4 | 17.7 | 42.6 | 39.7 |
| PH7-22B | 110 | 24.3 | 26.2 | 73.9 | 91.9 | 102.7 | 1.5 | 163.7 | 334.7 | 375.3 | 89.3 | | | |
| PH7-23B | 115 | 14.9 | 40.2 | 94.8 | 97.1 | 121.4 | 1.3 | 299.4 | | | | | | |
| PH7-24B | 120 | 22.7 | 42.9 | 39.4 | 84.9 | 88.5 | 1.8 | 569.4 | 646.4 | 702.9 | 89.0 | 21.8 | 44.5 | 33.7 |
| PH7-25B | 125 | 12.2 | 22.2 | 122.5 | 114.2 | 119.6 | 1.1 | 346.2 | 732.4 | 811.0 | 89.2 | | | |
| PH7-26B | 130 | 13.7 | 23.3 | 117.0 | 109.3 | 121.1 | 1.2 | 1274.2 | 624.5 | 719.1 | 89.6 | | | |
| PH7-27B | 135 | 8.5 | 24.2 | 130.1 | 152.6 | 150.5 | 1.1 | 1283.3 | 684.4 | 705.3 | 88.4 | 24.3 | 38.3 | 37.4 |
| PH7-28B | 140 | 15.9 | 30.5 | 126.4 | 186.7 | 202.1 | 1.1 | 2271.7 | 810.3 | 895.2 | 89.1 | | | |
| PH7-29B | 145 | 15.9 | 19.0 | 128.9 | 147.3 | 166.9 | 1.0 | 1142.5 | 701.4 | 772.9 | 89.1 | 23.6 | 41.5 | 35.0 |
| PH7-30B | 150 | 16.3 | 17.3 | 137.0 | 132.1 | 145.2 | 1.0 | 561.8 | 596.5 | 678.6 | 89.5 | | | |
| PH7-31B | 155 | 23.9 | 46.9 | 134.3 | 217.7 | 262.9 | 1.1 | 3450.8 | 1805.4 | 2099.8 | 89.7 | | | |
| PH7-32B | 160 | 13.1 | 14.5 | 44.3 | 60.9 | 62.8 | 1.8 | 775.4 | 538.5 | 587.3 | 89.0 | | | |
| PH7-33B | 165 | 5.1 | 17.3 | 85.5 | 82.6 | 92.6 | 1.4 | 455.3 | 454.6 | 408.1 | 86.6 | 21.3 | 43.5 | 35.1 |

| | | | | | | | | | | | |
|---------------|-----|------|------|-------|-------|-------|-----|-------|-------|-------|------|
| PH7-34B | 170 | 9.5 | 10.9 | 78.7 | 93.3 | 97.7 | 1.5 | 755.0 | 649.4 | 688.6 | 88.7 |
| PH7-35B | 175 | 15.6 | 12.9 | 142.7 | 129.9 | 155.2 | 0.9 | 474.2 | 565.5 | 610.4 | 88.9 |
| PH7-36B | 180 | 9.6 | 7.2 | 87.3 | 84.6 | 90.0 | 1.4 | | | | |
| PH7-37B | 185 | 28.8 | 7.5 | 119.5 | 114.4 | 136.1 | 1.1 | | 452.6 | | 88.9 |
| Natural GW | | 0.2 | -1.5 | 252.9 | 156.3 | | | | | | |

400μM

| Sample ID | Depth | NO ₂ ⁻ | NH ₄ ⁺ | NO ₃ ⁻ | DON | N _{ex} | NO ₃ ⁻ removal | DOC | TA | DIC | DIC _{OM} | C1 | C2 | C3 |
|-----------|-------|------------------------------|------------------------------|------------------------------|-------|-----------------|---|-------|--------|---------|-------------------|------|------|------|
| | | μM | | | | | μM/hr | μM | | | % | | | |
| PH7-1C | 5 | 0.0 | 113.5 | 1.7 | 67.2 | 147.1 | 3.4 | 972.2 | 2471.9 | 4518.5 | 44.8 | 20.4 | 43.4 | 36.2 |
| PH7-2C | 10 | 0.2 | 61.5 | 148.9 | 46.8 | 118.8 | 2.1 | 238.3 | 966.2 | 1898.4 | 48.9 | | | |
| PH7-3C | 15 | 1.2 | 70.5 | 227.2 | 186.5 | 282.4 | 1.5 | 228.7 | 1752.5 | 3382.5 | 47.9 | | | |
| PH7-4C | 20 | 1.3 | 25.5 | 268.5 | 204.4 | 276.3 | 1.1 | 35.9 | 798.3 | 1812.7 | 55.8 | | | |
| PH7-5C | 25 | 0.8 | 24.4 | 269.4 | 209.2 | 280.2 | 1.1 | 18.1 | 970.2 | 1103.7 | 12.0 | 8.5 | 73.7 | 17.8 |
| PH7-6C | 30 | 0.3 | 0.6 | 384.4 | 304.5 | 381.5 | 0.2 | 12.2 | 776.3 | 2219.4 | 64.8 | | | |
| PH7-7C | 35 | 0.0 | 1.8 | 385.8 | 311.0 | 387.1 | 0.2 | 11.1 | 911.2 | 2162.5 | 57.6 | | | |
| PH7-8C | 40 | 0.2 | 6.4 | 371.5 | 301.3 | 375.1 | 0.3 | 10.6 | 598.5 | 801.7 | 25.3 | 9.6 | 72.9 | 17.6 |
| PH7-9C | 45 | 1.9 | 12.1 | 256.1 | 201.0 | 253.3 | 1.2 | 16.7 | 886.2 | 1039.3 | 14.6 | | | |
| PH7-10C | 50 | 21.9 | 78.9 | 135.9 | 114.6 | 203.9 | 2.3 | 86.1 | 559.5 | 1831.5 | 69.3 | | | |
| PH7-11C | 55 | 16.9 | 162.1 | 150.6 | 193.1 | 345.8 | 2.1 | 823.8 | 284.8 | 1143.0 | 75.0 | 47.3 | 22.1 | 30.6 |
| PH7-12C | 60 | 8.5 | 136.1 | 169.9 | 148.3 | 284.7 | 2.1 | 330.4 | 1156.0 | 2185.1 | 46.9 | | | |
| PH7-13C | 65 | 5.2 | 55.5 | 212.3 | 165.8 | 247.8 | 1.6 | 144.7 | 356.7 | 364.0 | 2.0 | | | |
| PH7-14C | 70 | 13.0 | 10.2 | 165.9 | 136.1 | 176.5 | 2.0 | 137.0 | 932.2 | 13174.3 | 91.6 | | | |
| PH7-15C | 75 | 0.2 | 46.1 | 247.3 | 181.9 | 265.8 | 1.3 | 35.8 | 249.8 | 717.6 | 65.1 | 18.8 | 43.9 | 37.3 |
| PH7-16C | 80 | 10.2 | 64.5 | 188.3 | 145.9 | 233.8 | 1.8 | 46.3 | 1506.7 | 8402.2 | 81.2 | | | |
| PH7-17C | 85 | 3.3 | 52.1 | 181.9 | 126.9 | 203.0 | 1.9 | 38.9 | 1013.1 | 2703.3 | 62.3 | | | |
| PH7-18C | 90 | 5.2 | 43.4 | 182.0 | 137.8 | 204.2 | 1.9 | 47.2 | 572.5 | 6960.8 | 91.1 | 12.7 | 37.2 | 50.1 |
| PH7-19 | 95 | 9.5 | 59.7 | 243.5 | 179.6 | 270.8 | 1.3 | 35.1 | 1379.8 | 20209.8 | 91.2 | | | |
| PH7-20C | 100 | 1.2 | 104.2 | 211.3 | 175.8 | 292.1 | 1.6 | 299.6 | 1183.0 | 4760.9 | 74.7 | | | |

| | | | | | | | | | | | | | | |
|---------|-----|------|-------|-------|-------|-------|-----|-------|--------|--------|------|------|------|------|
| PH7-21C | 105 | 14.5 | 122.9 | 162.8 | 155.9 | 277.8 | 2.0 | 215.5 | 249.8 | 603.4 | 58.5 | 15.1 | 47.9 | 37.0 |
| PH7-22C | 110 | 22.4 | 103.8 | 185.7 | 171.2 | 286.8 | 1.8 | 180.2 | 585.5 | 692.4 | 15.4 | | | |
| PH7-23C | 115 | 17.8 | 91.7 | 221.2 | 197.9 | 313.3 | 1.5 | 329.1 | 1122.0 | 1659.9 | 32.2 | | | |
| PH7-24C | 120 | 20.8 | 95.3 | 207.7 | 215.8 | 328.4 | 1.6 | 398.9 | 539.5 | 647.7 | 16.6 | 32.4 | 32.9 | 34.7 |
| PH7-25C | 125 | 23.6 | 51.3 | 265.6 | 234.0 | 326.8 | 1.2 | 288.2 | 295.7 | 409.2 | 27.7 | | | |
| PH7-26C | 130 | 41.1 | 10.0 | 189.8 | 171.6 | 226.6 | 1.8 | 59.9 | 1351.8 | 8116.1 | 82.5 | | | |
| PH7-27C | 135 | 1.0 | 16.4 | 232.5 | 175.4 | 231.1 | 1.4 | 122.1 | 269.8 | 714.9 | 62.2 | | | |
| PH7-28C | 140 | 2.3 | 2.9 | 273.4 | 206.0 | 264.5 | 1.1 | | | | | | | |
| PH7-29C | 145 | 16.3 | 4.4 | 334.3 | 277.6 | 354.0 | 0.6 | 126.3 | 1072.1 | 1325.3 | 19.0 | 19.3 | 36.2 | 44.5 |
| PH7-30C | 150 | 9.5 | 4.1 | 344.3 | 276.9 | 353.6 | 0.5 | 60.0 | 1219.9 | 1838.7 | 33.5 | | | |
| PH7-31C | 155 | 23.6 | 4.4 | 319.8 | 278.0 | 348.6 | 0.8 | 85.1 | 654.4 | 873.1 | 25.0 | | | |
| PH7-32C | 160 | 35.0 | 10.5 | 337.0 | 315.7 | 400.8 | 0.6 | 125.7 | 897.2 | 1053.8 | 14.8 | | | |
| PH7-33C | 165 | | | | | | | 478.1 | 2113.2 | 3630.1 | 41.4 | 14.2 | 45.5 | 40.3 |

800 μ M

| Sample ID | Depth | NO ₂ ⁻ | NH ₄ ⁺ | NO ₃ ⁻ | DON | N _{ex} | NO ₃ ⁻ removal | DOC | TA | DIC | DIC _{OM} | C1 | C2 | C3 |
|-----------|-------|------------------------------|------------------------------|------------------------------|-------|-----------------|--------------------------------------|---------|-------|-------|-------------------|------|------|------|
| | | μ M | | | | | μ M/hr | μ M | | | % | | | |
| PH7-1D | 5 | 43.4 | 38.0 | 719.0 | 508.8 | 533.1 | 0.7 | 48.5 | 289.7 | 368.8 | 21.4 | | | |
| PH7-2D | 10 | 37.3 | 29.3 | 620.4 | 458.4 | 475.1 | 1.6 | 49.3 | 276.8 | 326.6 | 15.2 | 54.3 | 45.3 | 0.5 |
| PH7-3D | 15 | 37.1 | 22.1 | 627.8 | 460.9 | 479.7 | 1.5 | 42.0 | | | | | | |
| PH7-4D | 20 | 55.8 | 21.6 | 534.4 | 414.3 | 393.4 | 2.3 | 56.8 | 282.8 | 380.4 | 25.6 | | | |
| PH7-5D | 25 | 49.7 | 23.4 | 528.9 | 401.3 | 420.1 | 2.3 | 52.4 | 376.7 | 509.9 | 26.1 | | | |
| PH7-6D | 30 | 46.7 | 13.8 | 474.3 | 360.6 | 380.7 | 2.8 | 34.7 | 312.7 | 408.8 | 23.5 | 73.2 | 20.9 | 5.9 |
| PH7-7D | 35 | 35.7 | 8.1 | 432.5 | 332.8 | 302.5 | 3.1 | 32.8 | 265.8 | 359.7 | 26.1 | | | |
| PH7-8D | 40 | 59.0 | 16.8 | 485.9 | 376.7 | 326.8 | 2.7 | 30.9 | | | | 70.3 | 22.6 | 7.1 |
| PH7-9D | 45 | 30.2 | 57.3 | 573.4 | 452.4 | 407.2 | 2.0 | 438.3 | 362.7 | 450.6 | 19.5 | | | |
| PH7-10D | 50 | 6.1 | 56.3 | 548.1 | 421.5 | 423.9 | 2.2 | 803.2 | 305.7 | 401.6 | 23.8 | | | |
| PH7-11D | 55 | 3.5 | 43.8 | 545.5 | 432.3 | 473.1 | 2.2 | 1180.1 | 539.5 | 643.3 | 16.1 | 47.8 | 34.5 | 17.8 |
| PH7-12D | 60 | 7.6 | 21.3 | 808.0 | 622.5 | 658.8 | 0.1 | 821.2 | 358.7 | 417.1 | 14.0 | | | |
| PH7-13D | 65 | 14.5 | 20.9 | 808.6 | 628.5 | 618.3 | 0.0 | 1132.6 | 258.8 | 295.3 | 12.3 | | | |

| | | | | | | | | | | | | | | |
|---------|-----|------|------|-------|-------|-------|------|--------|--------|--------|------|------|------|------|
| PH7-14D | 70 | 22.2 | 17.2 | 824.4 | 604.0 | 637.5 | -0.1 | 542.4 | 402.7 | 407.4 | 1.1 | | | |
| PH7-15D | 75 | 16.4 | 11.9 | 827.7 | 594.1 | 622.4 | -0.2 | 605.5 | | | | 44.5 | 32.2 | 23.3 |
| PH7-16D | 80 | 26.7 | 30.8 | 700.6 | 548.6 | 568.9 | 0.9 | 437.9 | 255.8 | 375.7 | 31.9 | | | |
| PH7-17D | 85 | 11.4 | 26.7 | 696.5 | 523.0 | 566.4 | 0.9 | 50.9 | 287.7 | 410.2 | 29.8 | | | |
| PH7-18D | 90 | 13.1 | 25.0 | 728.3 | 537.4 | 581.2 | 0.7 | 44.1 | 794.3 | 918.0 | 13.4 | 63.8 | 24.1 | 12.1 |
| PH7-19D | 95 | 32.2 | 18.4 | 574.1 | 439.4 | 424.2 | 2.0 | 39.7 | 416.6 | 545.3 | 23.5 | | | |
| PH7-20D | 100 | 82.3 | 26.6 | 472.4 | 396.0 | 415.2 | 2.8 | 51.6 | 494.6 | 653.9 | 24.3 | | | |
| PH7-21D | 105 | 58.9 | 27.5 | 530.1 | 428.7 | 392.7 | 2.3 | 41.8 | 759.3 | 948.4 | 19.8 | 65.6 | 33.4 | 0.9 |
| PH7-22D | 110 | 39.7 | 16.0 | 524.1 | 391.4 | 415.4 | 2.4 | 59.4 | 585.5 | 586.9 | 0.2 | | | |
| PH7-23D | 115 | 31.2 | 58.3 | 568.2 | 439.9 | 495.2 | 2.0 | 444.0 | 1236.9 | 1553.5 | 20.2 | | | |
| PH7-24D | 120 | 33.4 | 50.8 | 597.1 | 491.2 | 490.3 | 1.8 | 1119.3 | 1204.0 | 1267.2 | 4.9 | 59.8 | 23.4 | 16.8 |
| PH7-25D | 125 | 34.1 | 20.7 | 744.9 | 553.5 | 536.6 | 0.5 | 502.3 | 812.3 | 1112.9 | 26.9 | | | |
| PH7-26D | 130 | 23.3 | 15.7 | 815.5 | 590.4 | 608.5 | -0.1 | 447.6 | | | | | | |
| PH7-27D | 135 | 30.6 | 28.0 | 806.7 | 667.0 | 626.7 | 0.0 | 1688.5 | 466.6 | 575.4 | 18.8 | 56.4 | 21.0 | 22.6 |
| PH7-28D | 140 | 22.9 | 22.4 | 830.3 | 612.0 | 558.3 | -0.2 | 2046.0 | 567.5 | 584.1 | 2.8 | | | |
| PH7-29D | 145 | 31.9 | 19.2 | 794.8 | 636.8 | 622.7 | 0.1 | 1021.0 | 319.7 | 368.0 | 13.1 | 56.7 | 18.2 | 25.1 |
| PH7-30D | 150 | 29.2 | 16.3 | 833.6 | 659.7 | 661.7 | -0.2 | 668.2 | 426.6 | 514.7 | 17.1 | | | |
| PH7-31D | 155 | 38.8 | 24.0 | 716.6 | 637.3 | 577.7 | 0.8 | 1474.3 | 842.3 | 1037.3 | 18.7 | | | |
| PH7-32D | 160 | 15.5 | 30.0 | 797.5 | 624.3 | 674.6 | 0.1 | 1451.8 | 880.2 | 929.2 | 5.2 | | | |
| PH7-33D | 165 | 15.7 | 18.8 | 787.5 | 583.8 | 582.5 | 0.2 | 697.1 | 495.6 | 500.0 | 0.8 | 53.8 | 28.8 | 17.4 |
| PH7-34D | 170 | 33.0 | 14.7 | 814.7 | 591.3 | 596.2 | -0.1 | 518.7 | 385.7 | 405.2 | 4.8 | | | |
| PH7-35D | 175 | 23.0 | 13.2 | 825.0 | 617.4 | 616.2 | -0.1 | 485.3 | | | | | | |
| PH7-36D | 180 | 19.7 | 25.9 | 839.4 | 646.0 | 650.5 | -0.3 | | 829.3 | 971.4 | 14.5 | | | |
| PH7-37D | 185 | 15.6 | 11.5 | 768.1 | 593.2 | 552.8 | 0.4 | | | | | | | |

Table 2: Sediment physical, chemical, and hydraulic properties

| Sample ID | Depth | Organic Content | Moisture Content | Porosity | Density | Hydraulic Conductivity | 15N | N weight % | 13C | C weight % | |
|-----------|-------|-----------------|------------------|----------|-------------------|------------------------|------|------------|-------|------------|-------|
| | | | | | | | | | | C/N | C/N |
| | cm | % | | | g/cm ³ | cm/sec | AIR | | VPDB | | |
| PH10-1 | 5 | <LOD | 12.5 | 48.7 | 2.5 | | 2.4 | 0.287 | -22.0 | 0.89 | 3.1 |
| PH10-2 | 10 | 1.9 | 11.0 | 46.8 | 2.0 | 0.0 | 2.3 | 0.277 | -22.1 | 0.51 | 1.8 |
| PH10-3 | 15 | 2.4 | 10.7 | 52.4 | 2.5 | 0.0 | 0.5 | 0.184 | -24.8 | 0.28 | 1.5 |
| PH10-4 | 20 | <LOD | 12.2 | 48.7 | 2.5 | 0.0 | 2.9 | 0.173 | -27.9 | 0.34 | 2.0 |
| PH10-5 | 25 | 4.2 | 12.1 | 49.0 | 2.0 | | 0.6 | 0.117 | -33.6 | 0.22 | 1.8 |
| PH10-6 | 30 | 2.9 | 11.8 | 41.9 | 2.0 | 0.0 | 2.1 | 0.100 | -28.7 | 0.12 | 1.2 |
| PH10-7 | 35 | 4.9 | 11.8 | 47.9 | 2.0 | 0.0 | 2.0 | 0.067 | -25.3 | 0.07 | 1.0 |
| PH10-8 | 40 | 7.0 | 34.3 | 64.9 | 2.5 | | 1.7 | 0.058 | -27.7 | 2.45 | 42.2 |
| PH10-9 | 45 | 12.1 | 42.5 | 64.8 | 2.0 | | 2.0 | 0.055 | -27.0 | 3.22 | 59.1 |
| PH10-10 | 50 | 22.3 | 25.3 | 52.4 | 2.5 | 0.0 | 1.4 | 0.053 | -27.3 | 0.15 | 2.9 |
| PH10-11 | 55 | 12.0 | 15.7 | 43.2 | 2.0 | 0.0 | 2.2 | 0.031 | -26.2 | 0.15 | 4.9 |
| PH10-12 | 60 | 1.6 | 16.1 | 39.0 | 2.0 | 0.0 | 2.3 | 0.030 | -27.0 | 0.24 | 8.0 |
| PH10-13 | 65 | 2.6 | 16.9 | 50.0 | 2.5 | 0.0 | 2.3 | 0.025 | -24.3 | 0.14 | 5.5 |
| PH10-14 | 70 | 2.6 | 16.8 | 41.5 | 1.6 | 0.0 | -0.4 | 0.023 | -27.7 | 0.07 | 3.1 |
| PH10-15 | 75 | 3.6 | 18.7 | 40.0 | 1.7 | 0.0 | 0.6 | 0.018 | -24.1 | 0.10 | 5.5 |
| PH10-16 | 80 | 1.1 | 18.2 | 42.9 | 1.8 | 0.0 | 1.9 | 0.018 | -26.2 | 0.40 | 22.2 |
| PH10-17 | 85 | 1.9 | 21.1 | 40.8 | 1.7 | 0.0 | 2.1 | 0.017 | -25.6 | 0.30 | 17.8 |
| PH10-18 | 90 | <LOD | 30.0 | 42.0 | 1.7 | 0.0 | 2.7 | 0.016 | -25.3 | 0.21 | 13.3 |
| PH10-19 | 95 | 5.4 | 40.3 | 58.3 | 2.5 | | 3.1 | 0.016 | -23.1 | 2.88 | 183.6 |
| PH10-20 | 100 | 8.3 | 35.6 | 48.7 | 2.5 | | 3.1 | 0.012 | -23.5 | 1.72 | 139.6 |
| PH10-21 | 105 | 7.0 | 39.9 | 58.3 | 2.5 | | 2.8 | 0.012 | -23.0 | 4.72 | 393.6 |
| PH10-22 | 110 | 6.8 | 31.1 | 52.2 | 2.3 | 0.0 | 4.7 | 0.011 | -25.3 | 0.26 | 23.3 |

| | | | | | | | | | | | |
|---------|-----|------|------|------|-----|-----|-----|-------|-------|------|-------|
| PH10-23 | 115 | 5.7 | 20.4 | 41.9 | 2.0 | 0.0 | 2.5 | 0.011 | -26.1 | 0.17 | 15.1 |
| PH10-24 | 120 | 1.8 | 37.5 | 55.2 | 1.9 | | 1.6 | 0.011 | -23.7 | 4.62 | 421.6 |
| PH10-25 | 125 | 4.2 | 30.0 | 57.4 | 2.5 | | 1.1 | 0.011 | -24.2 | 1.03 | 94.2 |
| PH10-26 | 130 | 4.2 | 20.4 | 48.7 | 2.5 | 0.0 | 2.6 | 0.011 | -24.5 | 0.58 | 53.8 |
| PH10-27 | 135 | 2.0 | 26.9 | 60.0 | 2.5 | 0.0 | 2.1 | 0.011 | -23.7 | 0.99 | 93.9 |
| PH10-28 | 140 | 5.5 | 28.7 | 58.3 | 2.5 | 0.0 | 2.5 | 0.010 | -23.7 | 1.20 | 122.5 |
| PH10-29 | 145 | 4.3 | 23.4 | 48.7 | 2.5 | 0.0 | 4.0 | 0.010 | -26.7 | 0.28 | 29.4 |
| PH10-30 | 150 | <LOD | 19.4 | 44.4 | 2.5 | 0.0 | 3.0 | 0.010 | -24.7 | 0.31 | 32.8 |
| PH10-31 | 155 | <LOD | 17.1 | 52.4 | 2.5 | 0.0 | 2.1 | 0.009 | -22.5 | 0.43 | 46.9 |
| PH10-32 | 160 | 3.8 | 15.5 | 42.9 | 2.5 | 0.0 | 3.3 | 0.008 | -24.8 | 0.30 | 38.1 |
| PH10-33 | 165 | 1.9 | 16.0 | 47.4 | 2.5 | 0.0 | 4.6 | 0.007 | -23.3 | 0.14 | 19.8 |
| PH10-34 | 170 | 2.2 | 17.3 | 50.0 | 2.5 | 0.0 | 4.1 | 0.006 | -25.1 | 0.10 | 16.0 |
| PH10-35 | 175 | 3.0 | 17.8 | 50.0 | 2.5 | 0.0 | 3.2 | 0.005 | -25.2 | 0.37 | 67.1 |
| PH10-36 | 180 | <LOD | 18.3 | 54.5 | 2.5 | 0.0 | 2.1 | 0.005 | -25.8 | 0.23 | 42.4 |
| PH10-37 | 185 | 6.1 | 15.7 | 54.5 | 2.5 | 0.0 | 3.7 | 0.005 | -27.0 | 0.21 | 45.0 |
| PH10-38 | 190 | 1.8 | 17.4 | 43.2 | 2.0 | 0.0 | 3.0 | 0.003 | -27.3 | 0.21 | 61.7 |

Sediment
Mineralog
ic
Properties

| Sample ID | Depth | Montmorillonite | Kaolinite | Nordstrandite | Goethite | Microcline | Albite | Nontronite | Glauconite |
|-----------|-------|-----------------|-----------|---------------|----------|------------|--------|------------|------------|
| | cm | % intensity | | | | | | | |
| PH10-1 | 5 | | | | | | | | |
| PH10-2 | 10 | 1.8 | 1.5 | 3.7 | 18.1 | 1.3 | 0.6 | 1.0 | 0.0 |
| PH10-3 | 15 | 2.4 | 2.0 | 5.7 | 20.1 | 1.4 | 0.8 | 1.8 | 0.0 |
| PH10-4 | 20 | 2.9 | 4.1 | 18.5 | 22.1 | 1.6 | 1.3 | 2.7 | 1.2 |
| PH10-5 | 25 | 6.9 | 51.0 | 74.2 | 30.3 | 3.3 | 3.7 | 16.7 | 0.0 |
| PH10-6 | 30 | 4.5 | 31.5 | 48.4 | 28.8 | 3.9 | 3.9 | 14.8 | 5.4 |

| | | | | | | | | | |
|---------|-----|-----|------|------|------|-----|-----|------|-----|
| PH10-7 | 35 | 5.6 | 44.5 | 55.9 | 25.6 | 4.4 | 3.8 | 12.3 | 5.1 |
| PH10-8 | 40 | 4.8 | 5.0 | 13.0 | 21.4 | 0.0 | 2.2 | 0.0 | 2.9 |
| PH10-9 | 45 | 4.5 | 3.6 | 8.3 | 19.0 | 0.0 | 1.0 | 5.7 | 2.2 |
| PH10-10 | 50 | 3.3 | 3.0 | 8.7 | 18.8 | 0.0 | 1.2 | 3.3 | 1.5 |
| PH10-11 | 55 | 5.8 | 14.5 | 32.2 | 19.8 | 2.1 | 2.2 | 6.0 | 2.5 |
| PH10-12 | 60 | 5.4 | 15.5 | 40.2 | 25.4 | 3.2 | 3.3 | 9.3 | 3.5 |
| PH10-13 | 65 | 2.3 | 4.8 | 8.6 | 22.5 | 1.7 | 0.0 | 2.9 | 1.2 |
| PH10-14 | 70 | 5.4 | 20.2 | 23.4 | 23.6 | 2.4 | 2.5 | 6.0 | 2.5 |
| PH10-15 | 75 | 4.9 | 21.6 | 22.2 | 23.1 | 1.8 | 1.5 | 6.4 | 3.1 |
| PH10-16 | 80 | 3.2 | 1.4 | 2.1 | 20.9 | 1.1 | 0.0 | 1.5 | 0.0 |
| PH10-17 | 85 | 4.6 | 20.5 | 18.5 | 21.7 | 2.3 | 1.7 | 5.0 | 2.3 |
| PH10-18 | 90 | 2.7 | 7.6 | 8.1 | 20.4 | 1.8 | 1.4 | 4.2 | 2.1 |
| PH10-19 | 95 | 3.2 | 5.6 | 0.8 | 20.7 | 1.4 | 0.0 | 4.4 | 1.9 |
| PH10-20 | 100 | 2.9 | 8.1 | 8.2 | 20.3 | 1.1 | 0.9 | 3.7 | 1.6 |
| PH10-21 | 105 | 3.6 | 7.5 | 5.7 | 22.2 | 0.0 | 1.5 | 4.8 | 2.3 |
| PH10-22 | 110 | 2.7 | 9.9 | 12.6 | 19.7 | 1.7 | 1.1 | 4.0 | 1.9 |
| PH10-23 | 115 | 4.1 | 15.7 | 15.5 | 21.7 | 2.0 | 1.6 | 5.9 | 2.7 |
| PH10-24 | 120 | 3.7 | 7.8 | 5.9 | 23.0 | 1.7 | 1.6 | 5.0 | 2.3 |
| PH10-25 | 125 | 3.4 | 10.8 | 9.2 | 22.1 | 0.0 | 0.0 | 6.3 | 2.7 |
| PH10-26 | 130 | 3.0 | 14.2 | 12.8 | 21.9 | 1.7 | 1.3 | 4.6 | 2.2 |
| PH10-27 | 135 | 2.2 | 4.6 | 4.2 | 21.1 | 0.0 | 0.9 | 3.2 | 1.4 |
| PH10-28 | 140 | 2.0 | 4.1 | 3.2 | 21.0 | 0.9 | 0.0 | 2.3 | 0.9 |
| PH10-29 | 145 | 2.7 | 13.6 | 15.2 | 20.7 | 1.3 | 1.2 | 4.5 | 2.2 |
| PH10-30 | 150 | 3.3 | 1.2 | 1.1 | 24.8 | 1.1 | 0.4 | 1.3 | 0.0 |
| PH10-31 | 155 | 1.6 | 0.0 | 0.0 | 21.2 | 1.0 | 0.4 | 0.8 | 0.5 |
| PH10-32 | 160 | 1.7 | 0.7 | 0.0 | 20.9 | 1.0 | 0.5 | 0.9 | 0.0 |
| PH10-33 | 165 | 2.2 | 1.1 | 0.0 | 19.6 | 0.8 | 0.0 | 1.0 | 0.0 |
| PH10-34 | 170 | 2.0 | 2.8 | 0.0 | 20.8 | 0.8 | 0.6 | 1.2 | 2.1 |
| PH10-35 | 175 | 1.8 | 2.2 | 0.0 | 21.5 | 0.9 | 0.0 | 1.1 | 1.2 |
| PH10-36 | 180 | 2.7 | 5.3 | 0.0 | 22.7 | 1.4 | 0.0 | 2.9 | 2.3 |

| | | | | | | | | | |
|---------|-----|-----|-----|-----|------|-----|-----|-----|-----|
| PH10-37 | 185 | 2.7 | 2.7 | 0.0 | 24.8 | 1.5 | 0.0 | 2.6 | 1.1 |
| PH10-38 | 190 | 1.9 | 3.1 | 0.9 | 21.5 | 1.3 | 0.0 | 2.4 | 0.8 |

Metals

| Sample ID | Depth | Organic content | Fe | Al | Mg | K | Na | Ca | Mn | B |
|-----------|-------|-----------------|----------------|------|------|------|------|------|------|------|
| | cm | % | g/kg | | | | | | | |
| PH10-1 | 5 | <LOD | 3.4258054 6 | 3.8 | 0.21 | 0.12 | 0.09 | 0.48 | 0.10 | 0.01 |
| PH10-2 | 10 | 1.9 | 4.6182124 3 | 6.2 | 0.18 | 0.13 | 0.04 | 0.25 | 0.12 | 0.02 |
| PH10-3 | 15 | 2.4 | 5.9 | 7.7 | 0.16 | 0.13 | 0.03 | 0.16 | 0.04 | 0.02 |
| PH10-4 | 20 | <LOD | 14.7 | 23.1 | 0.26 | 0.16 | 0.05 | 0.20 | 0.03 | 0.07 |
| PH10-5 | 25 | 4.2 | 16.3 | 23.0 | 0.14 | 0.08 | 0.05 | 0.19 | 0.02 | 0.08 |
| PH10-6 | 30 | 2.9 | 15.2 | 16.2 | 0.13 | 0.09 | 0.05 | 0.17 | 0.02 | 0.07 |
| PH10-7 | 35 | 4.9 | 11.8 | 14.0 | 0.09 | 0.04 | 0.06 | 0.19 | 0.02 | 0.06 |
| PH10-8 | 40 | 7.0 | 8.9 | 13.4 | 0.30 | 0.22 | 0.20 | 2.06 | 0.05 | 0.04 |
| PH10-9 | 45 | 12.1 | 7.3 | 11.8 | 0.22 | 0.11 | 0.20 | 1.58 | 0.04 | 0.04 |
| PH10-10 | 50 | 22.3 | 3.8 | 5.0 | 0.08 | 0.06 | 0.09 | 0.40 | 0.01 | 0.02 |
| PH10-11 | 55 | 12.0 | 11.2 | 13.2 | 0.12 | 0.06 | 0.10 | 0.37 | 0.07 | 0.05 |
| PH10-12 | 60 | 1.6 | 23.0 | 14.1 | 0.15 | 0.08 | 0.11 | 0.71 | 0.15 | 0.12 |
| PH10-13 | 65 | 2.6 | 12.6 | 9.2 | 0.20 | 0.17 | 0.16 | 0.41 | 0.07 | 0.05 |
| PH10-14 | 70 | 2.6 | 11.4 | 8.3 | 0.16 | 0.11 | 0.22 | 0.20 | 0.02 | 0.05 |
| PH10-15 | 75 | 3.6 | 5.8 | 7.9 | 0.28 | 0.20 | 0.35 | 0.22 | 0.02 | 0.03 |
| PH10-16 | 80 | 1.1 | 4.4 | 3.4 | 0.23 | 0.15 | 0.34 | 0.31 | 0.03 | 0.02 |
| PH10-17 | 85 | 1.9 | 5.7 | 6.6 | 0.22 | 0.18 | 0.28 | 0.26 | 0.02 | 0.02 |
| PH10-18 | 90 | <LOD | 9.2 | 9.6 | 0.57 | 0.45 | 0.51 | 0.51 | 0.04 | 0.04 |
| PH10-19 | 95 | 5.4 | 10.4 | 10.7 | 0.89 | 0.69 | 0.80 | 0.65 | 0.04 | 0.05 |
| PH10-20 | 100 | 8.3 | 11.4 | 9.9 | 0.87 | 0.57 | 0.72 | 0.62 | 0.04 | 0.05 |
| PH10-21 | 105 | 7.0 | 11.1 | 9.8 | 1.04 | 0.67 | 0.87 | 0.91 | 0.04 | 0.05 |
| PH10-22 | 110 | 6.8 | 7.0 | 7.7 | 0.39 | 0.29 | 0.40 | 0.40 | 0.02 | 0.03 |

| | | | | | | | | | | | |
|---------|-----|------|-----|------|-----|------|------|------|------|------|------|
| PH10-23 | 115 | | 5.7 | 5.5 | 5.9 | 0.17 | 0.11 | 0.20 | 0.20 | 0.02 | 0.02 |
| PH10-24 | 120 | | 1.8 | 10.7 | 9.7 | 1.05 | 0.70 | 0.79 | 0.73 | 0.05 | 0.05 |
| PH10-25 | 125 | | 4.2 | 9.0 | 8.2 | 0.75 | 0.47 | 0.67 | 0.59 | 0.04 | 0.04 |
| PH10-26 | 130 | | 4.2 | 5.1 | 5.4 | 0.24 | 0.14 | 0.28 | 0.25 | 0.03 | 0.02 |
| PH10-27 | 135 | | 2.0 | 6.9 | 7.5 | 0.63 | 0.46 | 0.63 | 0.49 | 0.04 | 0.03 |
| PH10-28 | 140 | | 5.5 | 5.5 | 6.2 | 0.46 | 0.33 | 0.53 | 0.46 | 0.03 | 0.03 |
| PH10-29 | 145 | | 4.3 | 4.3 | 5.0 | 0.14 | 0.06 | 0.39 | 0.16 | 0.01 | 0.02 |
| PH10-30 | 150 | <LOD | | 6.2 | 2.7 | 0.21 | 0.12 | 0.40 | 0.17 | 0.01 | 0.03 |
| PH10-31 | 155 | <LOD | | 14.7 | 3.3 | 0.27 | 0.11 | 0.54 | 0.20 | 0.02 | 0.08 |
| PH10-32 | 160 | | 3.8 | 6.7 | 3.0 | 0.26 | 0.15 | 0.48 | 0.14 | 0.01 | 0.03 |
| PH10-33 | 165 | | 1.9 | 12.2 | 3.4 | 0.30 | 0.16 | 0.46 | 0.17 | 0.03 | 0.06 |
| PH10-34 | 170 | | 2.2 | 34.1 | 4.9 | 0.34 | 0.15 | 0.58 | 0.34 | 0.05 | 0.19 |
| PH10-35 | 175 | | 3.0 | 23.7 | 3.8 | 0.30 | 0.13 | 0.55 | 0.21 | 0.03 | 0.12 |
| PH10-36 | 180 | <LOD | | 33.5 | 8.3 | 0.44 | 0.26 | 0.72 | 0.19 | 0.01 | 0.19 |
| PH10-37 | 185 | | 6.1 | 17.4 | 5.9 | 0.38 | 0.22 | 0.57 | 0.13 | 0.01 | 0.09 |
| PH10-38 | 190 | | 1.8 | 6.2 | 5.8 | 0.38 | 0.28 | 0.64 | 0.12 | 0.01 | 0.03 |

Metals
Contd.

| Sample ID | Depth | Organic content | Cr | Cu | Ni | Pb | Sr | Ti | V | Zn | |
|-----------|-------|-----------------|-------|-------|-------|------|------|-------|-------|-------|-------|
| | cm | % | mg/kg | | | | | | | | |
| PH10-1 | 5 | <LOD | 6.18 | 5.78 | 0.80 | 1.10 | 3.86 | 6.52 | 8.10 | 14.20 | |
| PH10-2 | 10 | | 1.9 | 7.59 | 6.53 | 1.91 | 1.77 | 2.58 | 20.15 | 11.29 | 9.99 |
| PH10-3 | 15 | | 2.4 | 9.06 | 6.33 | 2.41 | 1.23 | 2.00 | 23.25 | 13.86 | 7.91 |
| PH10-4 | 20 | <LOD | 28.23 | 10.12 | 4.36 | 2.19 | 2.95 | 16.63 | 36.92 | 10.81 | |
| PH10-5 | 25 | | 4.2 | 28.79 | 11.55 | 2.08 | 3.49 | 2.79 | 13.32 | 50.13 | 6.37 |
| PH10-6 | 30 | | 2.9 | 26.10 | 10.41 | 2.25 | 3.73 | 2.47 | 20.38 | 44.71 | 5.52 |
| PH10-7 | 35 | | 4.9 | 22.08 | 8.70 | 1.16 | 2.67 | 1.96 | 13.53 | 39.90 | 3.97 |
| PH10-8 | 40 | | 7.0 | 19.80 | 10.62 | 4.20 | 3.82 | 11.47 | 25.30 | 27.65 | 27.53 |

| | | | | | | | | | | |
|---------|-----|------|-------|------|------|------|-------|-------|-------|-------|
| PH10-9 | 45 | 12.1 | 16.75 | 9.83 | 2.21 | 5.36 | 8.89 | 9.43 | 22.39 | 25.21 |
| PH10-10 | 50 | 22.3 | 6.30 | 4.12 | 0.86 | 1.53 | 2.51 | 14.08 | 10.24 | 5.46 |
| PH10-11 | 55 | 12.0 | 16.86 | 7.73 | 1.47 | 2.61 | 1.77 | 21.30 | 32.40 | 5.63 |
| PH10-12 | 60 | 1.6 | 17.74 | 8.53 | 1.55 | 3.44 | 2.25 | 24.06 | 35.52 | 8.17 |
| PH10-13 | 65 | 2.6 | 11.27 | 5.69 | 2.40 | 2.56 | 2.45 | 21.50 | 22.22 | 9.11 |
| PH10-14 | 70 | 2.6 | 30.66 | 5.00 | 1.54 | 2.65 | 2.12 | 21.68 | 28.33 | 6.03 |
| PH10-15 | 75 | 3.6 | 11.42 | 4.96 | 2.21 | 2.30 | 3.41 | 20.06 | 19.13 | 5.79 |
| PH10-16 | 80 | 1.1 | 7.38 | 2.82 | 0.62 | 1.29 | 3.59 | 7.39 | 13.56 | 4.52 |
| PH10-17 | 85 | 1.9 | 9.94 | 4.52 | 2.04 | 1.26 | 3.13 | 19.94 | 15.69 | 6.11 |
| PH10-18 | 90 | <LOD | 17.59 | 7.02 | 3.67 | 4.26 | 7.06 | 15.75 | 23.77 | 13.71 |
| PH10-19 | 95 | 5.4 | 17.56 | 6.71 | 6.03 | 4.69 | 10.35 | 20.02 | 25.36 | 19.87 |
| PH10-20 | 100 | 8.3 | 16.01 | 7.06 | 4.45 | 4.54 | 10.03 | 10.51 | 24.65 | 18.27 |
| PH10-21 | 105 | 7.0 | 16.53 | 9.17 | 5.39 | 5.47 | 13.78 | 11.00 | 23.70 | 20.43 |
| PH10-22 | 110 | 6.8 | 10.56 | 6.43 | 2.97 | 2.17 | 5.51 | 19.36 | 17.89 | 9.66 |
| PH10-23 | 115 | 5.7 | 7.75 | 5.10 | 1.83 | 1.57 | 2.33 | 17.28 | 13.39 | 5.14 |
| PH10-24 | 120 | 1.8 | 15.55 | 7.26 | 5.35 | 4.96 | 12.28 | 14.50 | 23.15 | 18.78 |
| PH10-25 | 125 | 4.2 | 12.96 | 6.68 | 3.69 | 3.94 | 9.25 | 9.51 | 20.06 | 13.58 |
| PH10-26 | 130 | 4.2 | 7.77 | 4.94 | 1.34 | 2.28 | 3.34 | 11.24 | 14.05 | 5.21 |
| PH10-27 | 135 | 2.0 | 13.11 | 6.22 | 3.42 | 5.50 | 8.15 | 17.52 | 18.47 | 11.16 |
| PH10-28 | 140 | 5.5 | 10.58 | 5.18 | 2.61 | 2.61 | 6.75 | 20.30 | 16.24 | 8.81 |
| PH10-29 | 145 | 4.3 | 7.69 | 4.70 | 0.68 | 1.55 | 1.93 | 8.78 | 14.67 | 3.55 |
| PH10-30 | 150 | <LOD | 5.36 | 2.91 | 0.78 | 1.61 | 3.00 | 13.81 | 15.21 | 1.86 |
| PH10-31 | 155 | <LOD | 4.82 | 2.67 | 0.46 | 2.80 | 3.31 | 18.16 | 14.21 | 2.56 |
| PH10-32 | 160 | 3.8 | 4.59 | 2.31 | 0.72 | 1.59 | 3.00 | 31.00 | 8.70 | 2.13 |
| PH10-33 | 165 | 1.9 | 5.14 | 2.91 | 0.74 | 2.74 | 2.85 | 28.70 | 12.39 | 2.72 |
| PH10-34 | 170 | 2.2 | 5.41 | 3.29 | | 5.28 | 3.19 | 24.92 | 17.97 | 4.64 |
| PH10-35 | 175 | 3.0 | 5.16 | 2.80 | | 3.23 | 2.55 | 18.76 | 14.12 | 3.80 |
| PH10-36 | 180 | <LOD | 9.85 | 4.34 | 1.64 | 4.68 | 3.45 | 25.32 | 34.15 | 6.88 |
| PH10-37 | 185 | 6.1 | 8.52 | 3.39 | 1.42 | 2.55 | 2.66 | 20.78 | 26.89 | 5.09 |
| PH10-38 | 190 | 1.8 | 8.45 | 2.85 | 2.13 | 2.01 | 3.05 | 30.45 | 15.91 | 4.75 |

Pre-
treatment
sediment
DOM

| Sample ID | Depth | C1 | C2 | C3 |
|-----------|-------|------|------|------|
| | cm | % | | |
| PH10-1 | 5 | 22.8 | 43.2 | 34.0 |
| PH10-2 | 10 | 17.0 | 47.5 | 35.6 |
| PH10-3 | 15 | 9.2 | 52.4 | 38.4 |
| PH10-4 | 20 | 15.8 | 65.8 | 18.4 |
| PH10-5 | 25 | 12.4 | 72.1 | 15.5 |
| PH10-6 | 30 | 6.6 | 88.1 | 5.3 |
| PH10-7 | 35 | 11.8 | 81.1 | 7.1 |
| PH10-8 | 40 | 9.5 | 53.7 | 36.9 |
| PH10-9 | 45 | 22.8 | 43.6 | 33.6 |
| PH10-10 | 50 | 14.8 | 63.4 | 21.8 |
| PH10-12 | 55 | 5.9 | 60.7 | 33.4 |
| PH10-13 | 60 | 7.3 | 55.8 | 37.0 |
| PH10-14 | 65 | 43.8 | 32.6 | 23.7 |
| PH10-15 | 70 | 31.6 | 35.8 | 32.6 |
| PH10-16 | 75 | 19.2 | 45.9 | 35.0 |
| PH10-17 | 80 | 9.1 | 54.9 | 36.0 |
| PH10-18 | 85 | 17.7 | 40.4 | 41.9 |
| PH10-19 | 90 | 11.3 | 52.9 | 35.8 |
| PH10-20 | 95 | 9.1 | 57.0 | 33.9 |
| PH10-21 | 100 | 12.9 | 49.9 | 37.2 |
| PH10-22 | 105 | 9.6 | 54.4 | 36.0 |
| PH10-23 | 110 | 9.9 | 54.9 | 35.2 |
| PH10-24 | 115 | 38.3 | 31.7 | 30.0 |
| PH10-25 | 120 | 17.0 | 46.4 | 36.6 |
| PH10-26 | 125 | 10.9 | 53.7 | 35.5 |
| PH10-27 | 130 | 22.0 | 41.0 | 37.0 |

| | | | | |
|---------|-----|------|------|------|
| PH10-28 | 135 | 16.5 | 45.7 | 37.8 |
| PH10-29 | 140 | 9.7 | 53.2 | 37.0 |
| PH10-30 | 145 | 11.4 | 52.2 | 36.3 |
| PH10-31 | 150 | 9.6 | 52.0 | 38.4 |
| PH10-32 | 155 | 8.2 | 54.5 | 37.3 |
| PH10-33 | 160 | 17.9 | 43.3 | 38.7 |
| PH10-34 | 165 | 16.5 | 42.8 | 40.7 |
| PH10-35 | 170 | 25.0 | 42.3 | 32.7 |
| PH10-36 | 175 | 10.7 | 48.1 | 41.1 |
| PH10-37 | 180 | 17.2 | 60.6 | 22.1 |
| PH10-38 | 185 | 12.2 | 51.7 | 36.1 |

Radiocarbon

| Sample ID | Depth | $\delta^{14}C$ | F modern | F modern error | Age |
|-----------|-------|----------------|----------|----------------|-----------|
| | cm | Δ | | | yrs |
| PH7-11 | 55 | -19.5 | 0.9887 | 0.0019 | 90 +/- 15 |
| PH7-22 | 110 | 218.65 | 1.2289 | 0.0029 | >Modern |
| PH11-11 | 55 | 104.1 | 1.1134 | 0.0023 | >Modern |
| PH11-24 | 120 | 59.58 | 1.0685 | 0.0022 | >Modern |